Микро- и наноэлектромеханические системы на базе сегнетэлектрических структур и методы их исследования

Andrei Kholkin

Department of Ceramic and Glass Engineering &
Center for Research in Ceramic and Composite Materials
University of Aveiro
Portugal

СПбГПУ, 24 июня 2011 года

Acknowledgements

Former and current students and postdocs:

V. Shvartsman, I. Bdikin, D. Kiselev, G. Song, A. Emelyanov, S. Iakovlev, N. Vyshatko, H. Amorin, J. Perez

Dr. Paul Muralt (EPFL, Lausanne)

Prof. Alexei Gruverman (NCSU)

Dr. Nikolay Pertsev (F. Z. Juelich)

Prof. Doru Lupascu (U. Dresden)

Dr. S-H. Kim (Inostek)

Outline

- Introduction
- Overview of MEMS
- Basics of piezoelectric effect in bulk materials and thin films
- Piezoelectric measurements: Laser Interferometry
- Piezoelectric measurements: Piezoresponse Force Microscopy
- Relaxor ferroelectrics: nanoscale vs. macroscopic response
- Summary

Where to read

Reports on Progress in Physics Sept., 2006

Nanoscale ferroelectrics: processing, characterization and future trends

A Gruverman[1] and A Kholkin[2]

[1] Department of Materials Science and Engineering, North Carolina State University, Raleigh, NC 27695-7920, USA
[2] Department of Ceramics & Glass Engineering, CICECO, University of Aveiro, 3810-193 Aveiro, Portugal

E-mail: Alexei_Gruverman@ncsu.edu and kholkin@cv.ua.pt

Received 25 April 2006, in final form 12 June 2006
Published 25 July 2006
Online at stacks.iop.org/RoPP/69/2443

Abstract

This review paper summarizes recent advances in the quickly developing field of nanoscal ferroelectrics, analyses its current status and considers potential future developments. Th paper presents a brief survey of the fabrication methods of ferroelectric nanostructures an investigation of the size effects by means of scanning probe microscopy. One of the focuses o the review will be the study of kinetics of nanoscale ferroelectric switching in inhomogeneou electrical and elastic fields. Another emphasis will be made on tailoring the electrical an mechanical properties of ferroelectrics with a viewpoint of fabrication of nanoscale domai structures.

"Scanning Probe Microscopy: Electrical and Electromechanical Phenomena at the Nanoscale", Springer, 2006.

Review of Ferroelectric Domain Imaging by Piezoresponse Force Microscopy

A. L. KHOLKIN, S. V. KALININ, A. ROELOFS, AND A. GRUVERMAN

This chapter describes the principles, theoretical background, recent developments, and applications of a local probe-based technique for nondestructive high-resolution ferroelectric domain imaging and manipulation—piezoresponse force microscopy (PFM). This technique has proven to be a powerful tool for the characterization of ferroelectric thin films, ceramics, and single crystals. Recent advances in application of PFM for studying a mechanism of polarization reversal at the nanoscale, domain dynamics, degradation effects, and size-dependent phenomena in ferroelectrics are reviewed in detail. Examples of using PFM for the characterization of various polar materials such as ferroelectric films, piezoelectric semiconductors, and ferroelectric relaxors are given.

Special Issue on "Nanoscale Ferroelectrics", TUFFC, Dec. 06

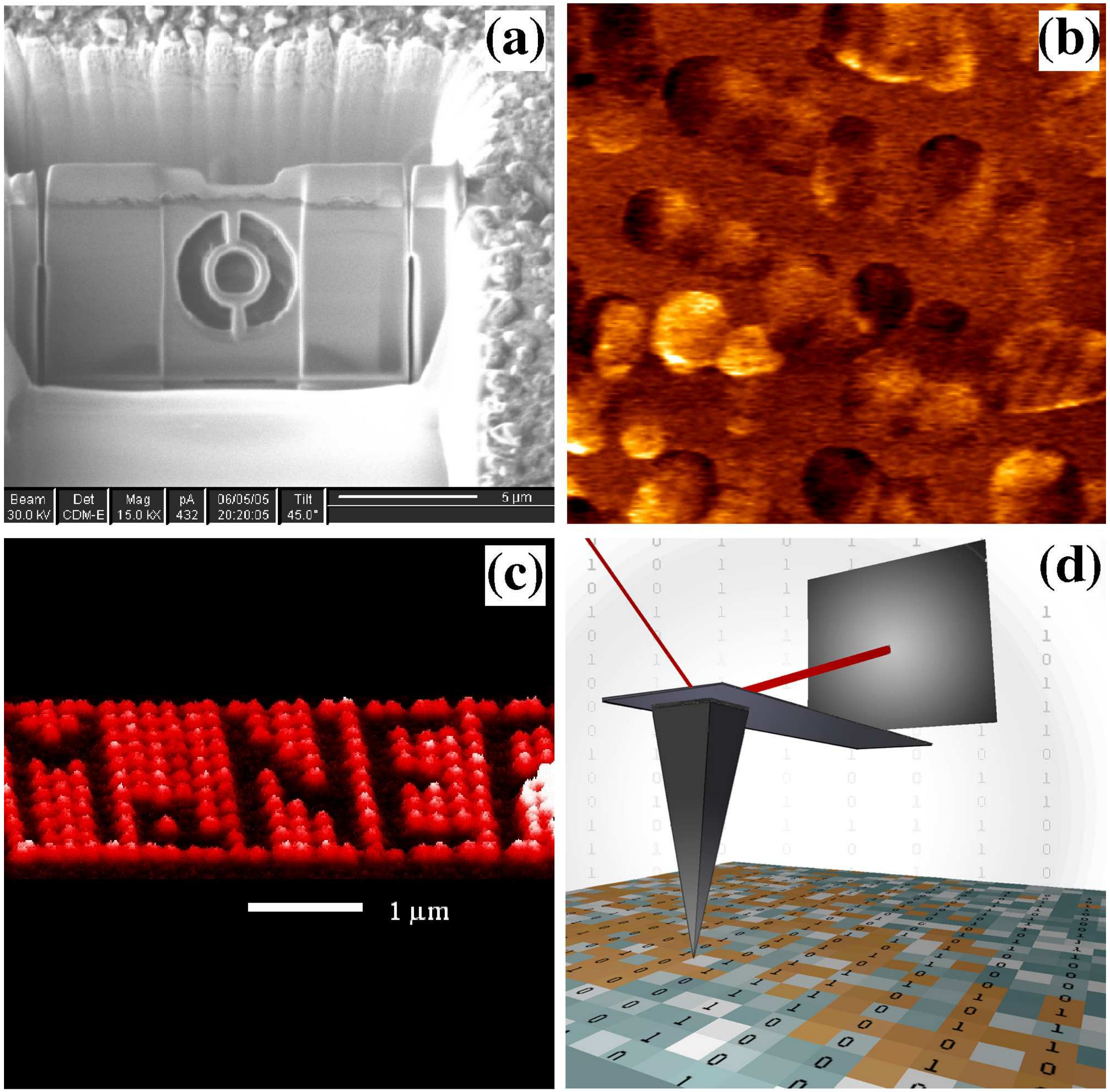

Actuation principles used in MEMS

- **Piezoelectric effect**
  -strong force, low displacement, good scalability, hard to integrate, high efficiency, fast response
- **Electrostatic effect**
  -weak force, low to moderate displacement, non-linearity, most easy to integrate, large voltages even for small gaps
- **Electromagnetic effect**
  -high displacement, low to moderate force, limited by heating of coils, slow response, hard to integrate
- **Thermal effect**
  -strong force, large displacement, slow, hard to control, low efficiency

Other principles...

- **Shape memory effect (austenite/martensite phase transition)**
  -5% strain (NiTi alloy),
  -slow response

- **Piezoresistivity**
  -easily processed
  -sensing only

- **Magnetostriction**
  -processing can be complicated (Terfenol-D)
  -similar performance to piezoelectrics

Possibilities provided by Si technology

• Most common structures

- Electrostatic drive

- Capacitive sensor

• Complex geometries

-Large strain with moderate force

-High sensitivity-large areas

• Easy processing

-30+ years of Si processing technology

- Surface micromachining

- Bulk surface micromachining

- LIGA process, etc…

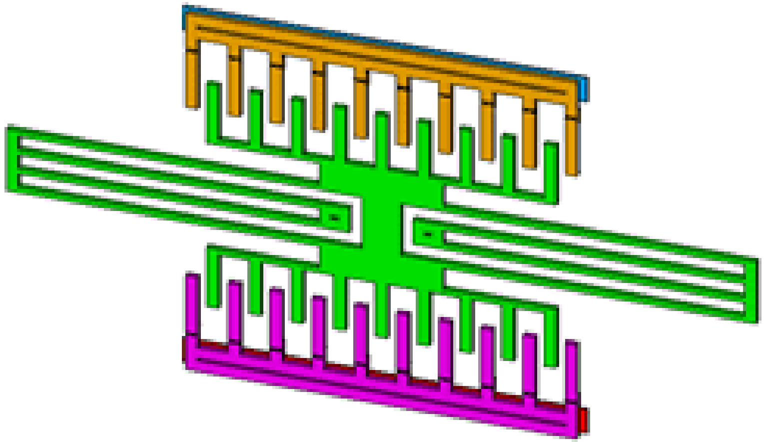

Schematic of linear electrostatic drive

Advantages of MEMS

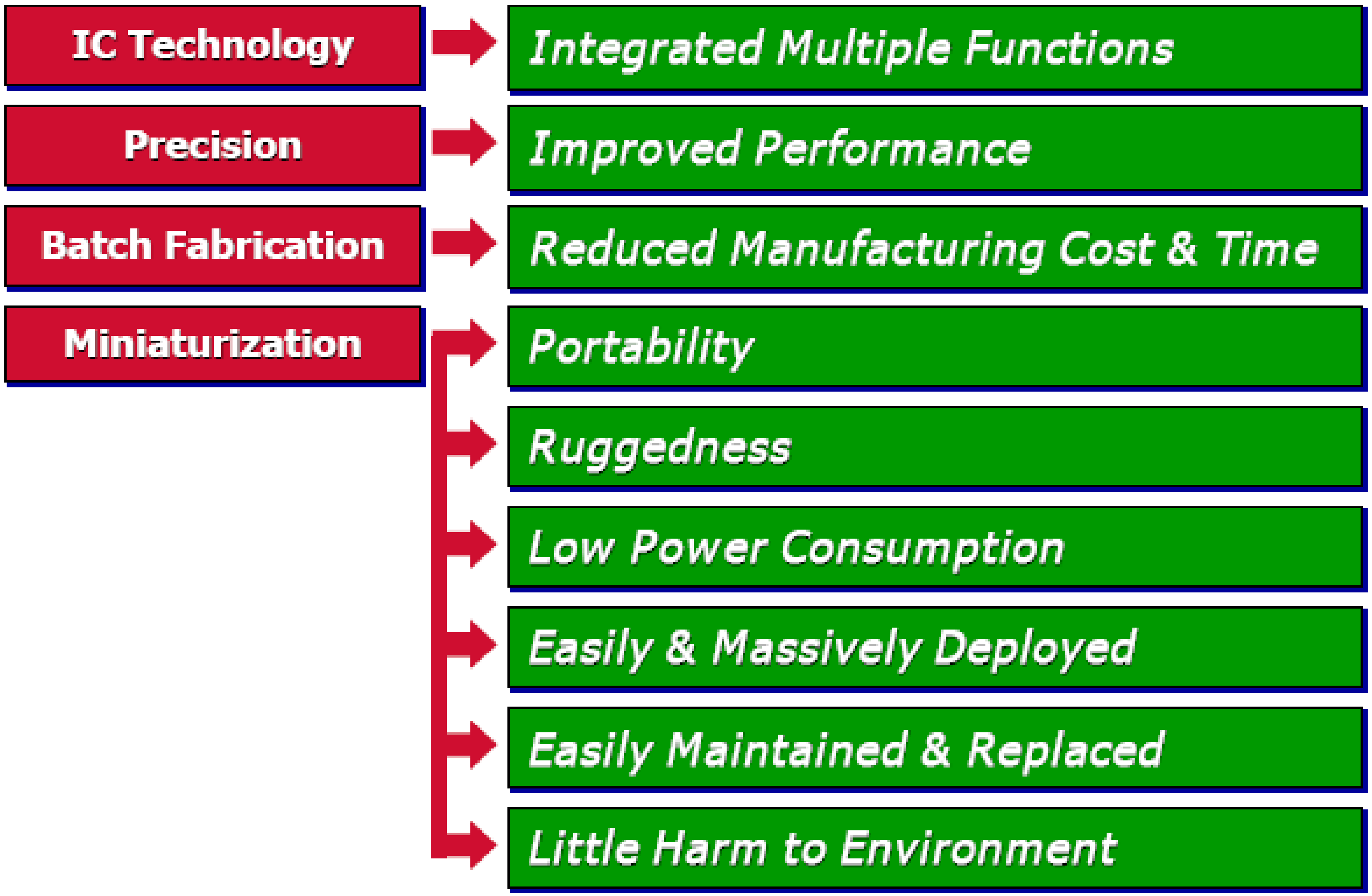

MEMS technologies

- Bulk micromachining
- Surface micromachining
- Wafer bonding
- LIGA and similar techniques
- Others

- MicroEDM
- 3D lithography
- Laser micromachining

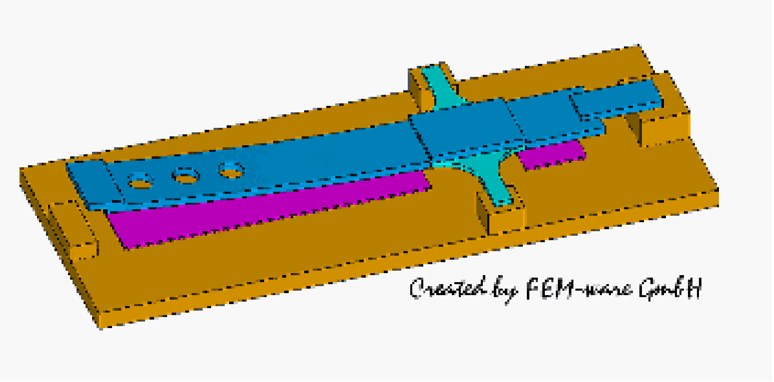

Wet etching of Si

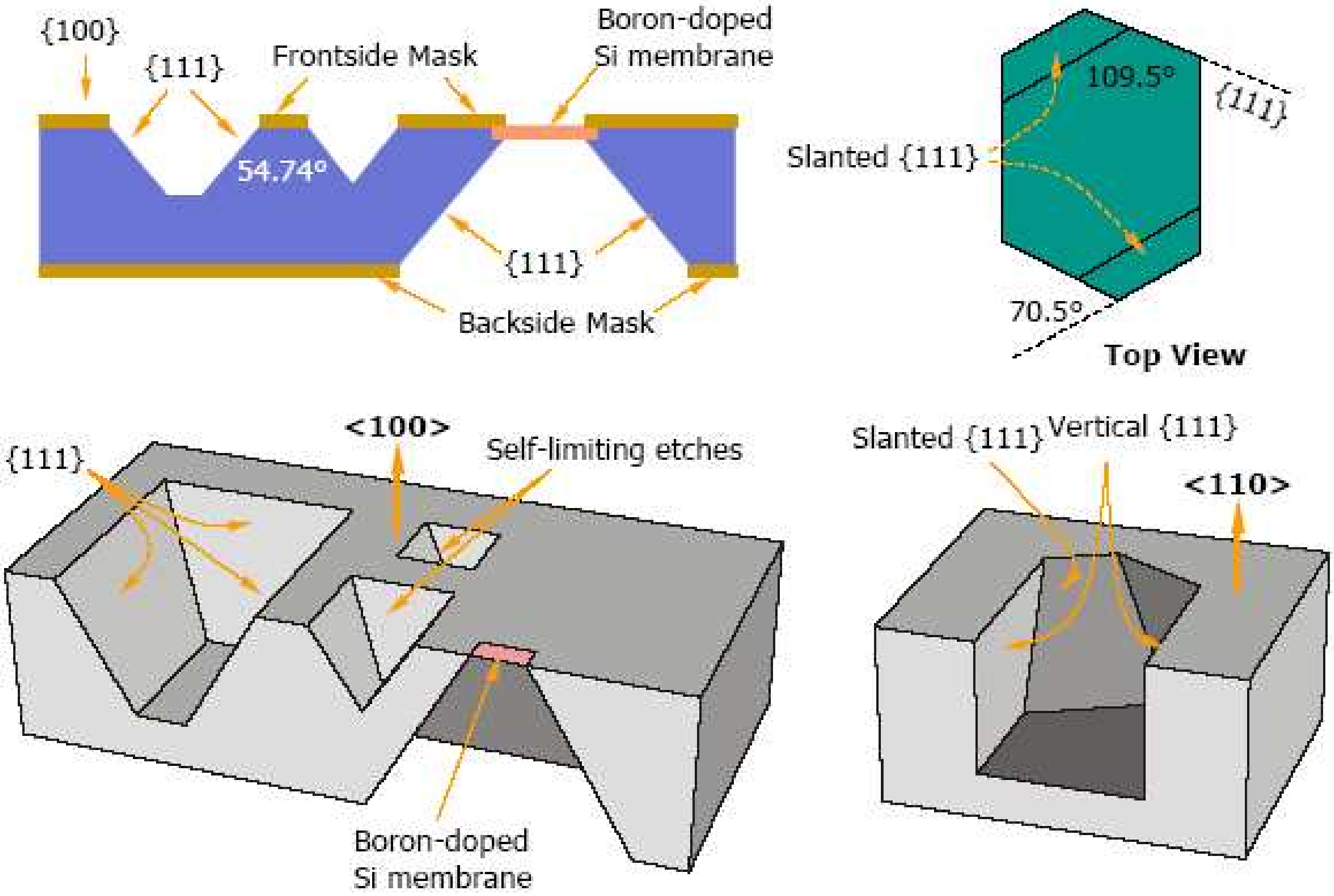

Dry etching of Si

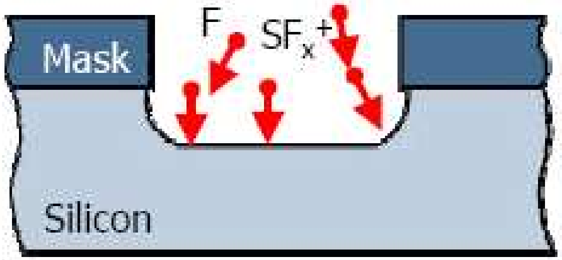

Etch

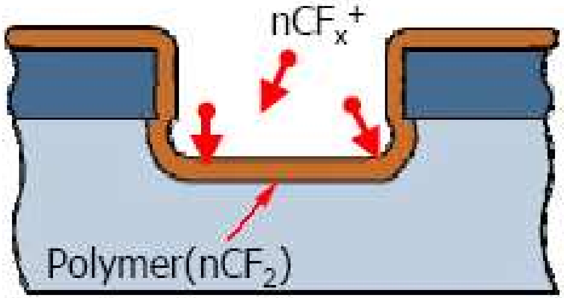

Deposit Polymer

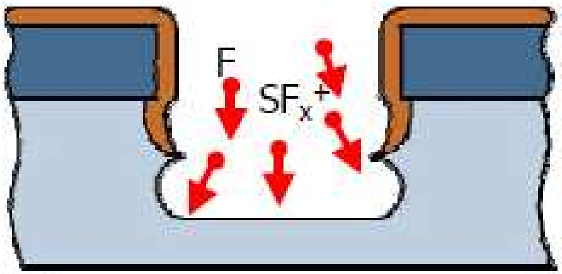

Etch

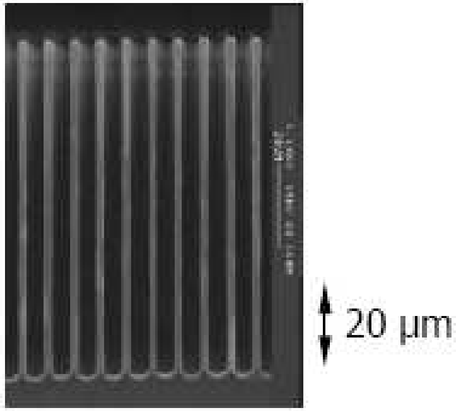

Trenches - *Surface Technology Systems*

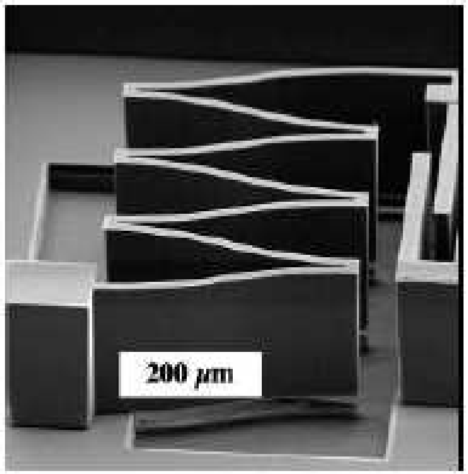

Spring - Klaassen, *et al*, 1995

Surface micromachining

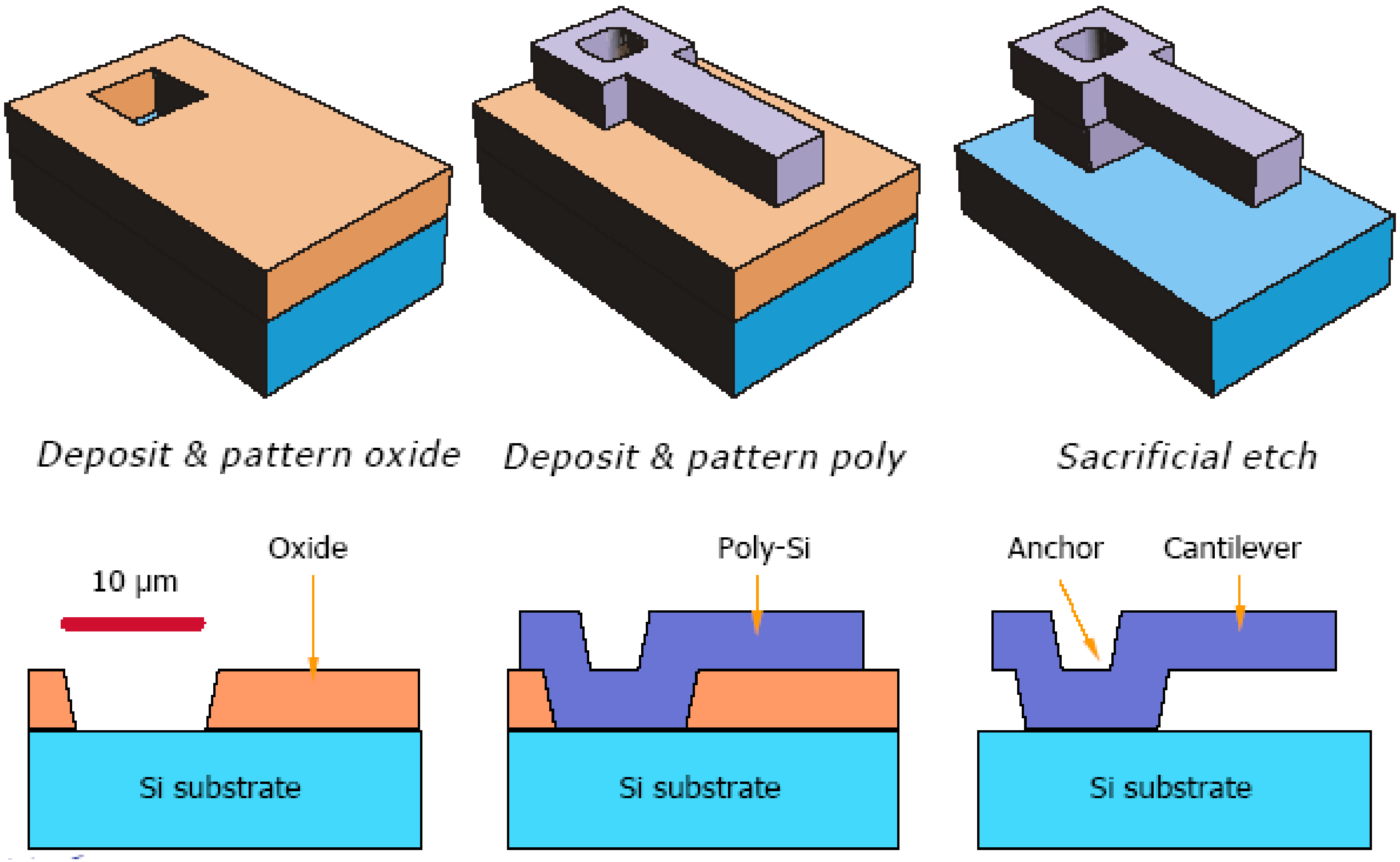

Piezoelectric micromotor (EPFL)

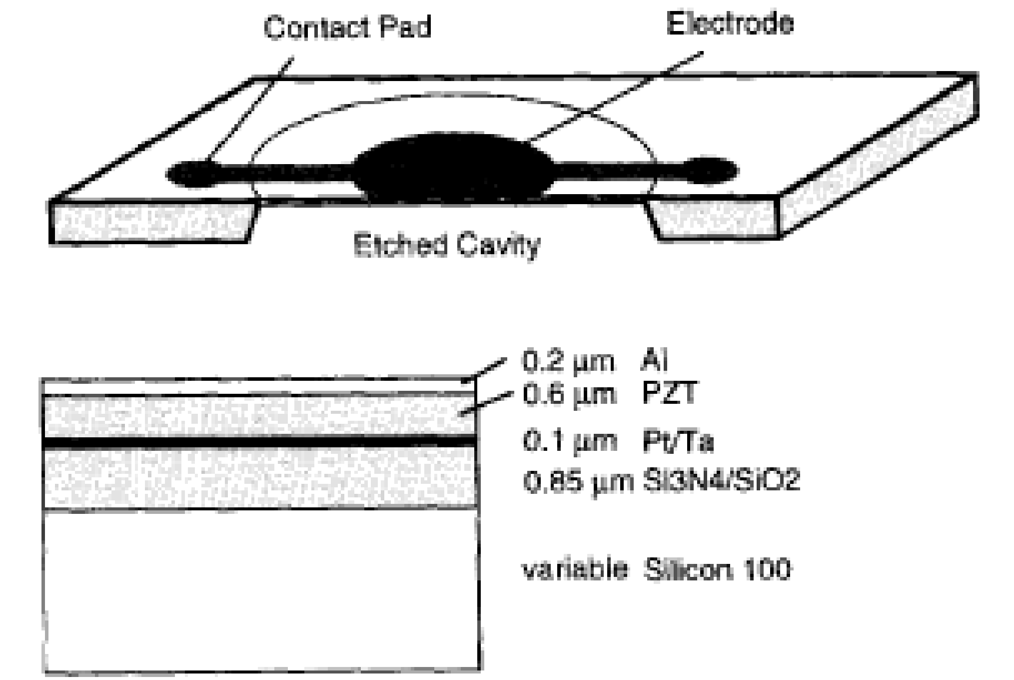

Fig. 1. Schematic drawing of the membrane with view onto the top side of the wafer and a schematic cross section through the films.

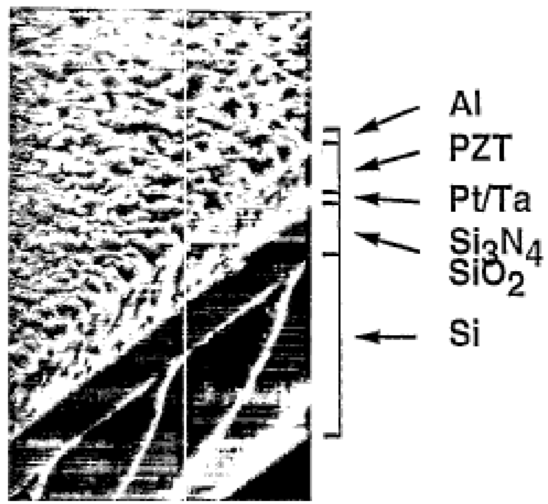

Fig. 2. Image of a cut through a membrane as obtained by scanning electron microscopy.

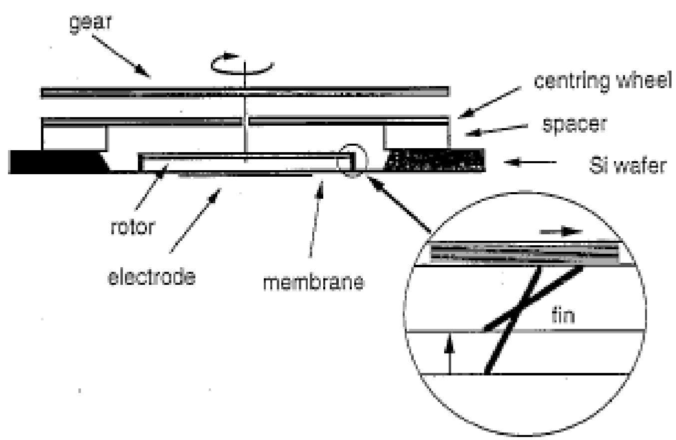

P. Muralt, A. Kholkin, M. Kohli, T. Maeder (Sens. Act. 96, 97 & 98)

Motor performance vs. PZT routes

Performance	Sol–gel no bias 94 kHz B_{10}	Sol–gel +2 V 94 kHz B_{10}	Sputter −2 V 21 kHz B_{00}	Sputter no bias 78 kHz B_{10}	Sputter −2 V 78 kHz B_{10}
Speed per a.c. voltage $F=2.4\times10^{-4}$ N (rpm/$V_{r.m.s.}$)	140	180	32	80	100
Torque per a.c. voltage $F=2.4\times10^{-4}$ N (nN m/$V_{r.m.s.}$)	4.3		1.8		3.9
Torque per a.c. voltage $F=9.8\times10^{-4}$ N (nN m/$V_{r.m.s.}$)	12		3.2		11

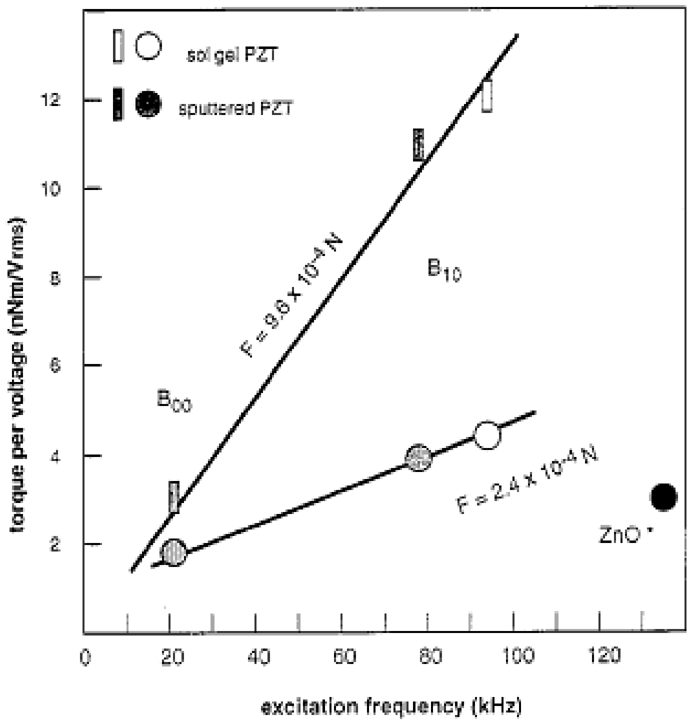

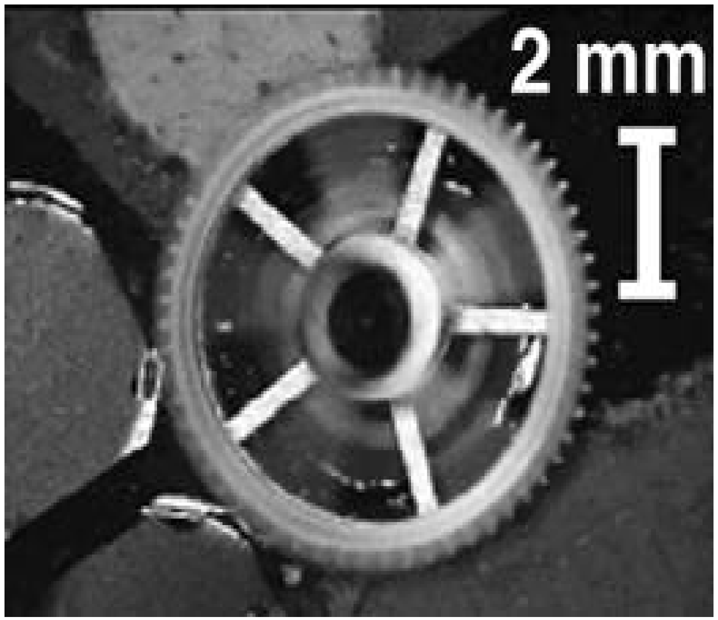

Piezoelectricity: Coupling between mechanical and electrical energies

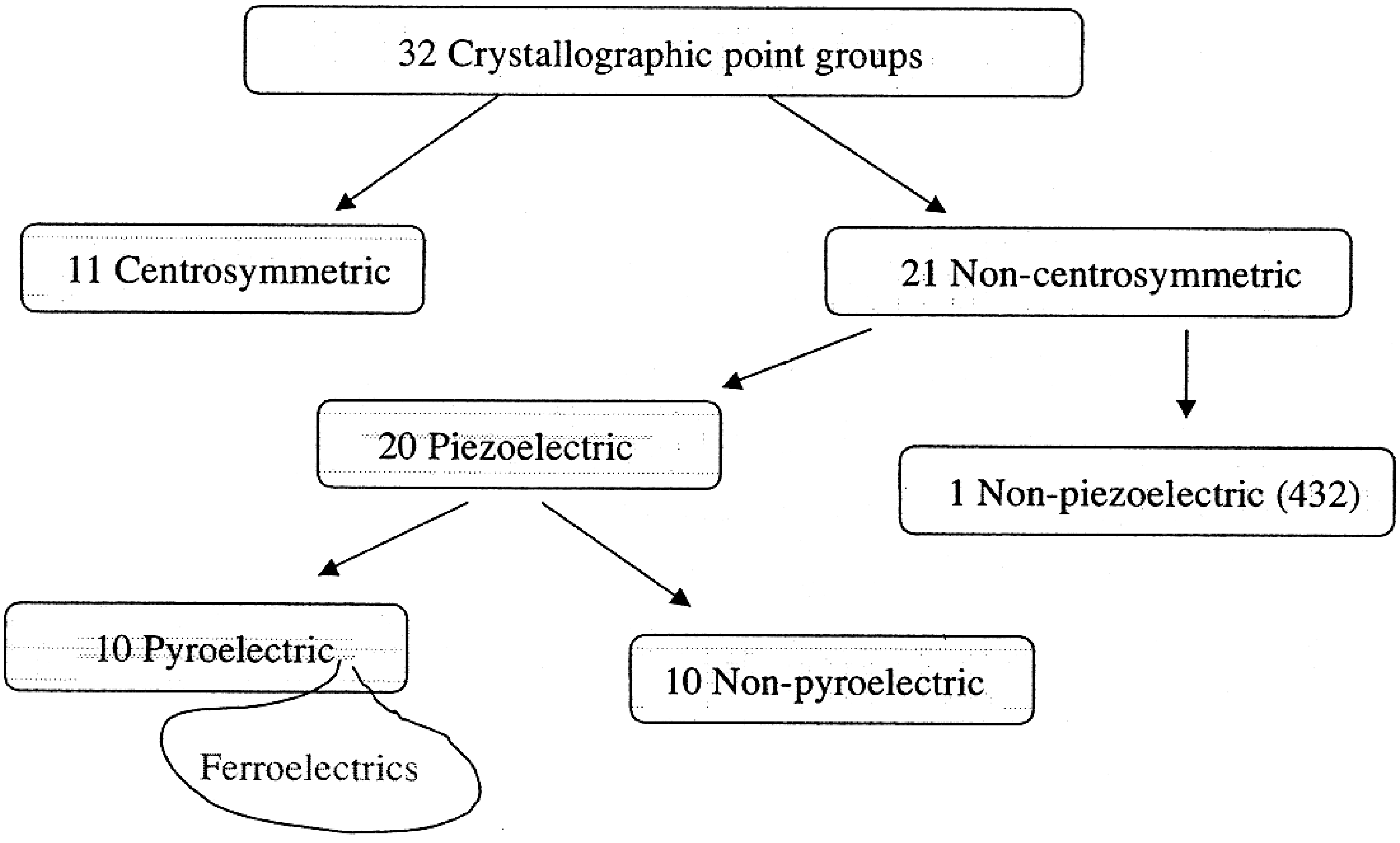

Direct piezoelectric effect:
Charge=d × force or
D=d × X (stress)

Converse piezoelectric effect:
Dispacement=d × Voltage or
x (strain)=d × E

or in general form

$$x_{ij} = \alpha_{ij}^{X,E} \Delta T + s_{ijkl}^{T,E} X_{kl} + d_{ijk}^{T,X} E_k$$

$$D_i = p_i^{X,E} \Delta T + d_{ikl}^{T,E} X_{kl} + \varepsilon_{ij}^{T,X} E_i$$

(X, E) independent variables
Other choices of independent variables are possible:
(X,D), (x, E), and (x, D)

Constitutive equations:

$$x_{ij} = s^{E}_{ijkl} X_{kl} + d^{X}_{ijk} E_k$$

$$D_i = d^{E}_{ikl} X_{kl} + \varepsilon^{X}_{ij} E_j$$

$$x = s^{D} X + g\, D$$

$$E = -g\, X + \beta^{X} D$$

$$X = c^{E} x - e\, E$$

$$D = e\, x + \varepsilon^{x} E$$

$$X = c^{D} x - h\, D$$

$$E = -h\, x + \beta^{x} D$$

$$d = \varepsilon^{X} g = e\, s^{E}$$

$$g = \beta^{X} d = h\, s^{D}$$

$$e = \varepsilon^{x} h = d\, c^{E}$$

$$h = \beta^{S} e = g\, c^{D}$$

Major piezoelectric coefficients

$d_{33}=(\Delta l/l)_{||}/E$ $d_{13}=(\Delta l/l)_{\perp}/E$ $d_{15}=(\Delta l/l)_{shear}/E$

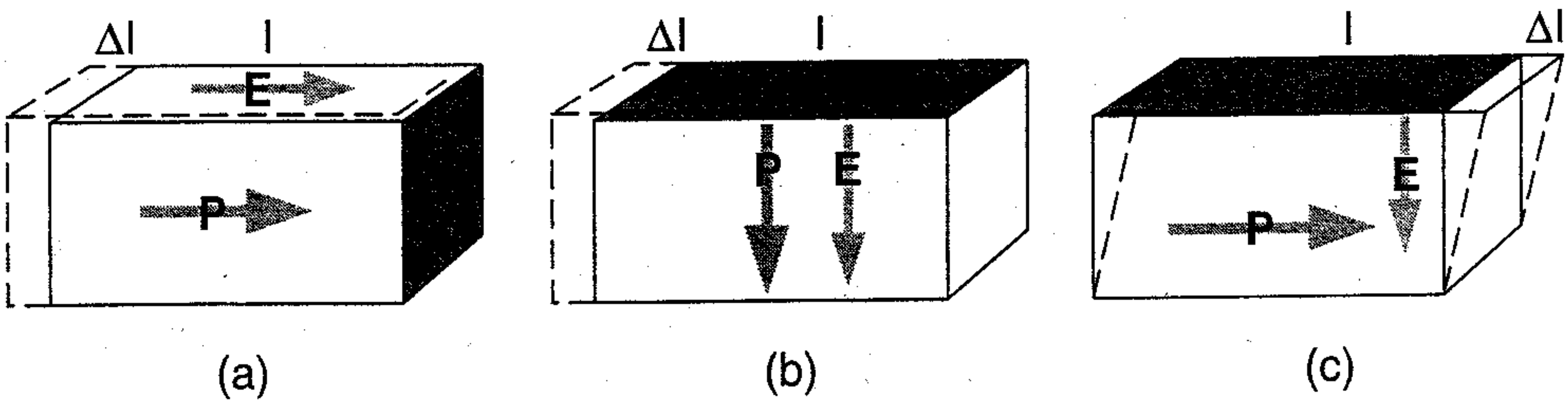

The choice of equations depends on boundary conditions:

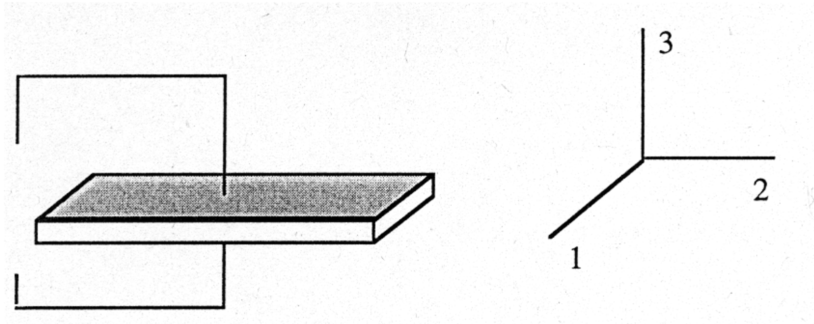

1D problem for a plate:

$E_1 = E_2 = 0$, $E_3 \neq 0$ but spatially constant → choose E as one independent variable.

$X_1 \neq 0$, $X_2 = X_3 = X_4 = X_5 = X_6 = 0$, → choose X as the other independent variable

$$x_1 = s_{11}^E X_1 + d_{31} E_3$$

$$D_3 = d_{31} X_1 + \varepsilon_{33}^X E_3$$

Clamping in thin films

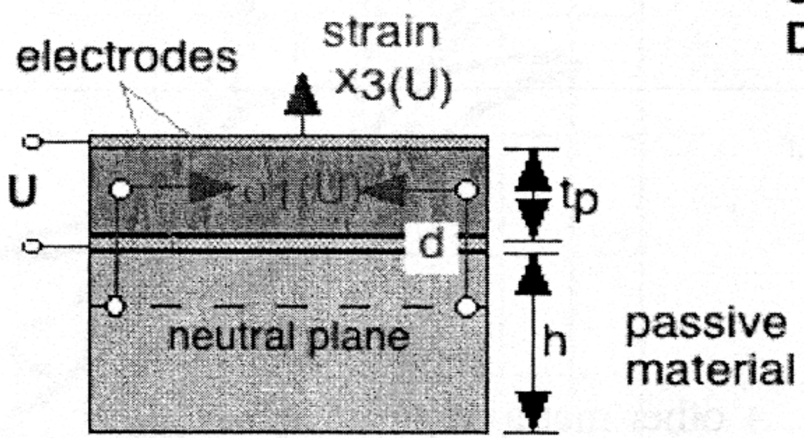

Converse effect

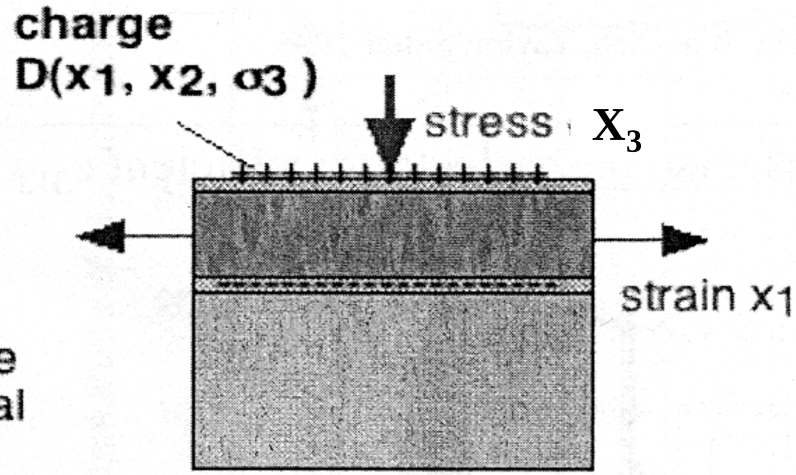

Direct effect

For ideal clamping (thin film on thick rigid substrate) the equations:

$$\frac{\sigma_1}{E_3} = \quad e_{31,f} = \frac{d_{31}}{s_{11}^E + s_{12}^E} = e_{31} - \frac{c_{13}^E}{c_{33}^E} e_{33} \qquad \left|e_{31,f}\right| > \left|e_{31}\right|$$

Muralt 1996

$$\frac{S_3}{E_3} = \quad d_{33,f} = \frac{e_{33}}{c_{33}^E} = d_{33} - \frac{2 s_{13}^E}{s_{11}^E + s_{12}^E} d_{31} \qquad < d_{33}$$

Royer & Kmetik 1992

$$\frac{D_3}{E_3} = \quad \varepsilon_{33,f} = \varepsilon_{33}^{\sigma} - \frac{2 d_{31}^2}{s_{11}^E + s_{12}^E}$$

Actuator:

$\sigma_{1,2} = -e_{31,f} * E_3$

$S_3 = d_{33,f} * E_3$

Sensor:

$D = e_{31,f} * (S_1 + S_2) + d_{33,f} * \sigma_3$

De-clamping in nanostructures

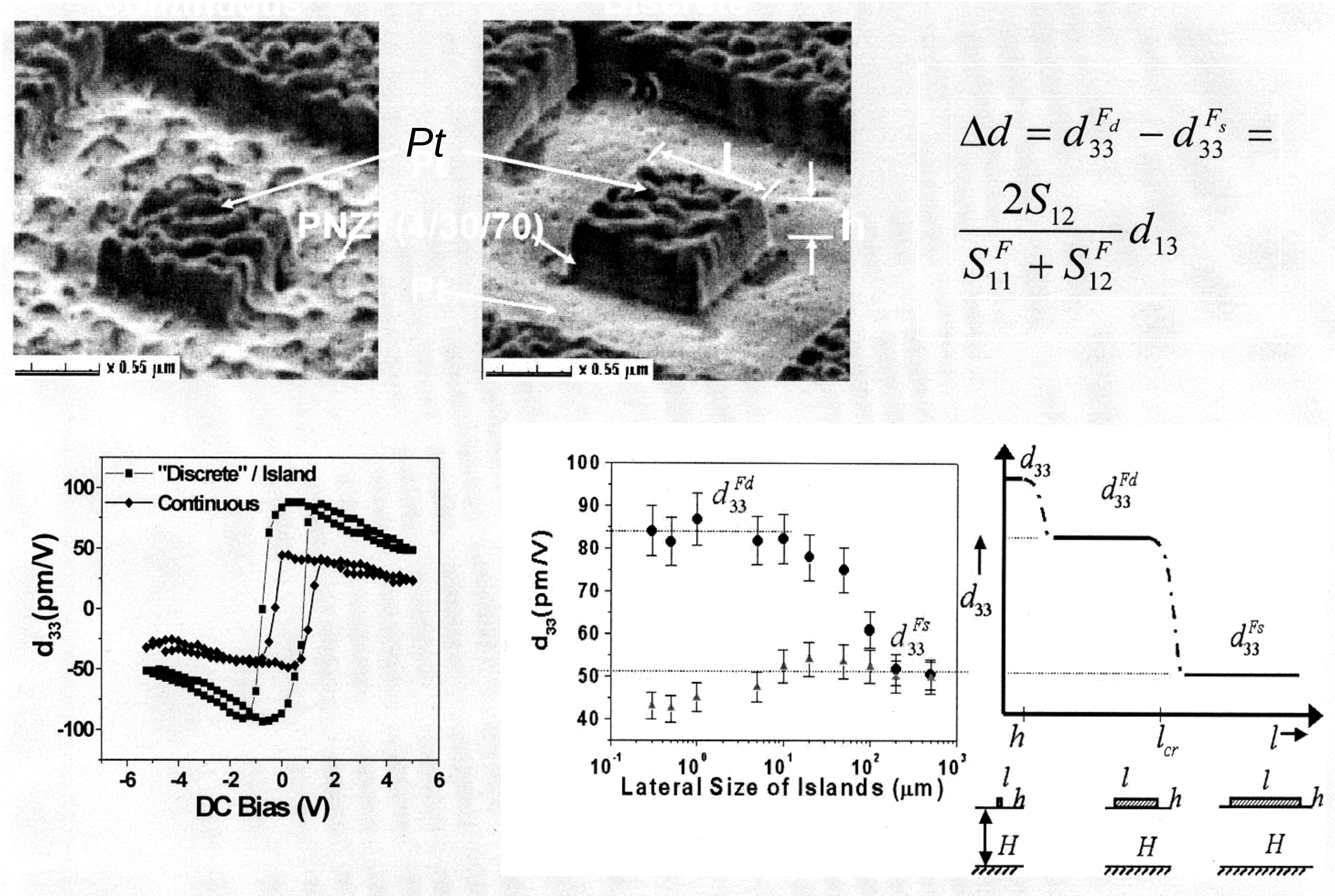

$$\Delta d = d_{33}^{F_d} - d_{33}^{F_s} = \frac{2S_{12}}{S_{11}^F + S_{12}^F} d_{13}$$

Nagaranjan et al. APL (2002)

Advantages of piezoelectric actuation

- High strain (up to 3-4 %)
- Unlimited resolution
- Rapid response (μs range)
- Good scalability
- High generative force
- Low power consumption
- Unlimited reliability
- *Problems with integration*

Giant strain in (001)-oriented $Pb(Zn,Nb)O_3$-8%PT

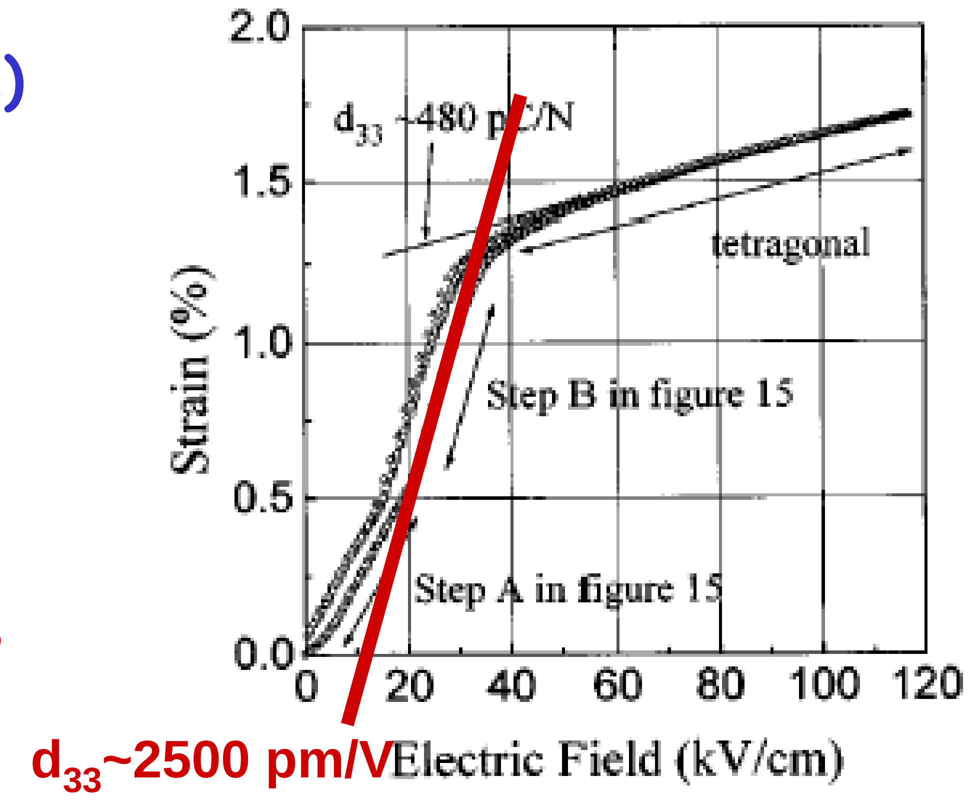

Park & Shrout, JAP (1997)

Examples of piezoelectric MEMS

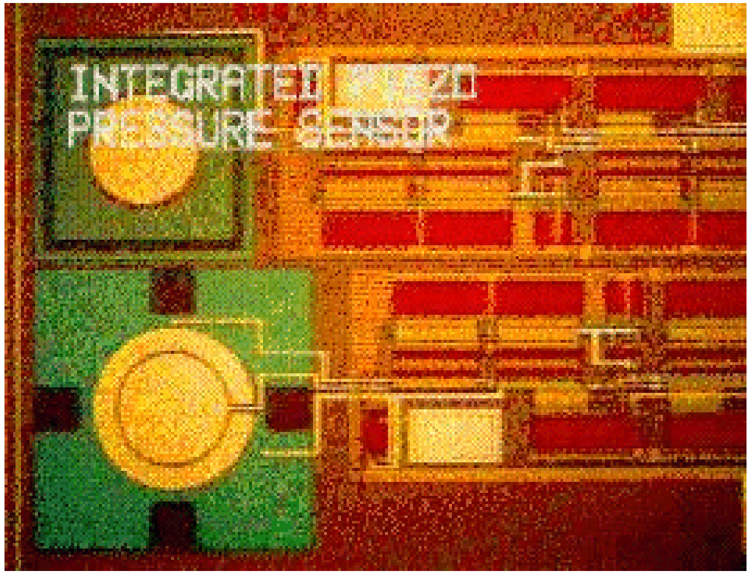

Acoustic pressure sensor
(U. of Minnesota)

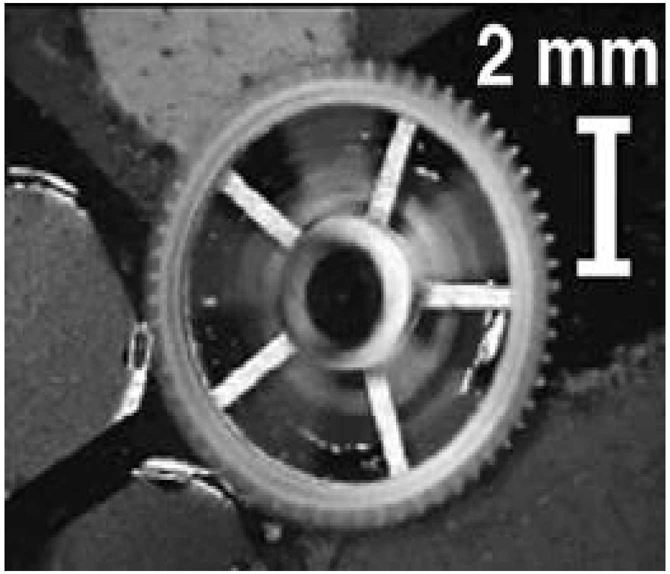

Piezoelectric micromotor
(EPFL, Switzerland)

Examples of piezoelectric MEMS (cont.)

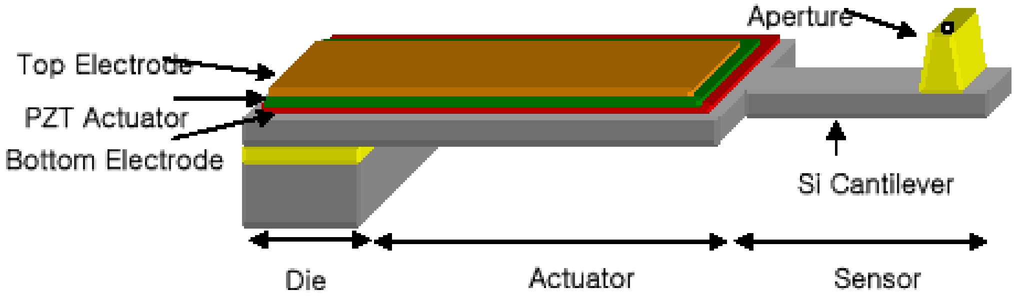

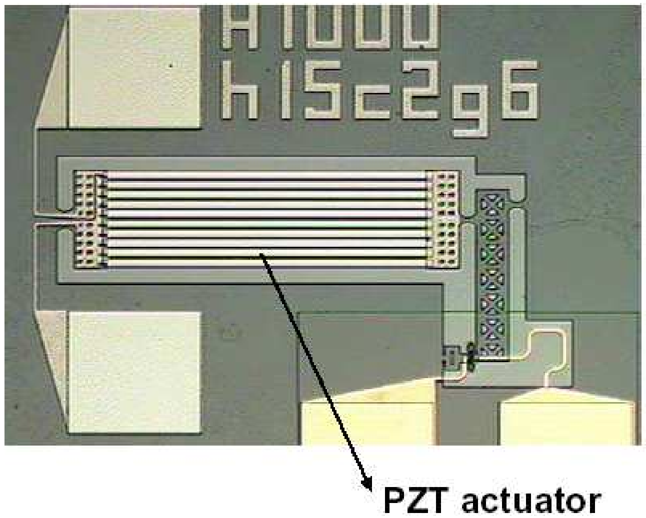

Piezo microswitch

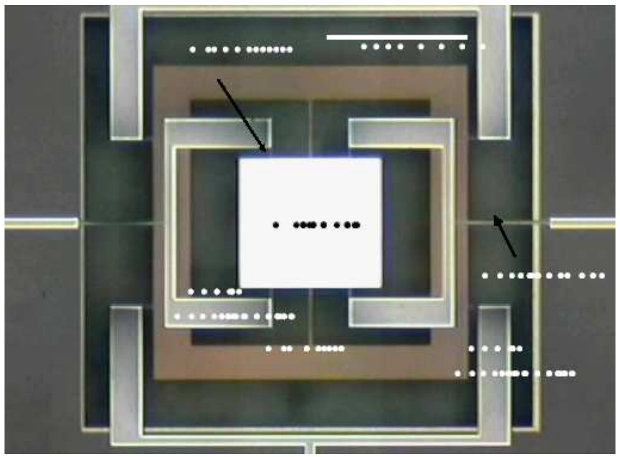

Tilting micromirror

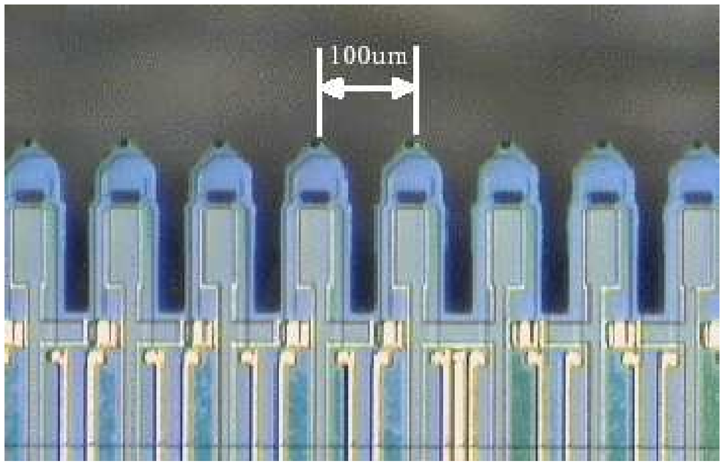

Cantilever array

Courtesy of Inostek, Inc. (S. Korea)

Examples of piezoelectric MEMS (cont.)

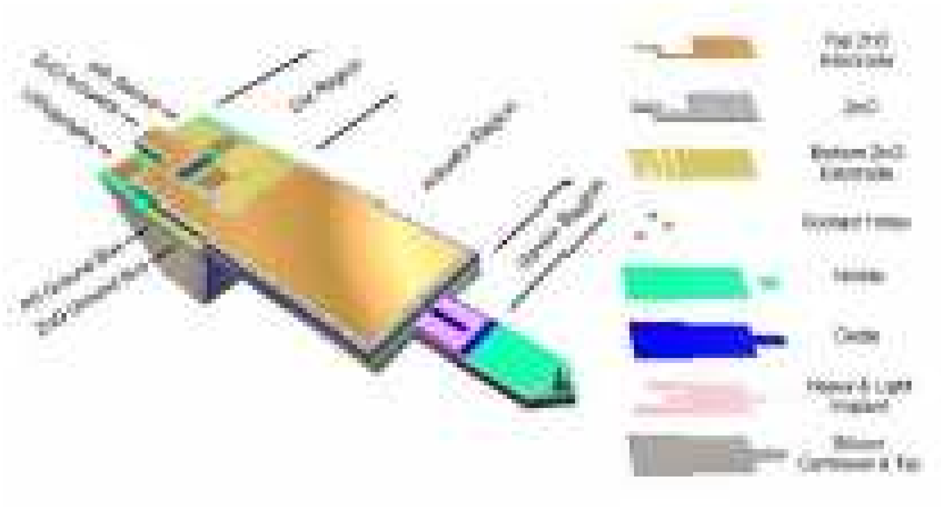

Sensor/actuator for AFM

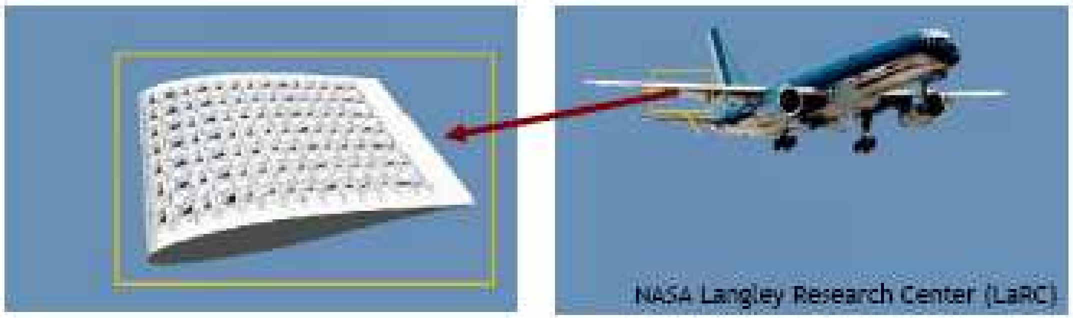

Smart wing for aircraft

Ferroelectric MEMS

• General features

- Small strains (1% max, 0.2%-0.5% more realistic)

Typically designs rely on "d_{31}" mode to increase strain:

diaphragms, bridges & cantilevers

-High sensitivity to stress (stress-compensating layers)

-Efficient electromecanical coupling (95% in some cases)

-Weak hysteresis (in some compositions)

-Excellent high-frequency potential

• Complicated processing

-two or more metal cations in compositions of interest (PZT, d_{33}= 250-600 pm/V))

-Typically contain Pb (need of lead-free materials)

-Oxidizing process atmospheres

Non-ferroelectric MEMS

• **Non-ferroelectric piezoelectric MEMS**

- ZnO $d_{33} \sim 4 \div 10$ pm/V (2 times larger than quarz)

- AlN $d_{33} \sim 2 \div 6$ pC/N (compatible with Si_3N_4)

-Modulation of *n* in ZnO-clad optical fiber

Much easier processing

-Relatively low-temperature growth

• **Comparatively small electromechanical response**

• **But must be deposited with specific crystallographic texture**

-i.e., piezoelectric axis normal to substrate

-*c*-oriented film for both ZnO and AlN

- **Advantages of FE MEMS**

-Potentially much larger piezoelectric response

- d_{33} values up to 2500 pm/V

-as deposited, FE films are NOT piezoelectric and poling

can produce piezoelectricity for any texture

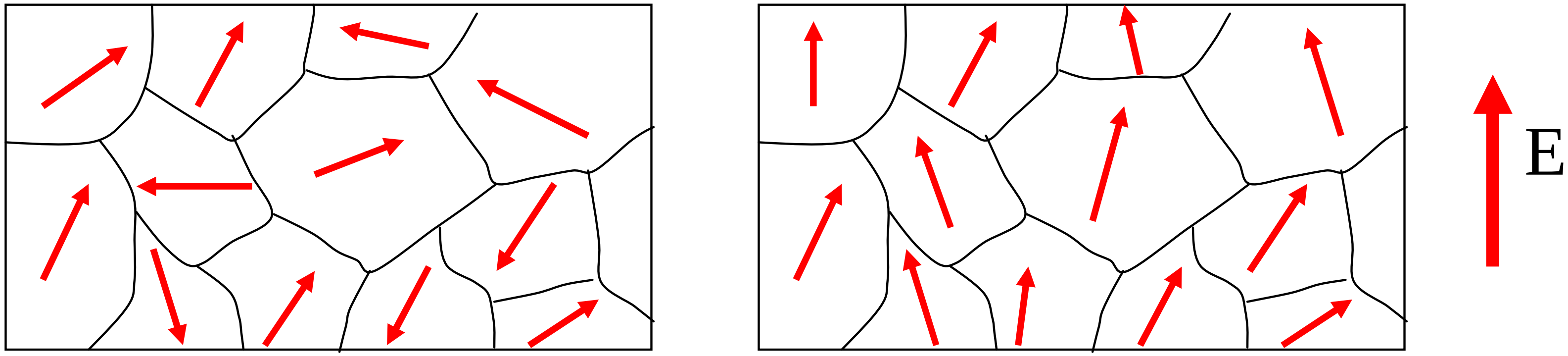

- No crystallographic texture required

- In some cases, random orientation gives best results

MEMS materials

• Same materials as in bulk ceramics

$Pb(Zr, Ti)O_3$ (PZT) solid solution – ferroelectric

$Pb(Mn_{1/3}Nb_{2/3})O_3$ – e lectrostrictors

Relaxor-$PbTiO_3$ solid solutions and new MPB systems

such as $BiScO_3$-$PbTiO_3$ (High T_c)

• Most research still on $Pb(Zr_xTi_{1-x})O_3$ solid solution

-x ~ 0.52 (morphotropic composition) ideal

-d_{33} coefficients approach now above 200 pm/V (unclamping)

•Non-lead containing compositions

-$BaTiO_3$, $(Sr_xBa_{1-x})NbO_3$, or $(K,Na)NbO_3$-based

- difficult to process

•Important observations

-bulk properties difficult to achieve in thin films

-scaling effects

- extrinsic vs. intrinsic contribution

Related issues

- Intrinsic contribution to piezoelectricity

$$d_{ijk} = 2Q_{ijkl}\varepsilon_0\varepsilon_{kl}P_l$$

large permittivity

large remanent polarization

- Extrinsic contribution to piezoelectricity

existence of non-180º domains

large spontaneous strain

multiple available domain variants

morphotropic compositions desirable

composition-induced symmetry transition

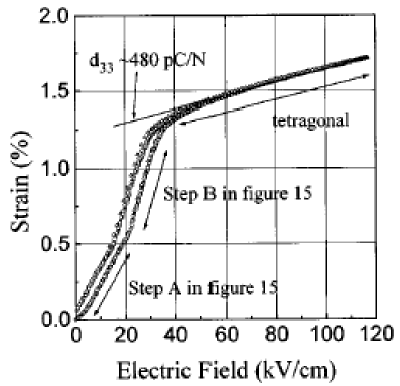

PZT vs. lead-free materials

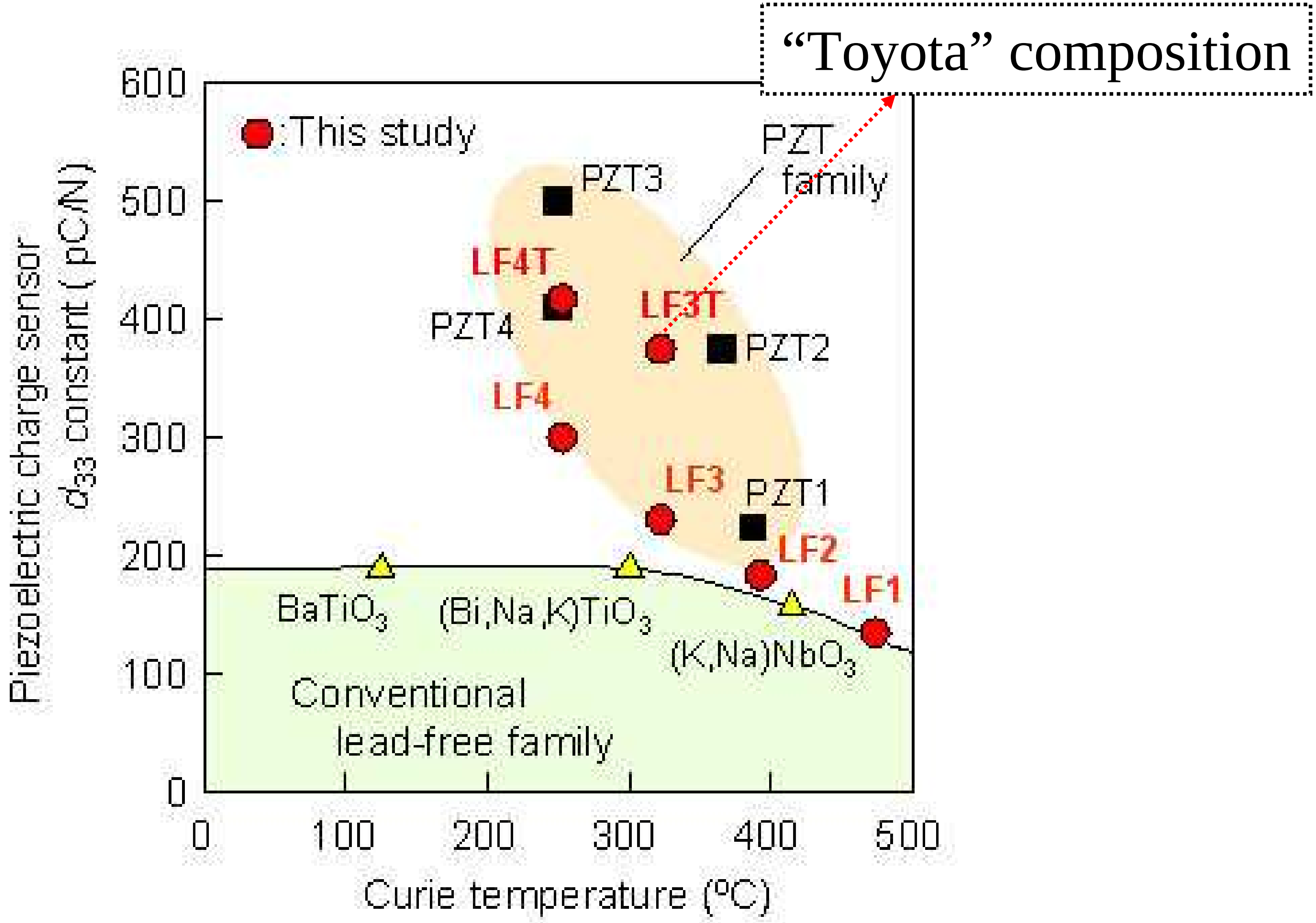

Y. Saito, et al. "Lead-free piezoceramics", *Nature*, **432**, Nov.4, 84-87 (2004).

Experimental evidence of domain wall contributions

Non-linearity

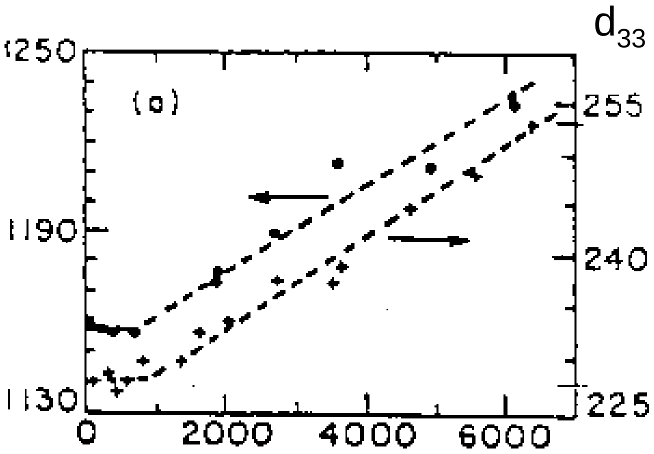

Q.M.Zhang et al, JAP **64**, 6445 (1988)

Temperature dependence of d_h

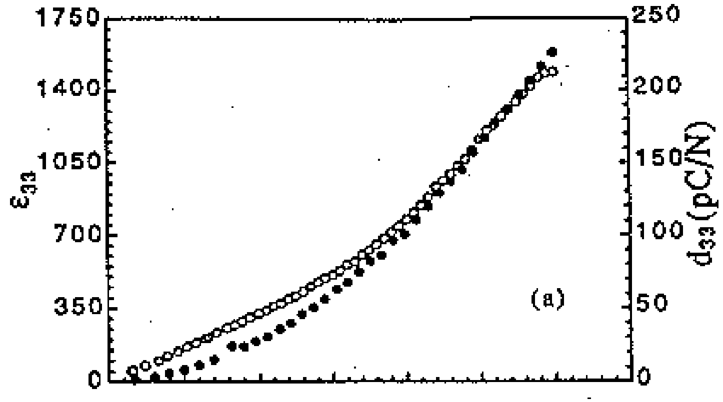

Q.M.Zhang et al, JAP **75**, 454 (1993)

Aging

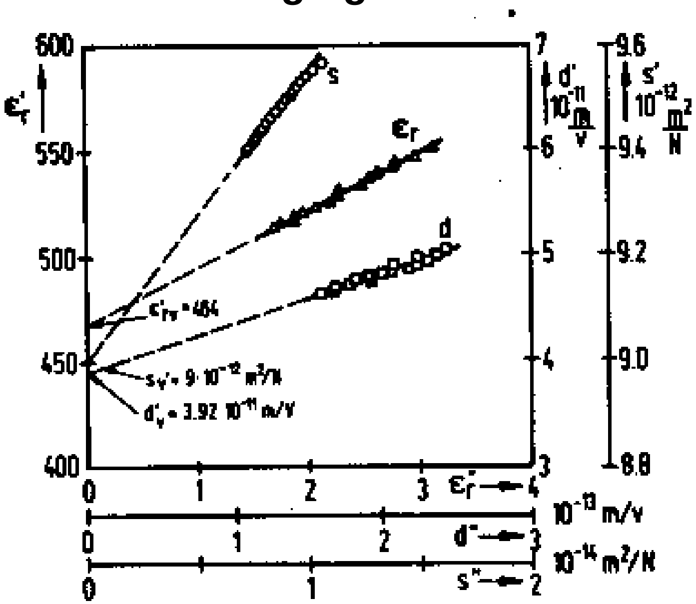

R.Herbiet et al, Ferroelectrics **76**, 319 (1987)

Theoretical predictions for extrinsic effect

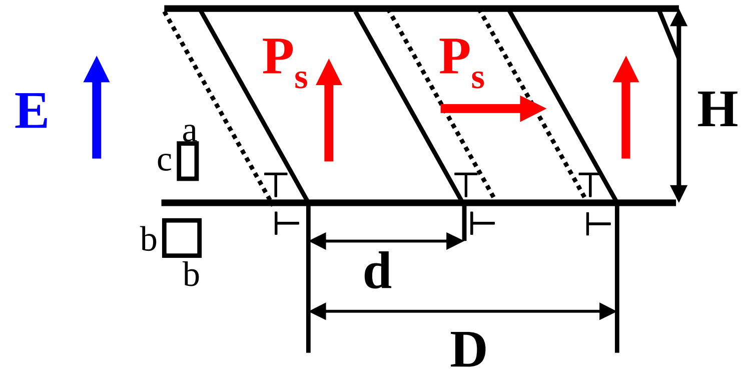

$$d_{ext} = 2\sqrt{2}(1-\frac{\nu}{1-\nu})(Q_{11}-Q_{12})\frac{P_s^3}{kD}$$

N. Pertsev & A. Emelyanov, APL (1997)

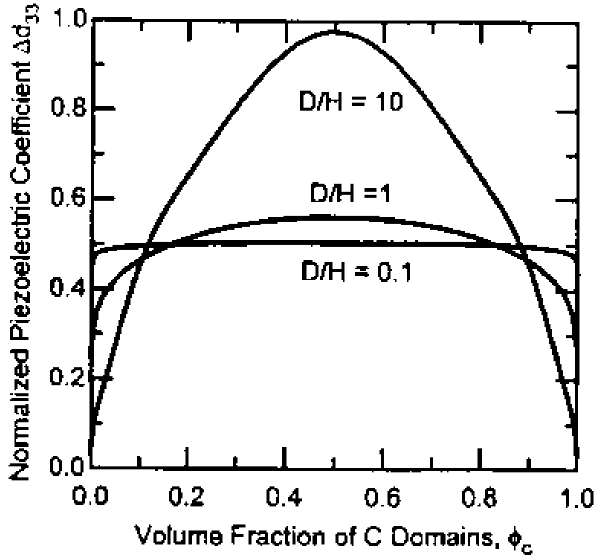

for D/H<<1

d_{ext}=70 pm/V $PbTiO_3$

d_{ext}=100 pm/V   PZT

Macroscopic characterization: laser interferometry

Michelson interferometer

- Vertical resolution – 0.003 Å
- Lateral resolution - 0.6 μm
- Frequency range <6 GHz

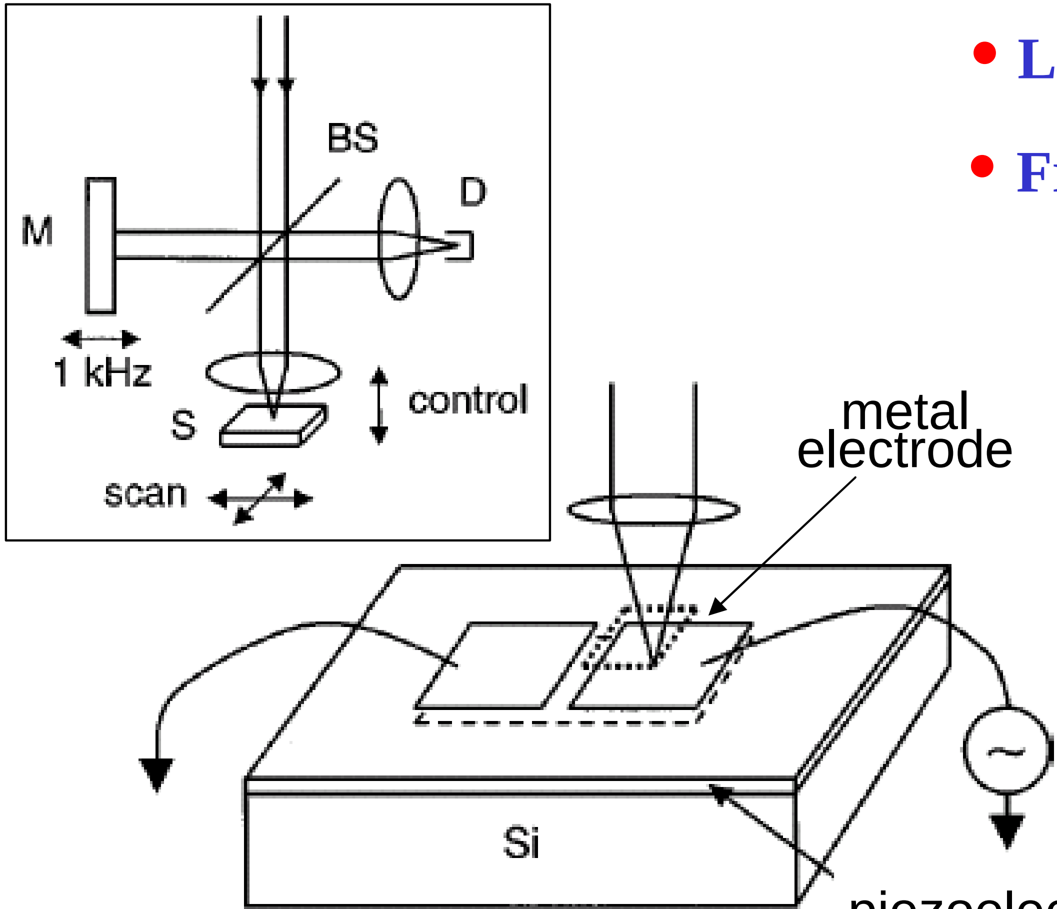

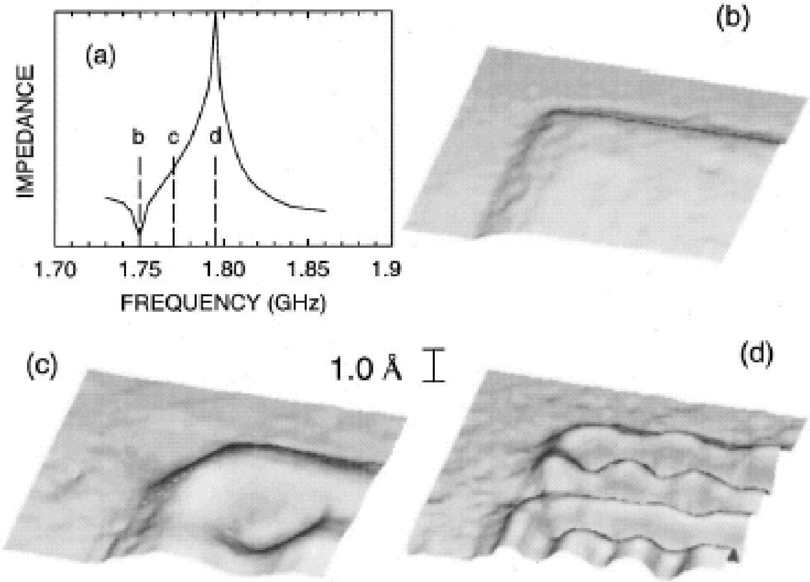

Kholkin et al Rev. Sci. Instr. **67** (1996)
Graebner et al. Appl. Phys. Lett. **78** (2001)

Piezoelectric measurements in thin films

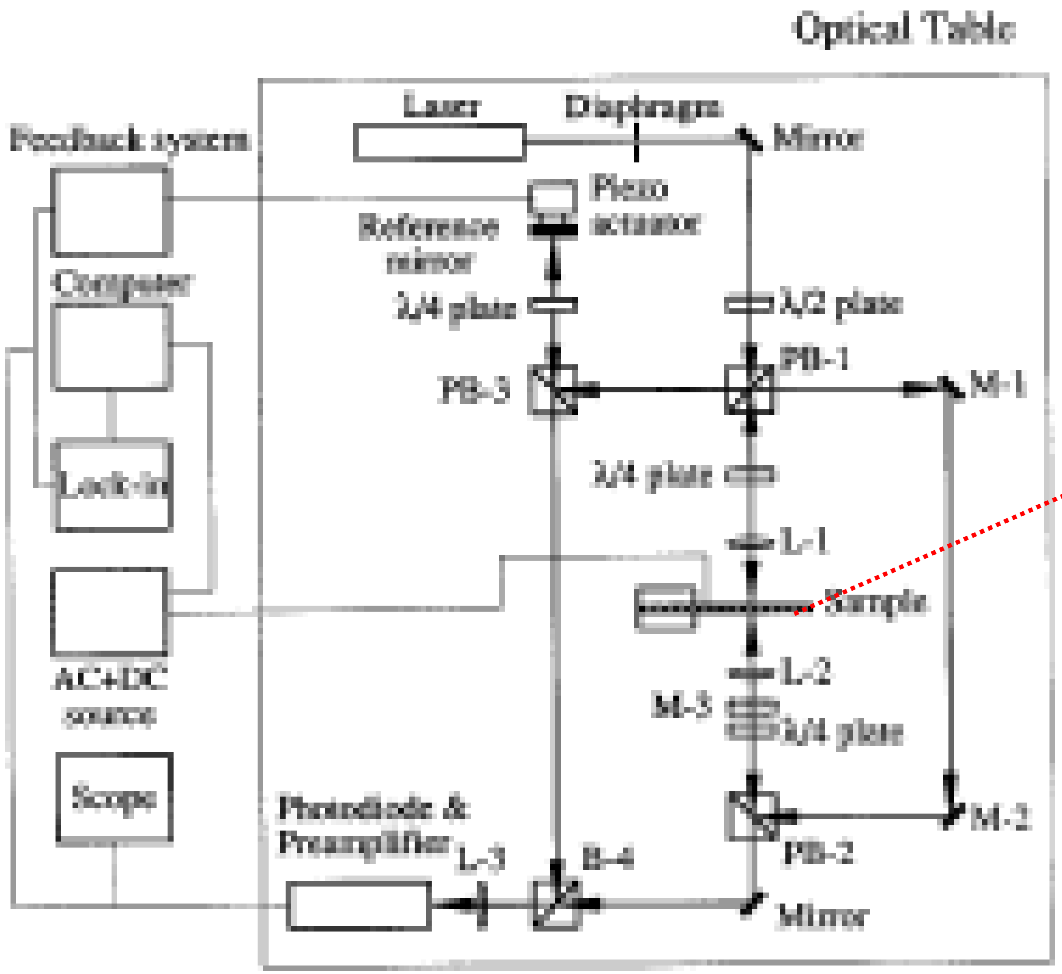

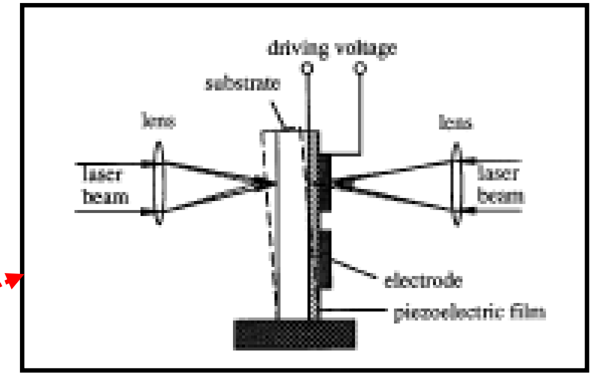

Kholkin et al., Rev. Sci. Instr. 1996

Simultaneous d_{33} and ε measurements

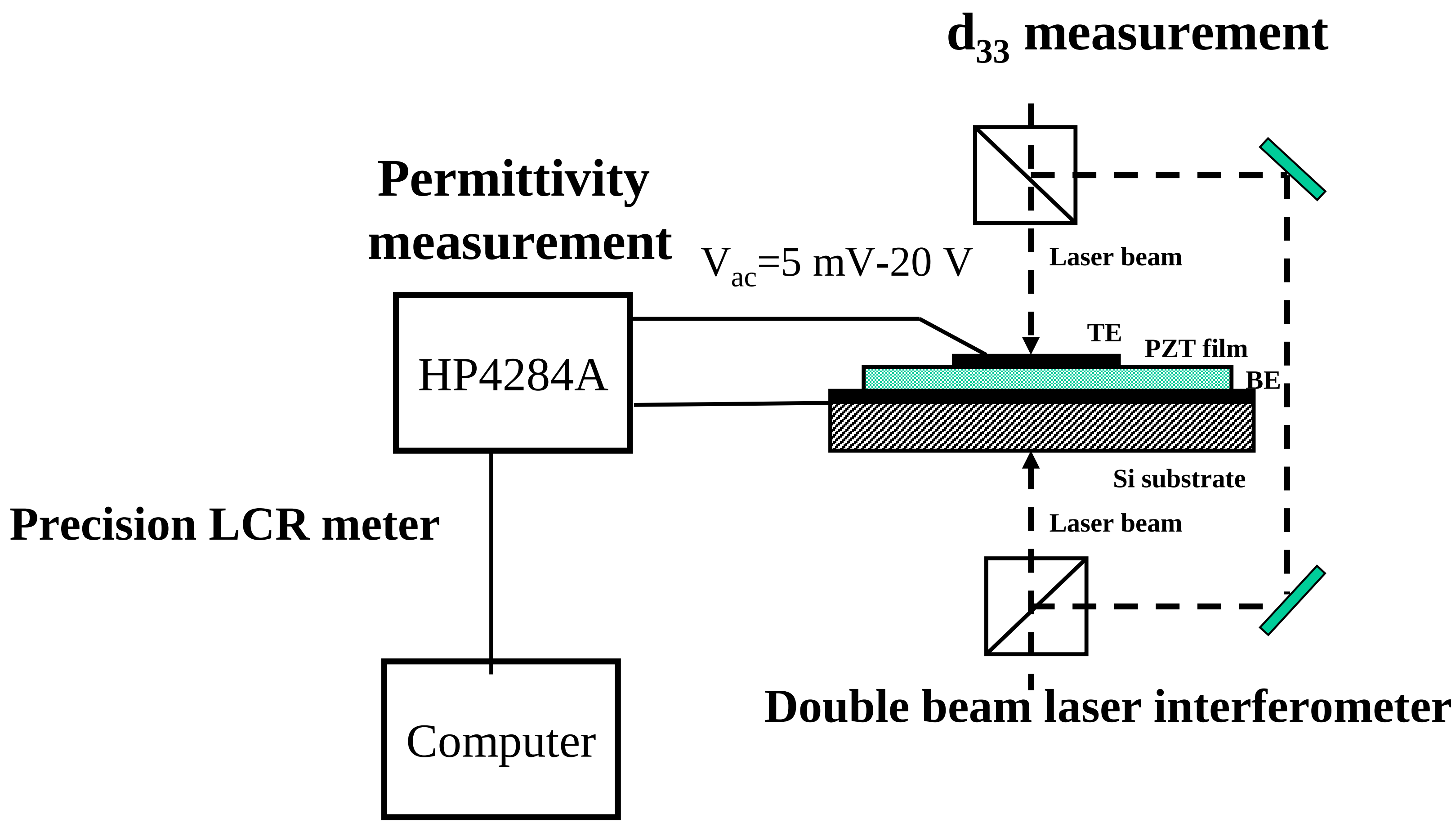

Substrate bending elimination

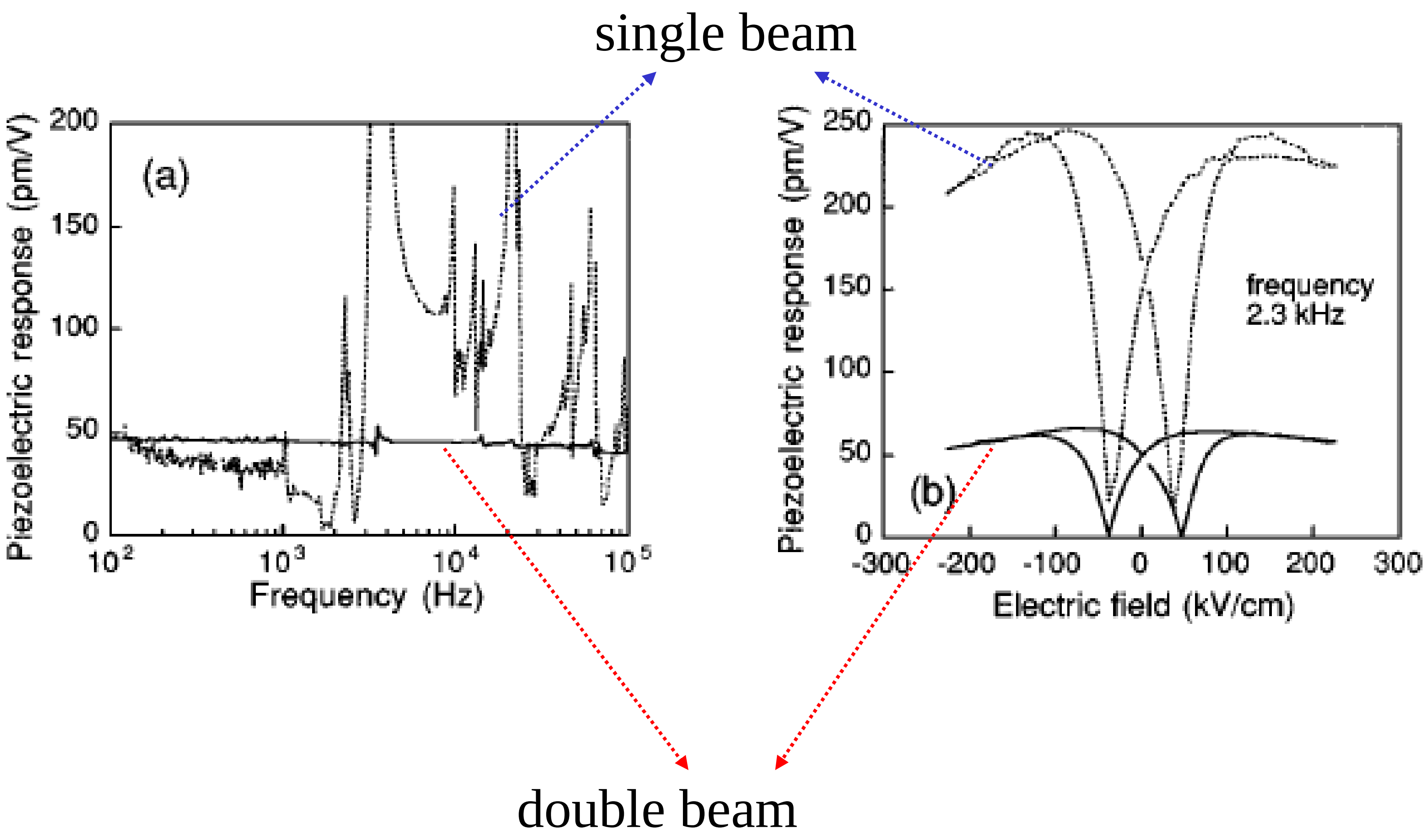

Double-beam laser interferometer

Key issues

- Single-mode laser with improved stability
- Short optical path
- Reduced environmental noise
- Active stabilization of the optical path length difference

Sensitivity

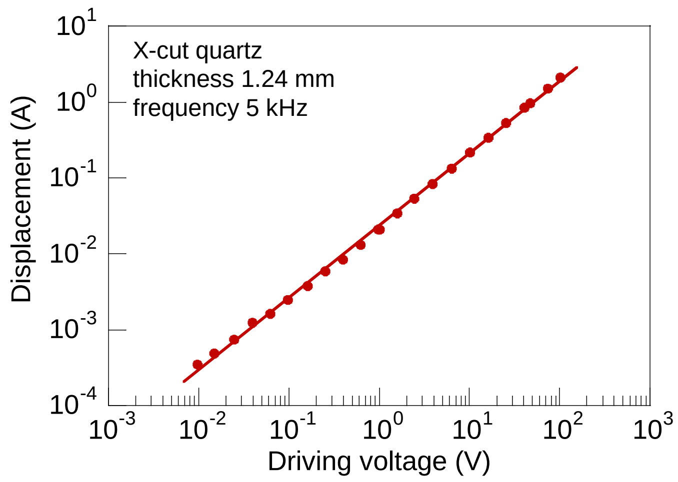

Stability

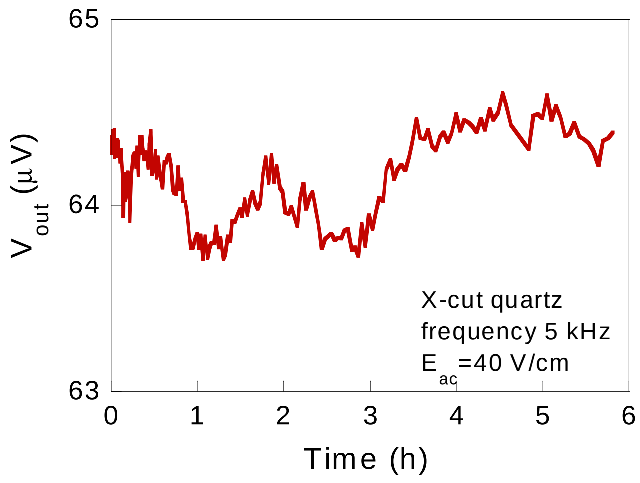

Bending in single-beam interferometer

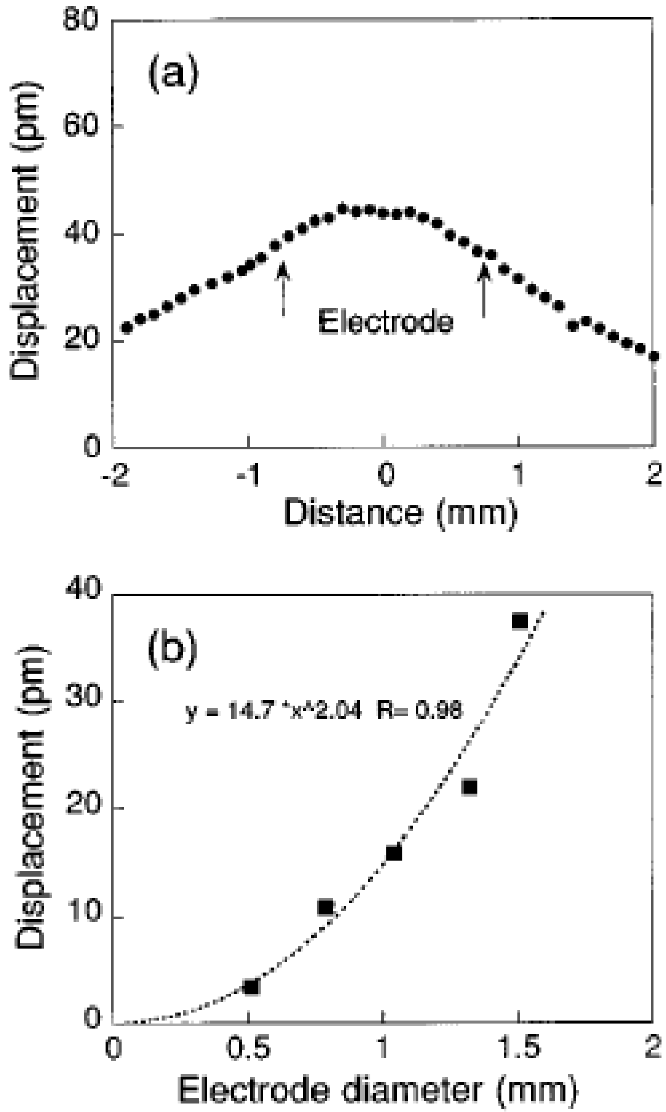

FIG. 2. (a) Deformation of the Si substrate induced by piezoelectric effect in the PZT film. Arrows indicate the edges of the top electrode. (b) Displacement of the top electrode as a function of the electrode diameter.

Typical values for PZT thin films

Reference	Effective d_{33}* (pm/V)	Meas. technique
K.F.Etzold et al. (1990)	8	converse effect
Z.Surowiak et al. (1992)	70-120	direct effect
K.Lefki and G.J.M. Dormans (1994)	400	direct effect
J.-F.Li et al. (1994)	140	converse effect
H.D.Chen et al. (1995)	196	converse effect
A.L.Kholkin et al. (1996)	40-110	converse effect
F.Xu et al. (1997)	150	direct effect

*PZT films of MPB composition and thickness ≤1 μm

For undoped PZT ceramics $\mathbf{d_{33} \approx 230}$ **pm/V**

Effect of the composition (sol-gel)

sol-gel PZT, thick. 0.3 µm, (111) orientation

poling curves

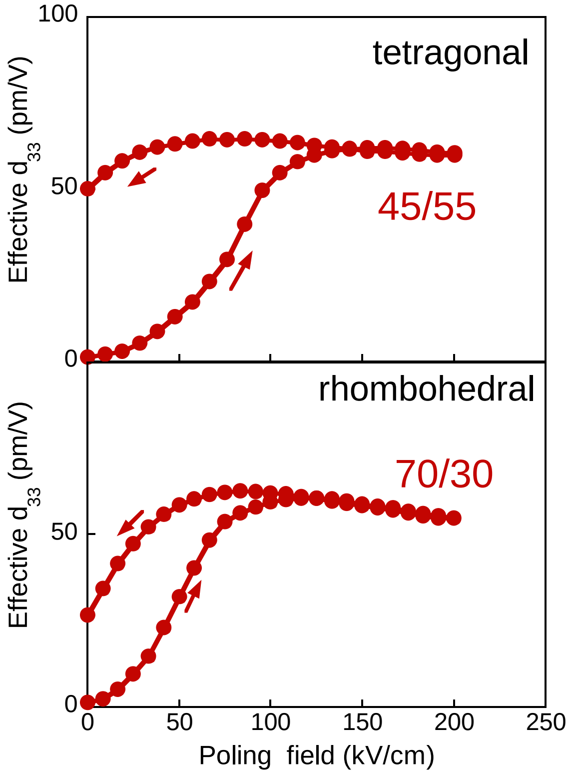

d_{33} as a function of composition

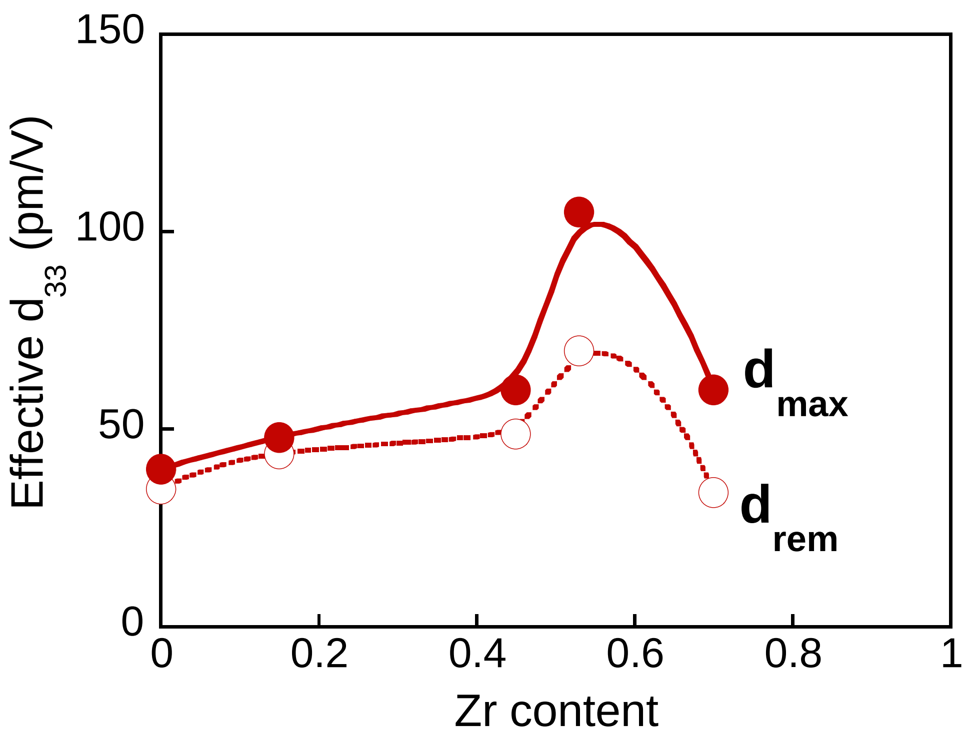

- significant depoling for MPB and rhombohedral compositions
- d_{33} for MPB composition is about half of the value for undoped PZT ceramics

Effect of the composition (sputtering)

sputtered PZT, thick. 0.3 µm, (111) orientation

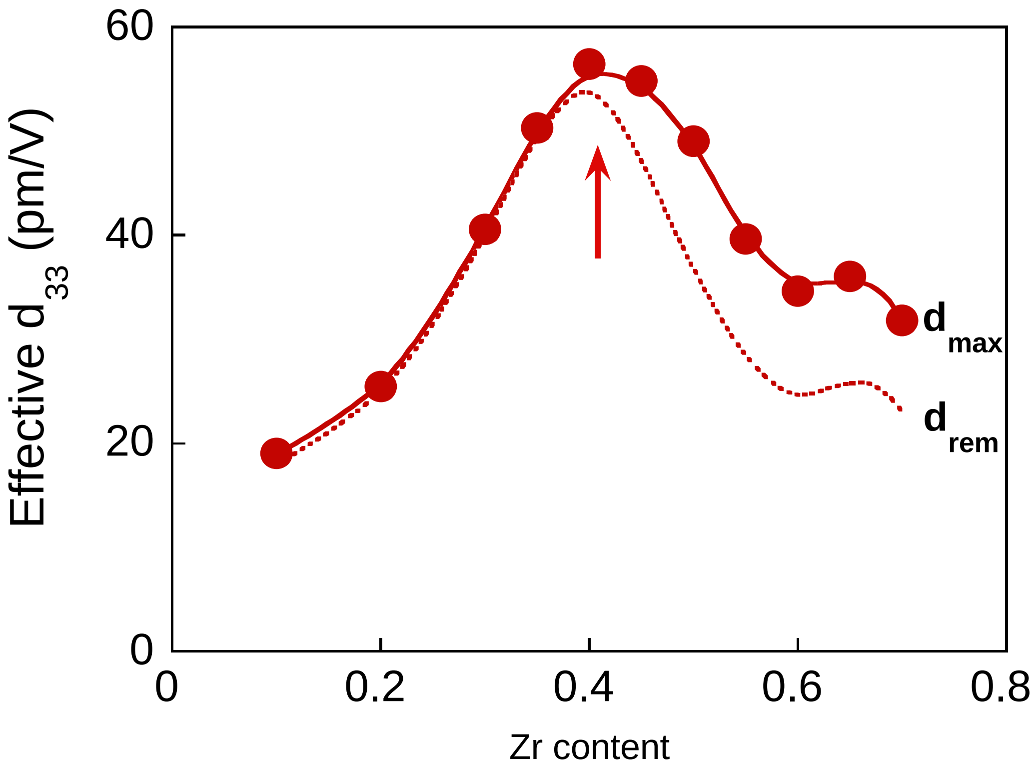

- In rhombohedral films non-180° domains may contribute to electromechanical strain under high ac-field

Intrinsic vs. Extrinsic effect

Linearized electrostriction equation

$$d_{33}=2Q_{11}\varepsilon_o\,\varepsilon\,P_r$$

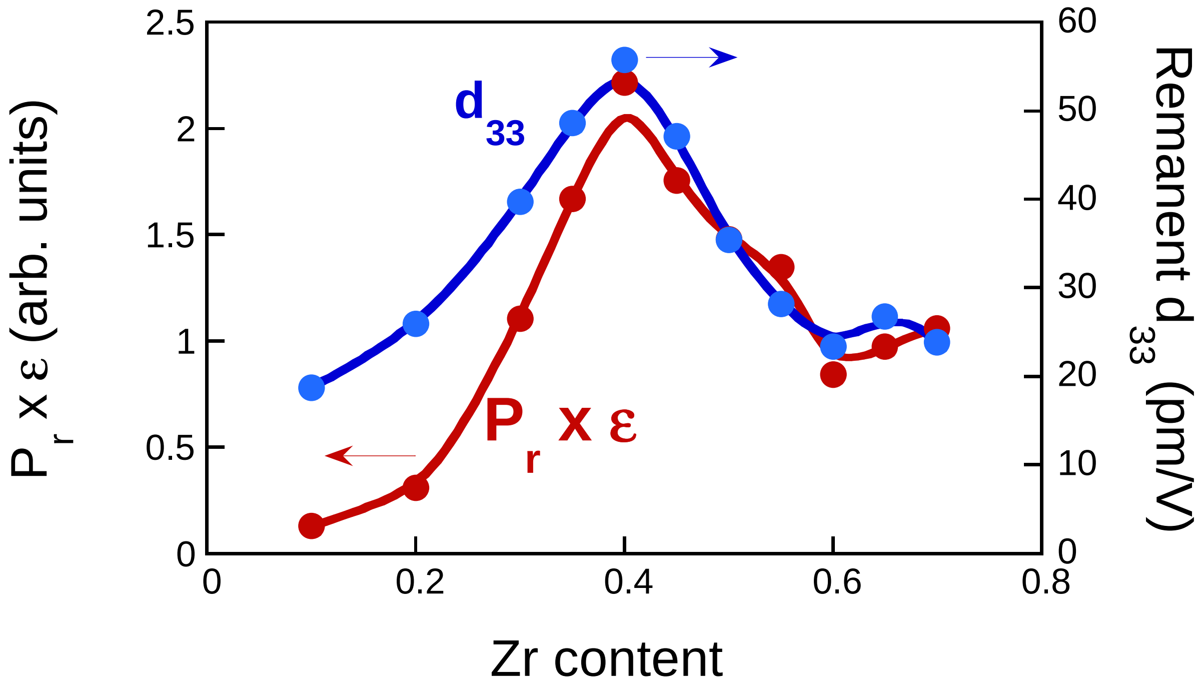

- $Q \approx 0.015\text{-}0.02\ m^4/C^2$ for rhombohedral compositions
- d_{33} is relatively high in tetragonal films due to non-switchable self-polarization

Effect of orientation

tetragonal (45/55)

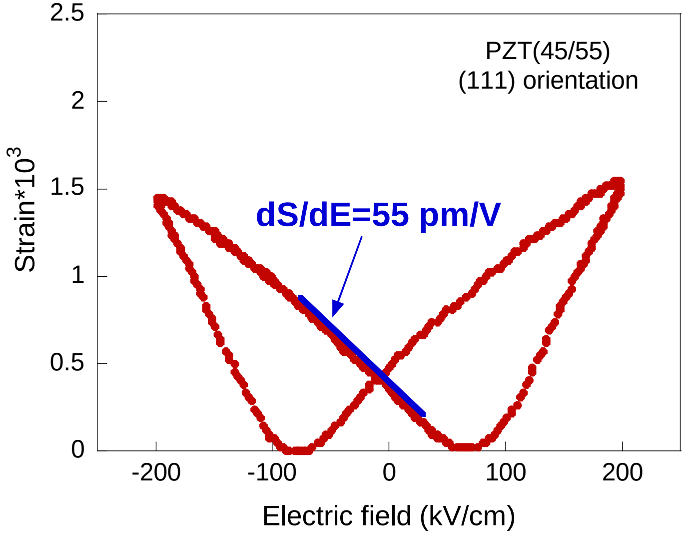

dS/dE≈d_{33}

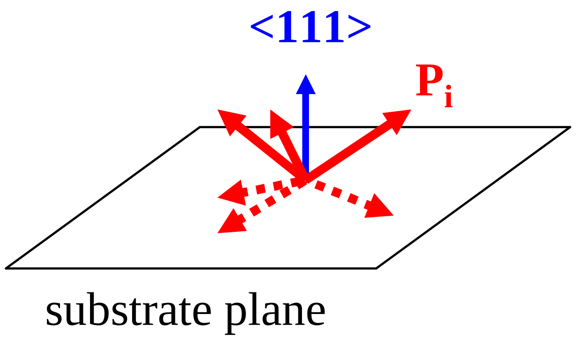

rhombohedral (70/30)

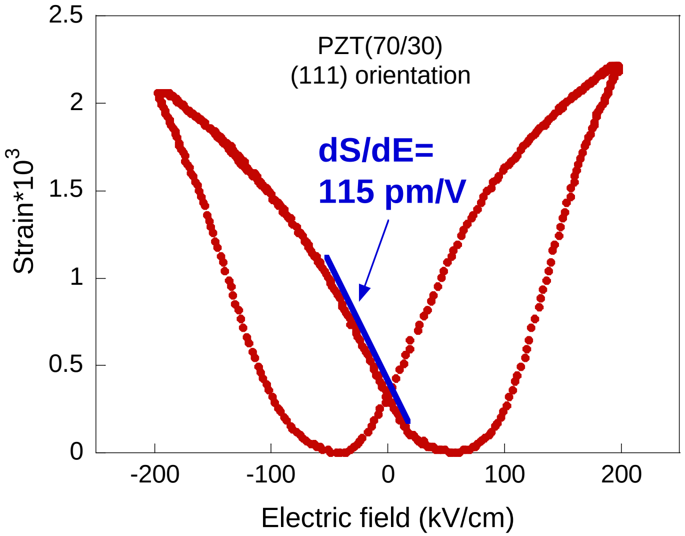

dS/dE>>d_{33}

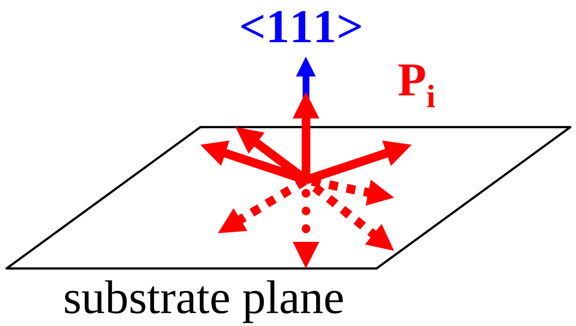

Piezoelectric non-linearity

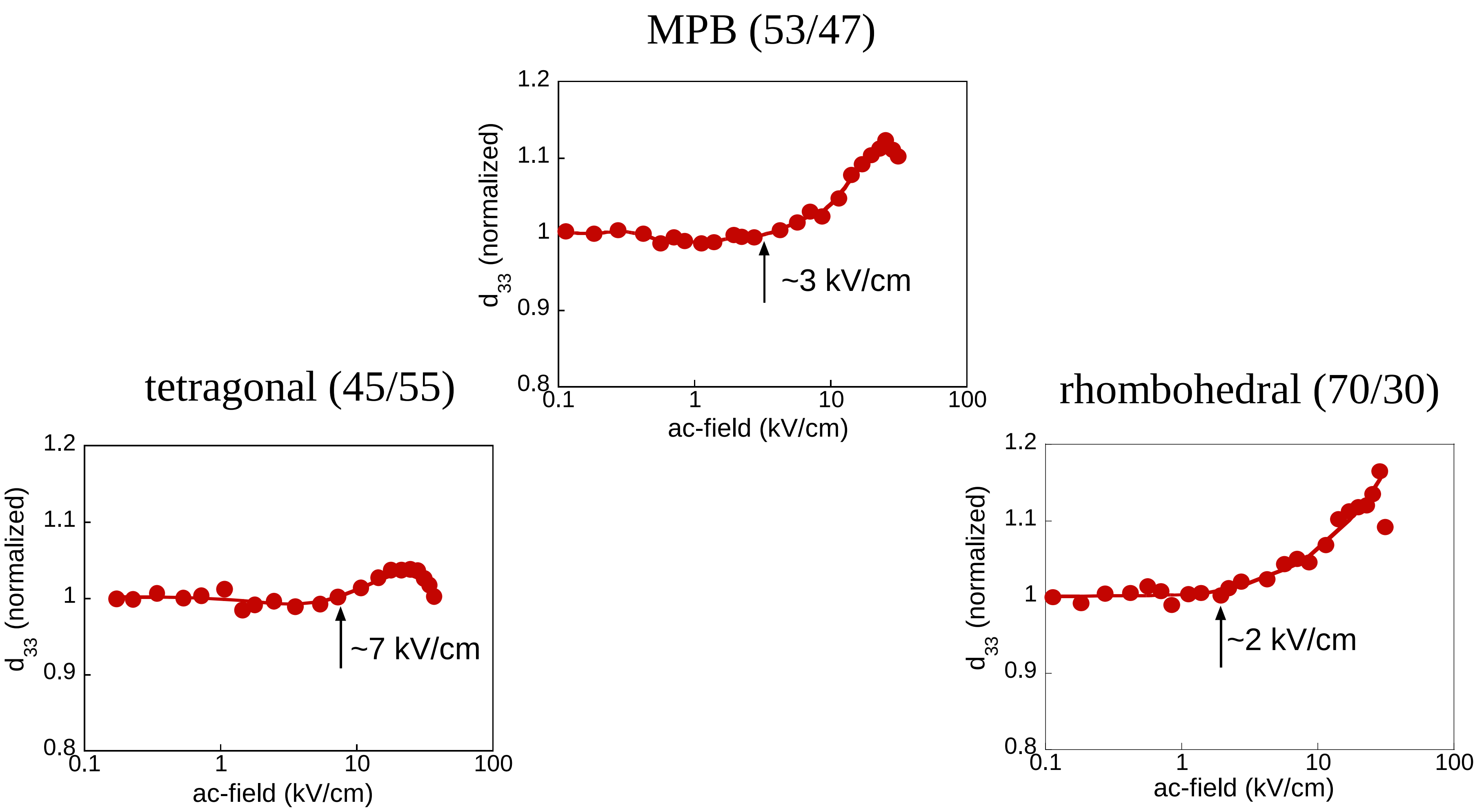

- 90° domains are almost inactive in tetragonal films
- domain wall contribution is evident in MPB and rhombohedral films

Effect of orientation

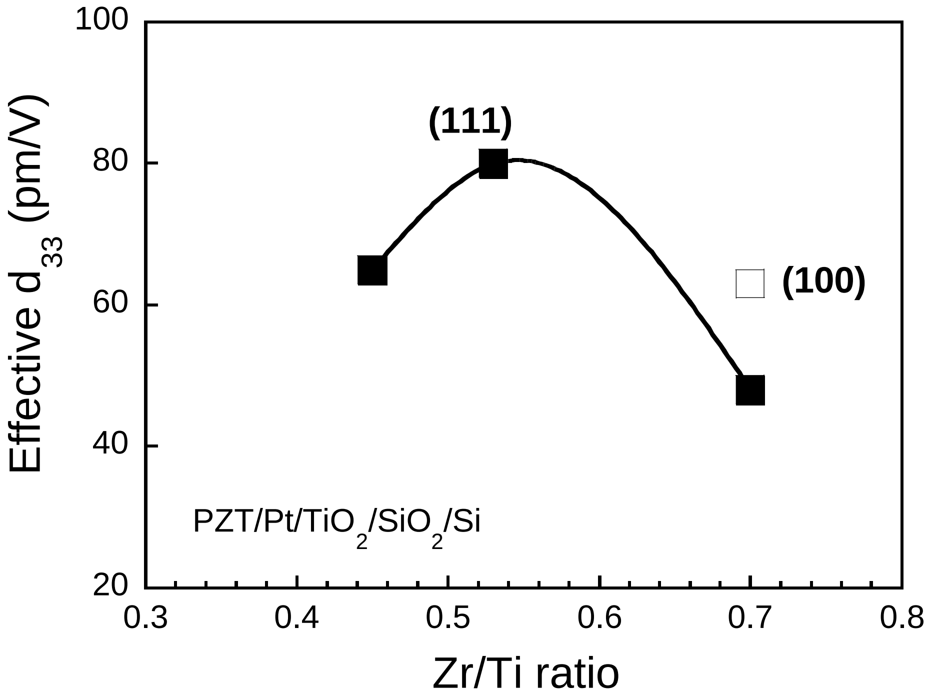

Comparison with calculations

<u>Tetragonal composition</u>

$$d_{31} = d_{32} = 2\varepsilon_o \varepsilon_{33} Q_{12} P_3$$
$$d_{33} = 2\varepsilon_o \varepsilon_{33} Q_{11} P_3$$
$$d_{15} = d_{24} = 2\varepsilon_o \varepsilon_{11} Q_{44} P_3$$

<u>Rhombohedral composition</u>

$$d_{11} = d_{22} = d_{33} = 2\varepsilon_o (\varepsilon_{33} Q_{11} + 2Q_{12}\varepsilon_{12}) P_3$$
$$d_{12} = d_{13} = d_{23} = 2\varepsilon_o [\varepsilon_{11} Q_{12} + \varepsilon_{12}(Q_{11} + Q_{12})] P_3$$
$$d_{14} = d_{25} = d_{36} = 2\varepsilon_o \varepsilon_{12} Q_{44} P_3$$
$$d_{15} = d_{16} = d_{24} = d_{26} = d_{34} = d_{35} = \varepsilon_o (\varepsilon_{11} + \varepsilon_{12}) Q_{44} P_3$$

*All thermodynamical coefficents are taken from Haun et al., Ferroelectrics **99,** 63 (1989)

Symmetry	Composition	Orientation	d_{33}(free)	d_{33}(clamped)	α	d_{33}(exp)
tetragonal	45/55	[111]	161	**58**	0.64	**62**
rhombohedral	70/30	[111]	63	**47**	0.25	**60**
		[001]	107	71	0.34	78
		[011]	88	42	0.52	—

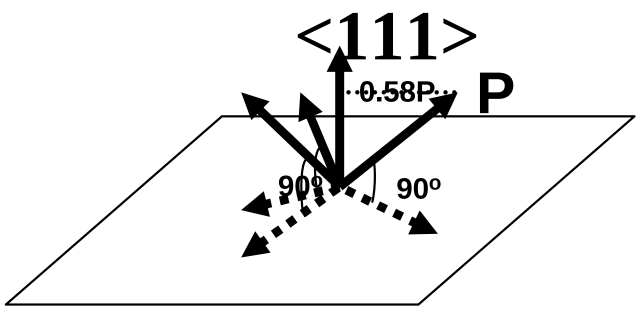

Dielectric vs. Piezoelectric nonlinearity

tetragonal (45/55)
<111> orientation

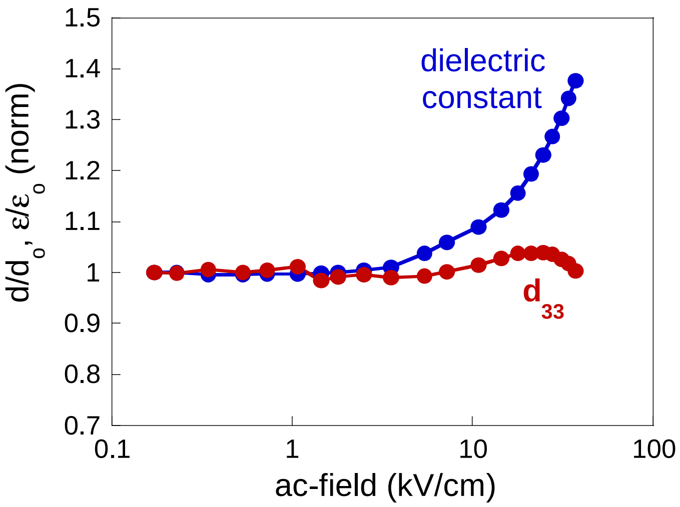

90° domains contribute
only to dielectric constant

MPB (53/47)
random orientation

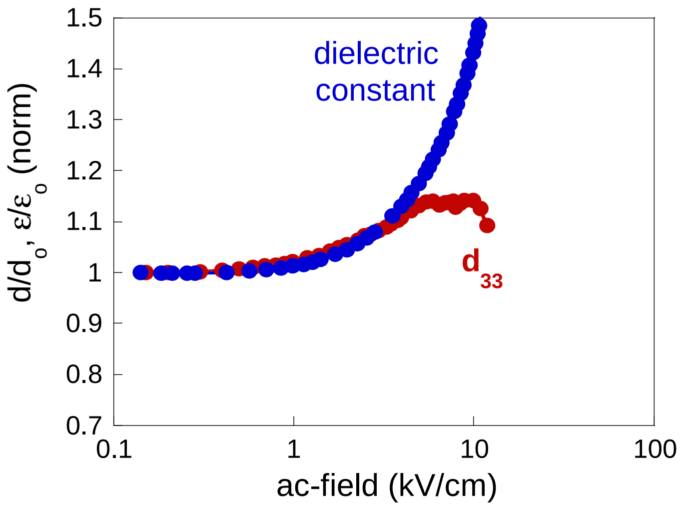

non 180° domains contribute
to both dielectric constant and d_{33}

Evidence of domain wall contribution

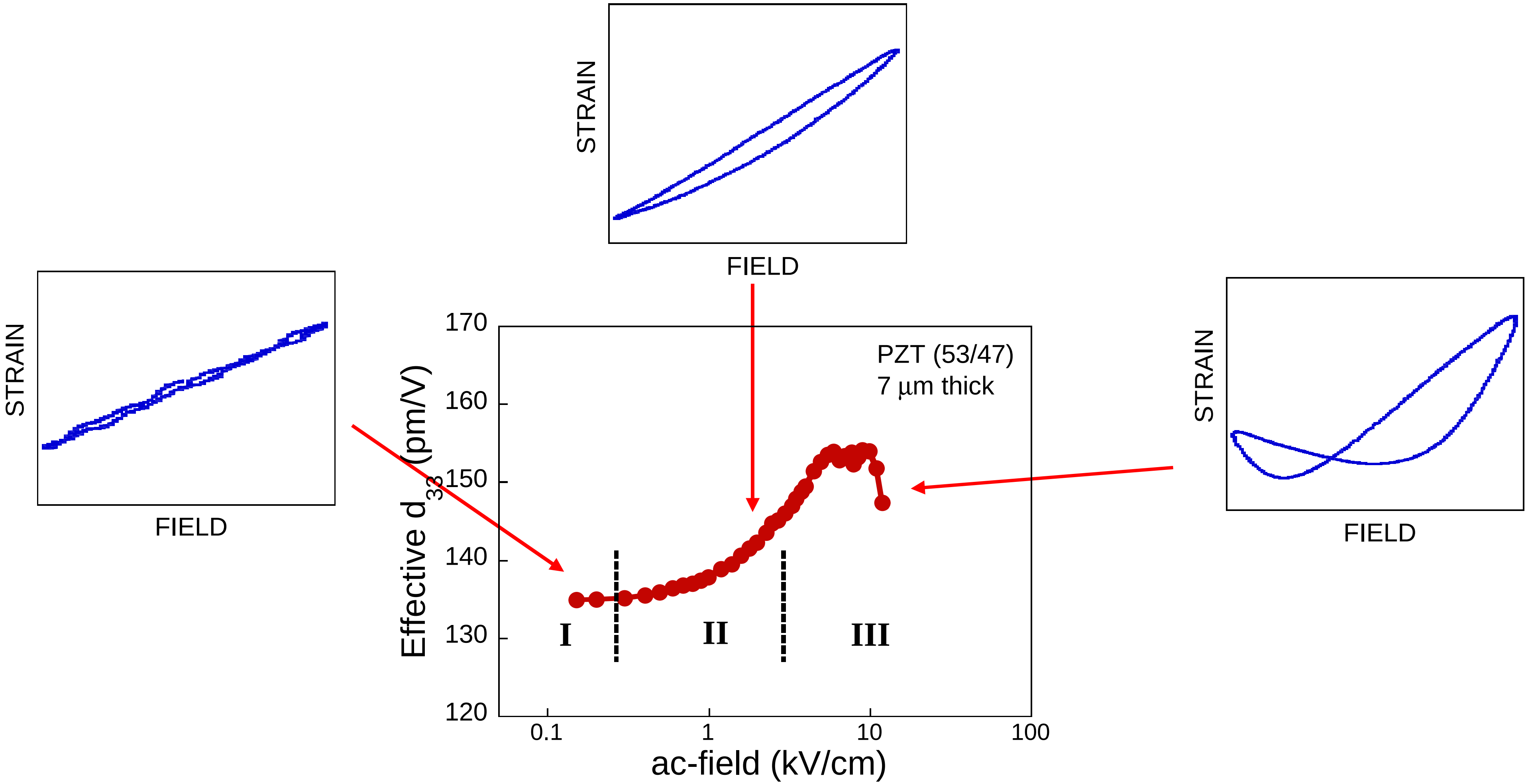

I - reversible domain wall motion
II - irreversible domain motion
III - depoling and switching

Bulk ceramics vs. thin/thick films

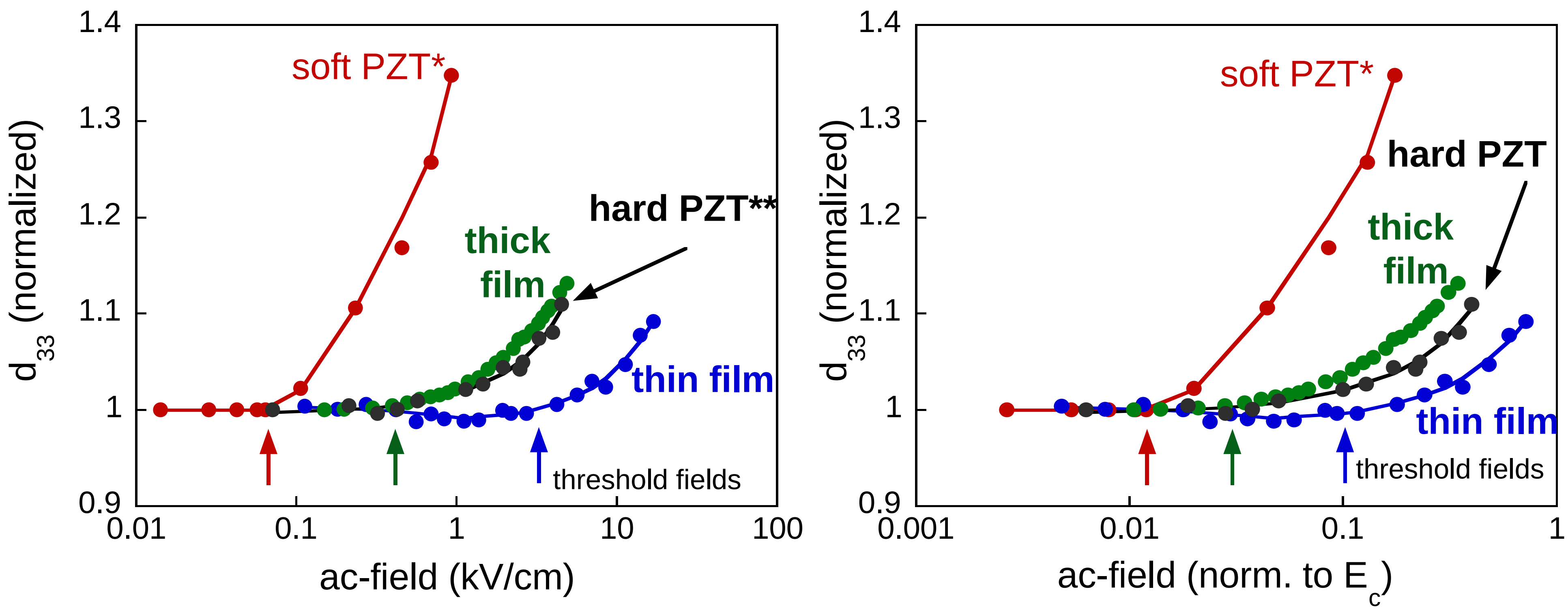

*Q.M.Zhang et al. JAP **64**, 6445 (1988), **V.Mueller and Q.M.Zhang, JAP **83**, 3754 (1998)

- non-linear piezoelectric properties are similar in thick films and hard PZT
- threshold field for irreversible domain wall motion is very high in thin films (≈0.1E_c)

Non-linearity in thick films

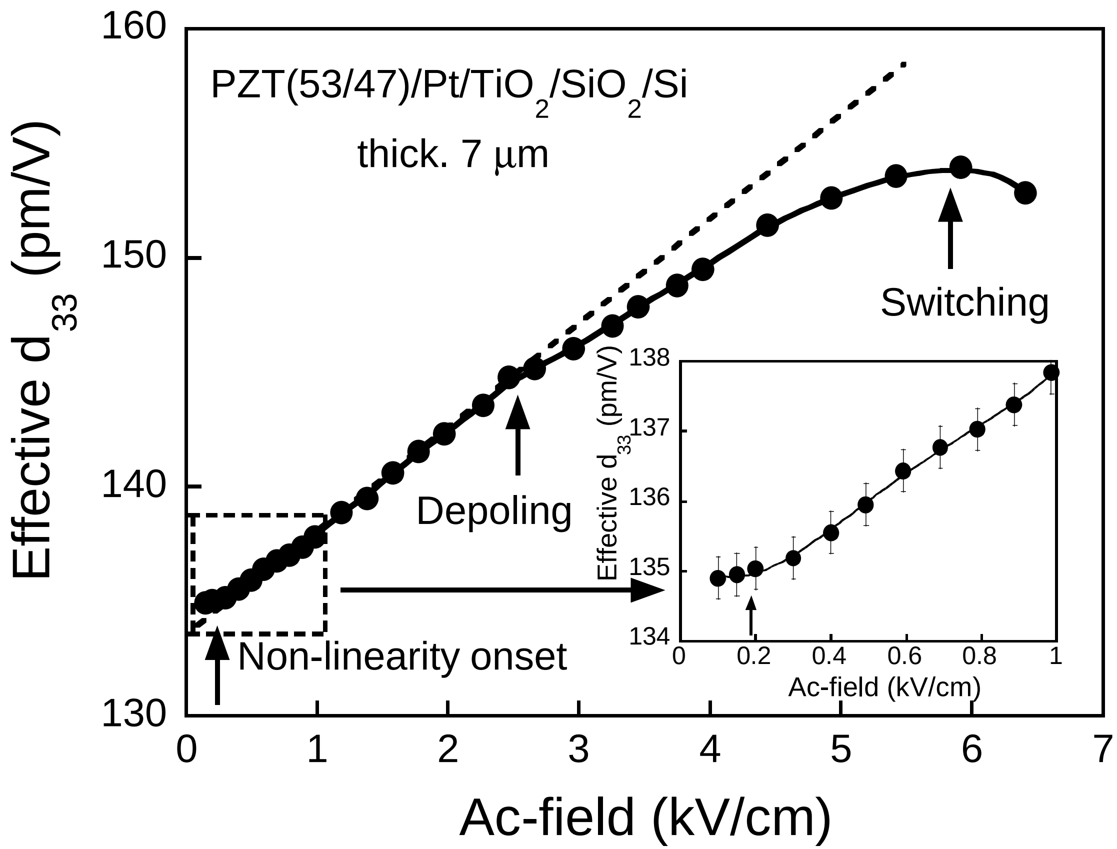

- Onset of non-linearity at ~0.2-0.3 kV/cm
- Quasi-linear response at higher fields
- Sub-linear behaviour at E>2.5 kV/cm (depoling)
- Switching at E>6 kV/cm

Modelling of piezoresponse

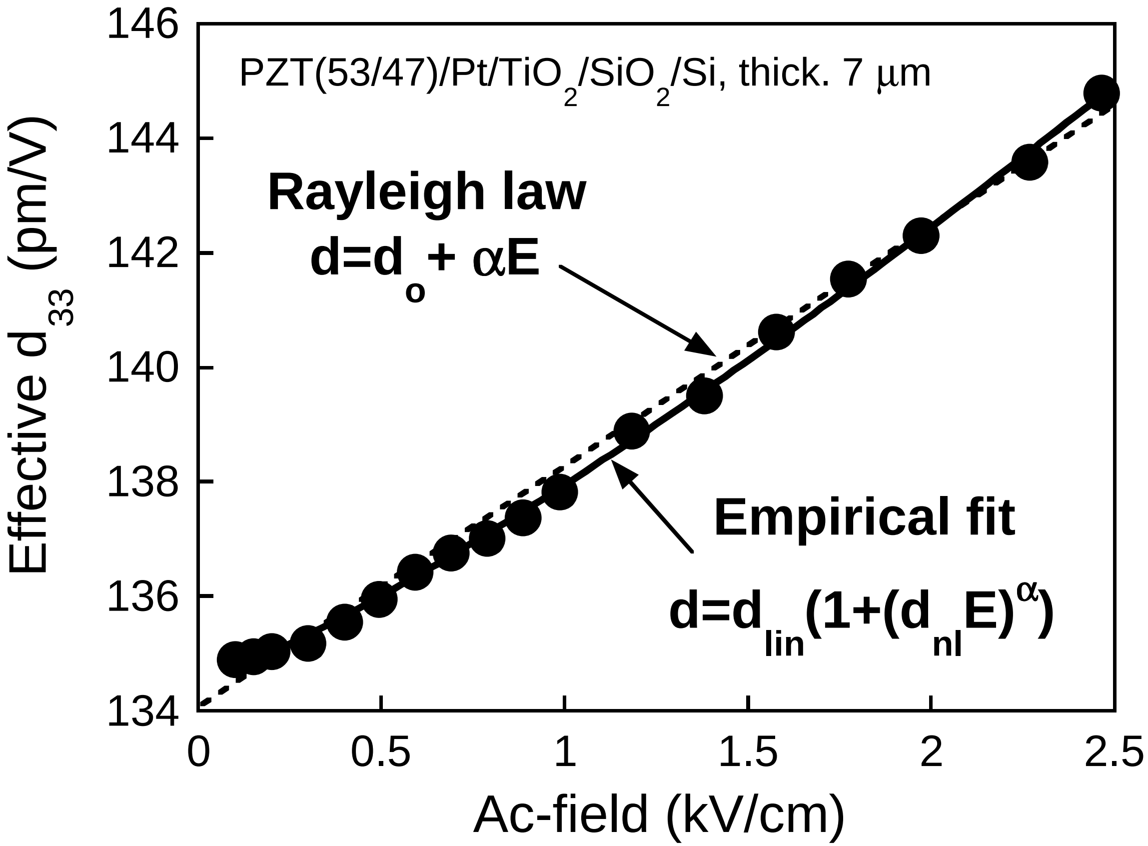

- Poor fit for Rayleigh law
- Non-linearity is better described by the empirical fit with α=1.2

Frequency dispersion

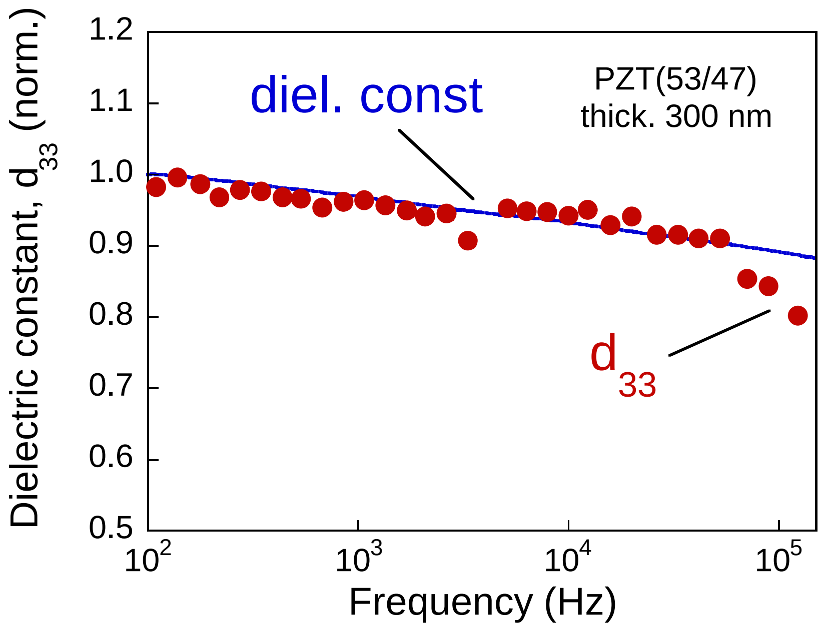

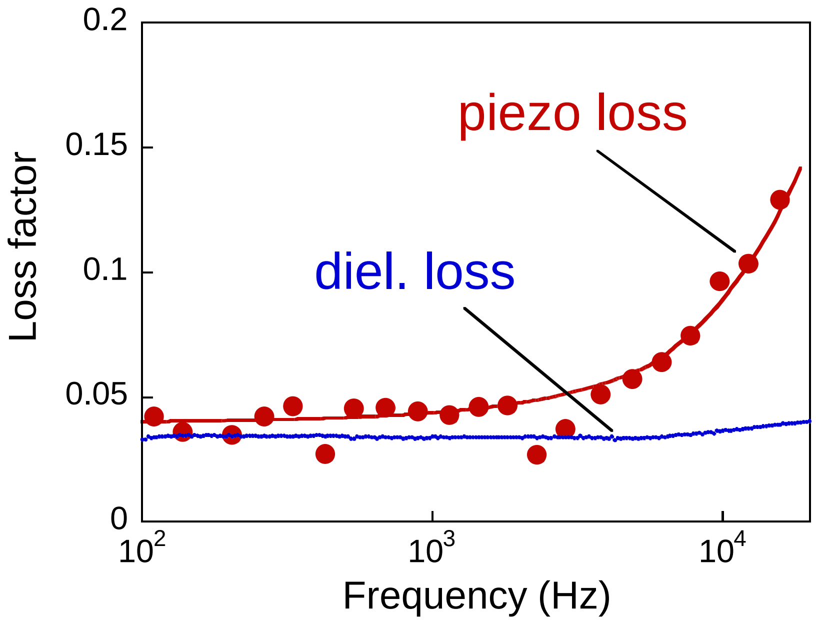

- frequency dispersion of d_{33} is close to dispersion of dielectric constant
- piezoelectric loss is close to dielectric loss

Aging after poling

A.Kholkin et al., Inegr. Ferroelectr. (1997)

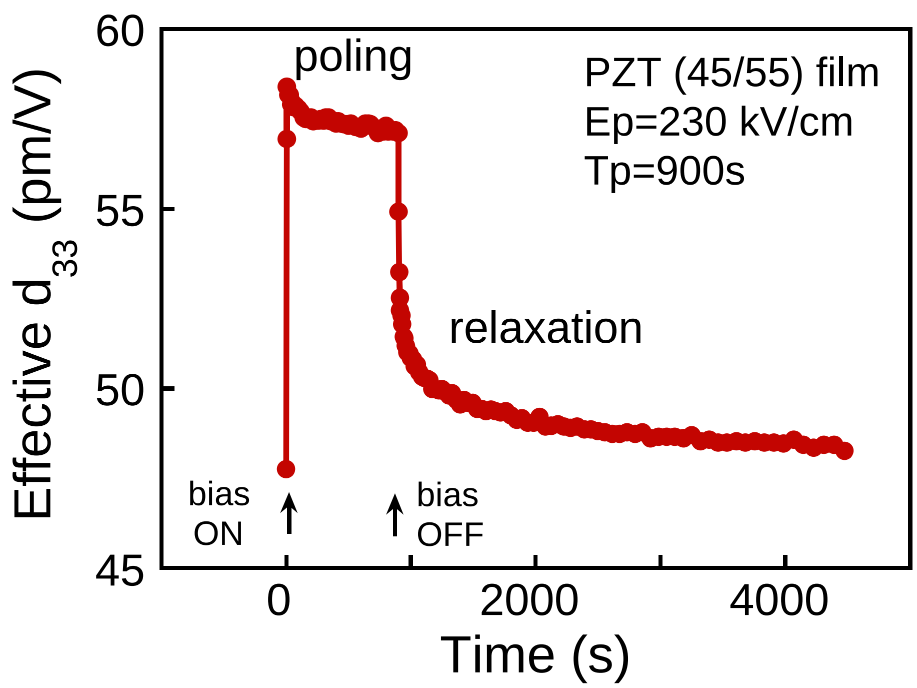

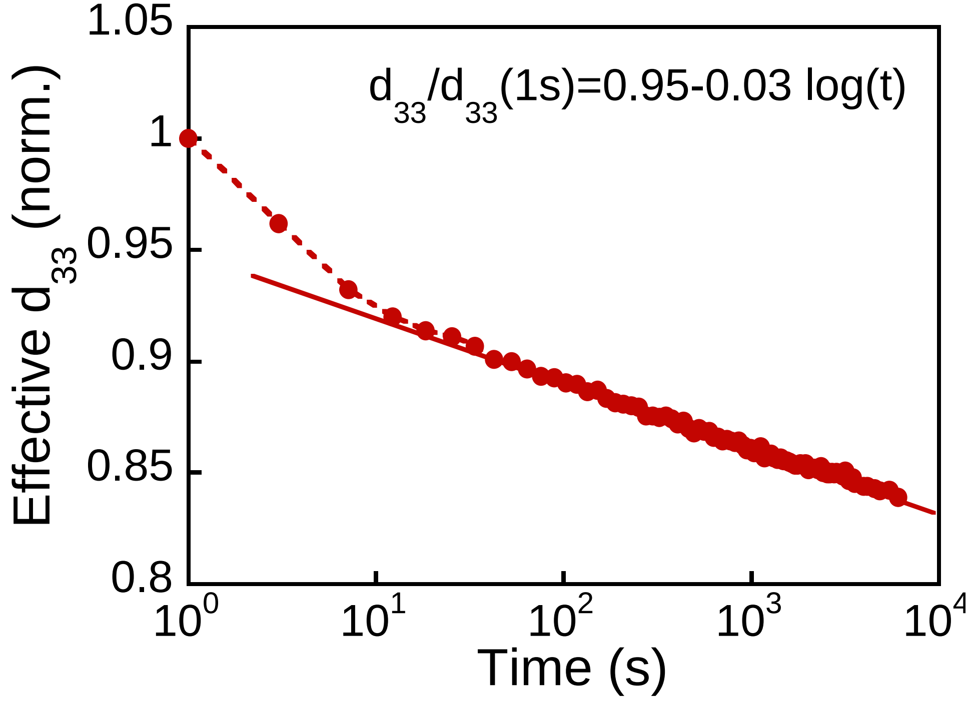

- two stages of d_{33} relaxation: fast depoling and slow logarithmic decrease
- aging rates ≈ 2÷5 %/dec depending on poling time

Thin films vs. Bulk ceramics

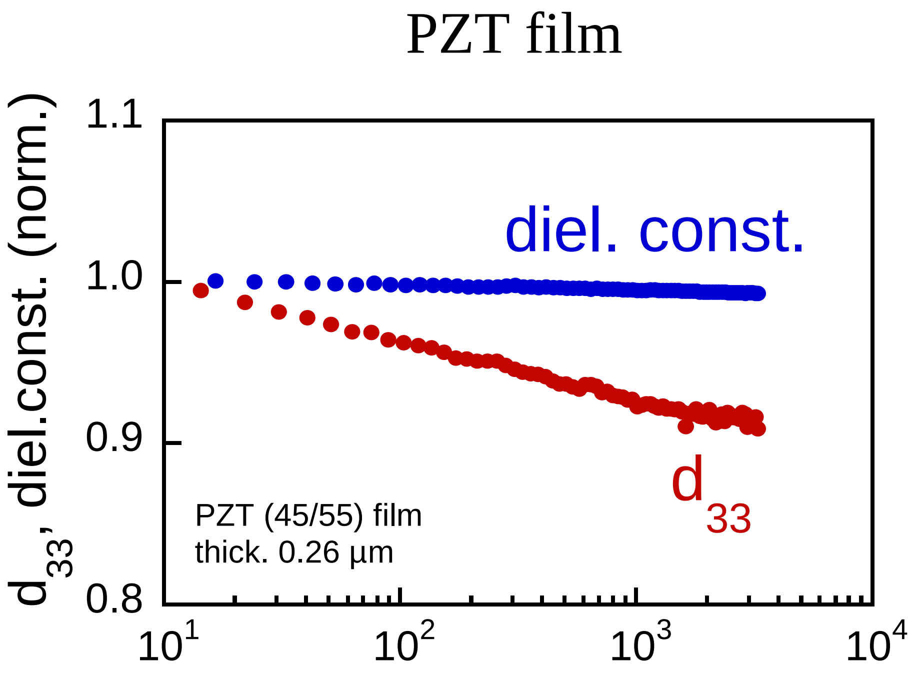

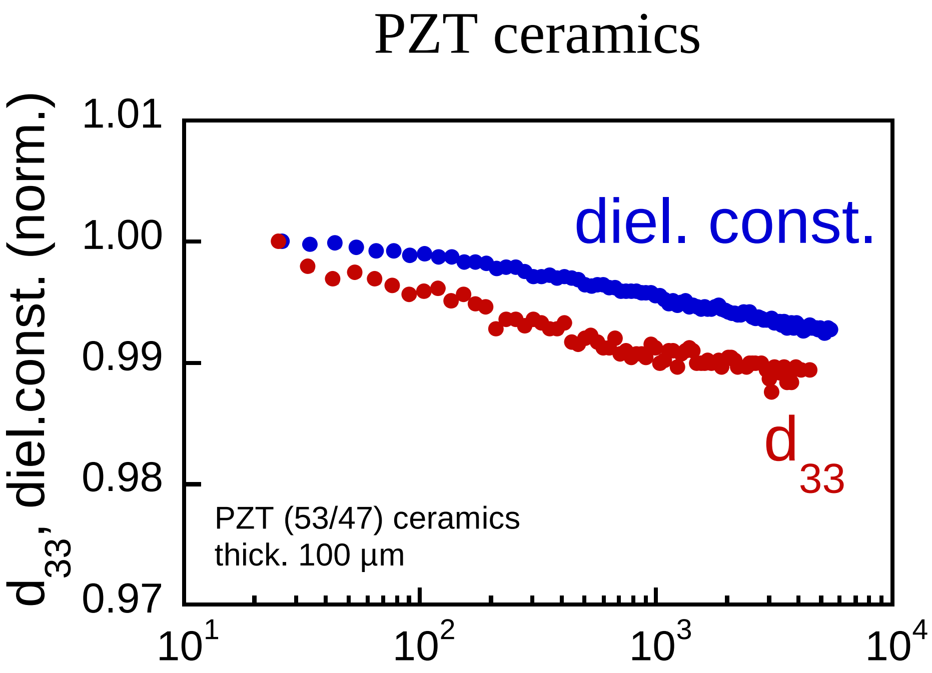

- d_{33} decays much faster than dielectric constant in PZT films
- aging of dielectric constant is comparable in films and ceramics

d_{33} aging vs. polarization retention

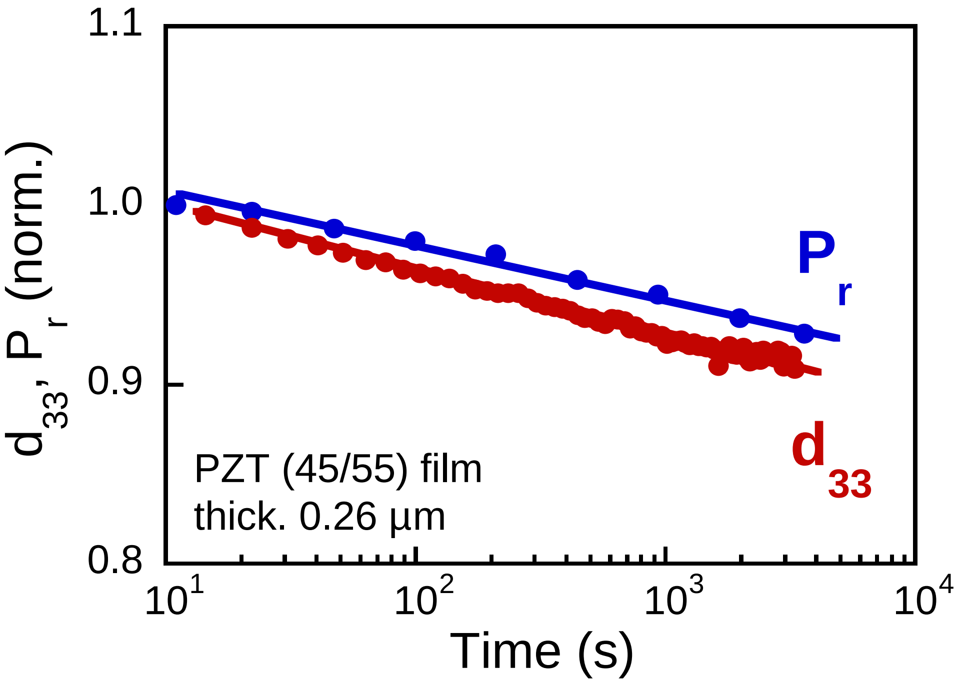

$$d_{33}(t)=2Q_{11}\varepsilon_o\varepsilon(t)P_r(t)$$

- aging of d_{33} is close to the reduction of P_r with time (retention)
- aging of d_{33} is due to <u>depoling</u> of PZT films rather than to the reduction of domain wall contribution

Case study: $PbTiO_3$:Ca

- simple tetragonal structure
- decrease of tetragonality with Ca addition
- high g_{33} coefficients
- high piezoelectric anisotropy for low Ca content

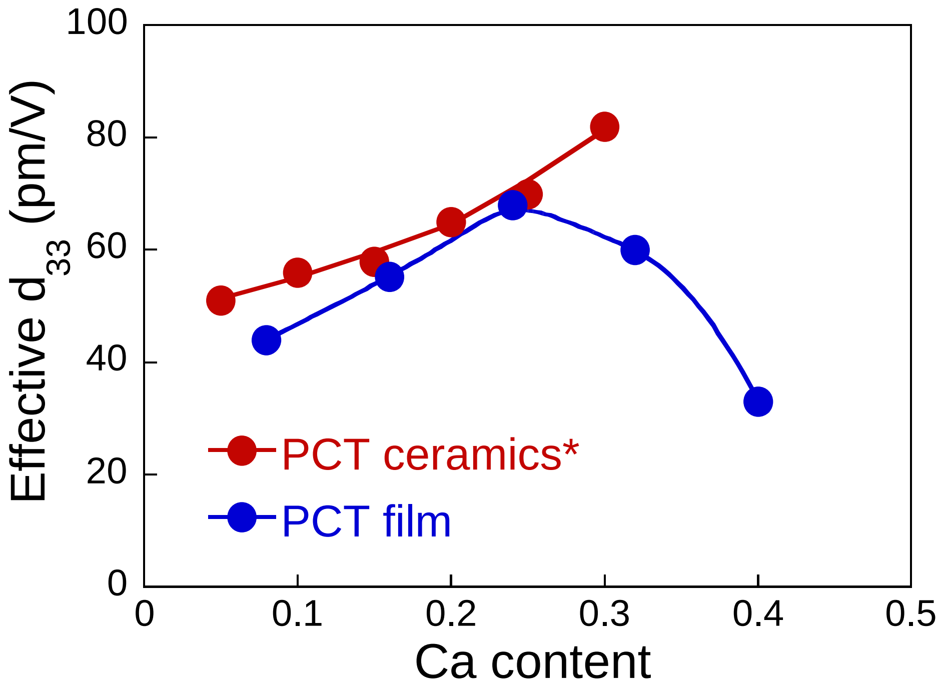

Giant strain in PCT films

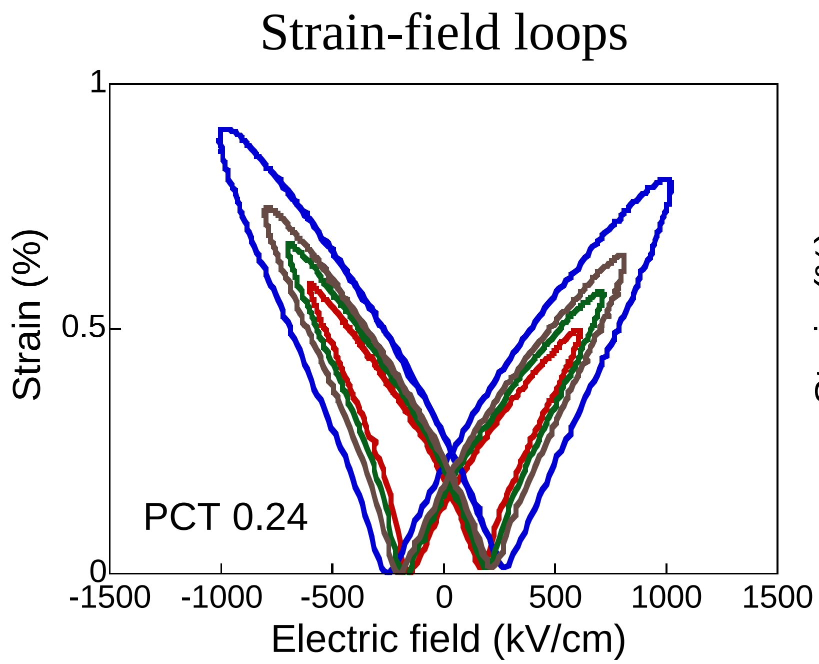

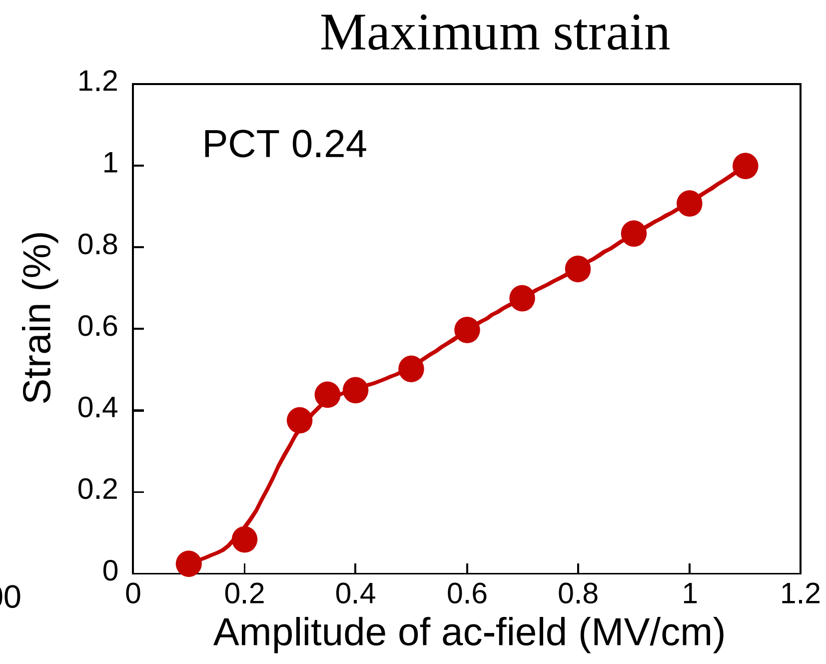

- High breakdown field results in a giant strain at 1 MV/cm (≈1 %)
- At high field strain is linear with the amplitude of ac-field

SBT films: absence of extrinsic strain

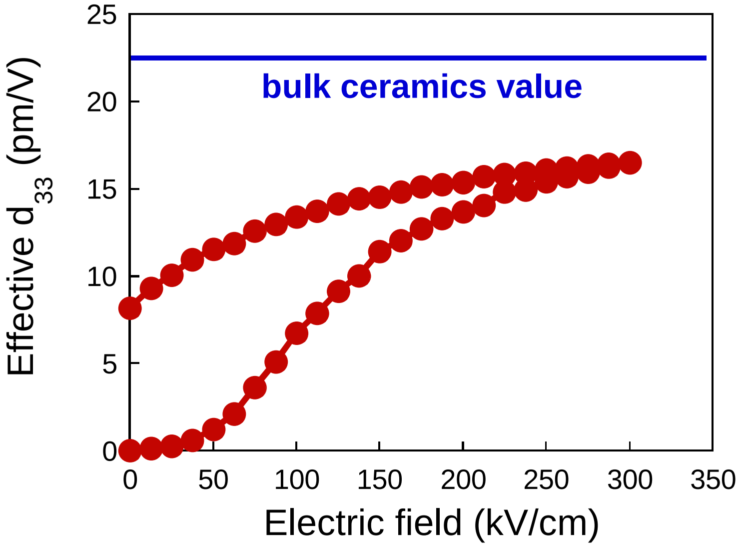

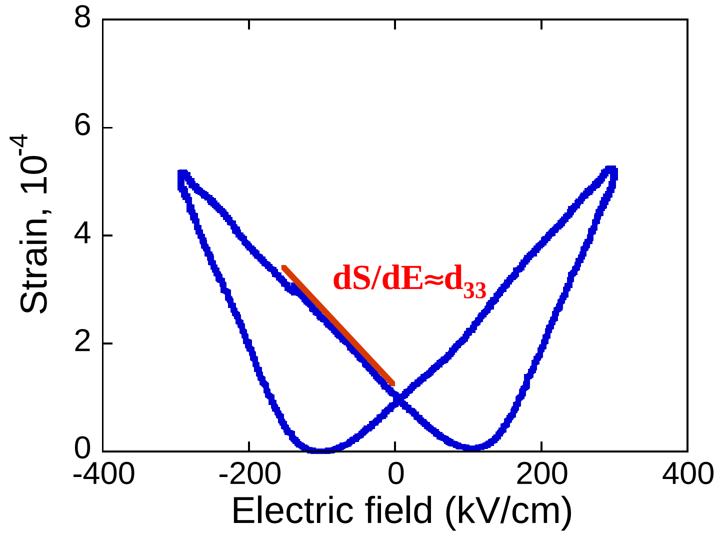

- $(d_{33})_{max}$ is about 75% of bulk ceramics value
- $d_{33} \approx dS/dE$ in contrast to PZT films

SBT films: absence of extrinsic strain

$S = Q_{11}P^2$

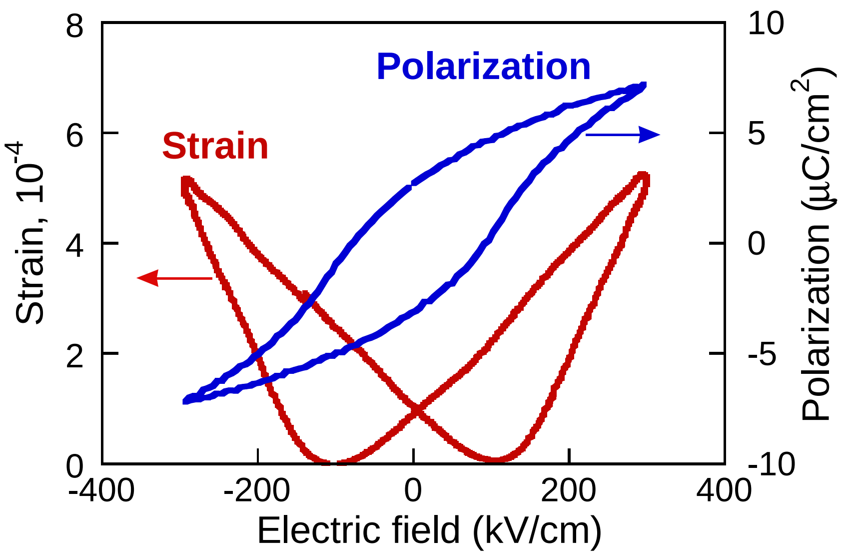

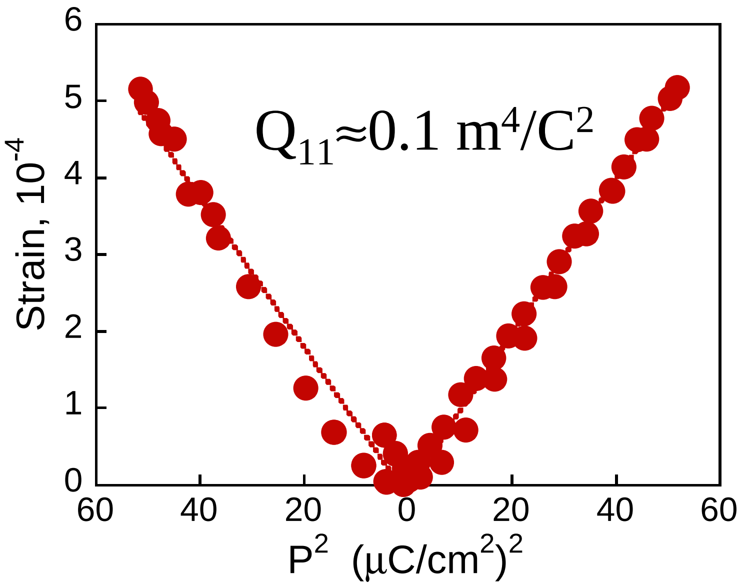

- pure electrostrictive strain behavior at $T \ll T_c$ ($Q_{11} \approx 0.1\ m^4/C^2$)

Domain pinning and voltage offset

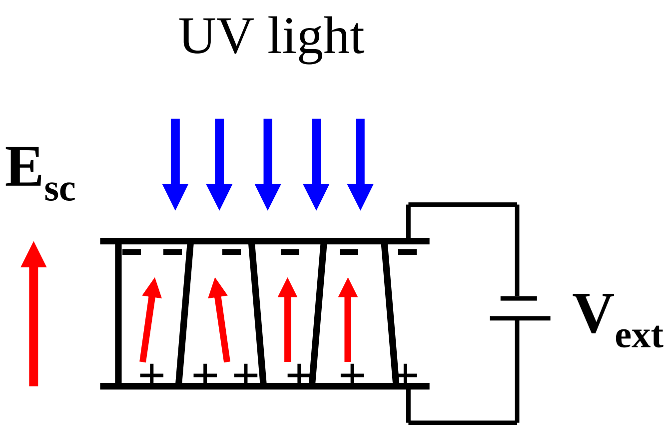

G.E.Pike et al, APL **66**, 484 (1995)

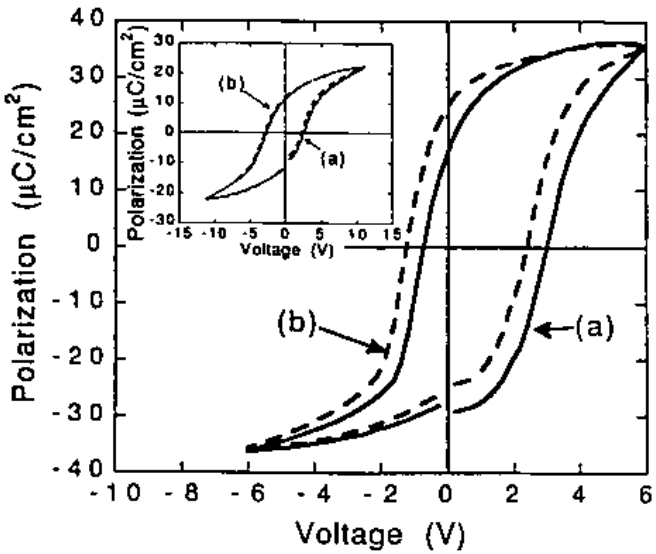

- electrons generated by UV light compensate polarization charge at the film-electrode interfaces
- voltage offset is due to the space-charge internal field

Piezoelectric fatigue: evidence of domain pinning

fatigue of polarization

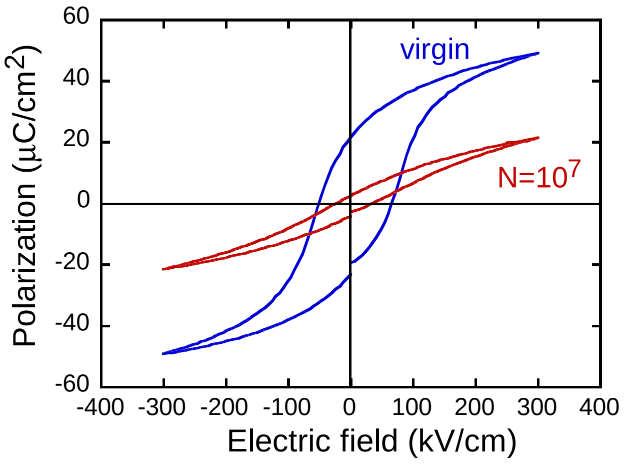

fatigue of d_{33}

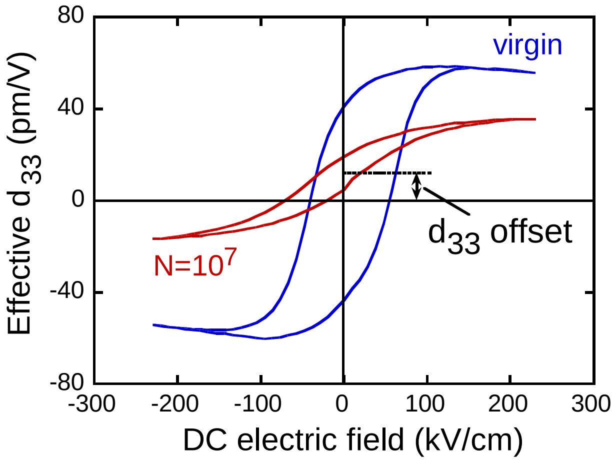

Polarization offset as a function of fatigue

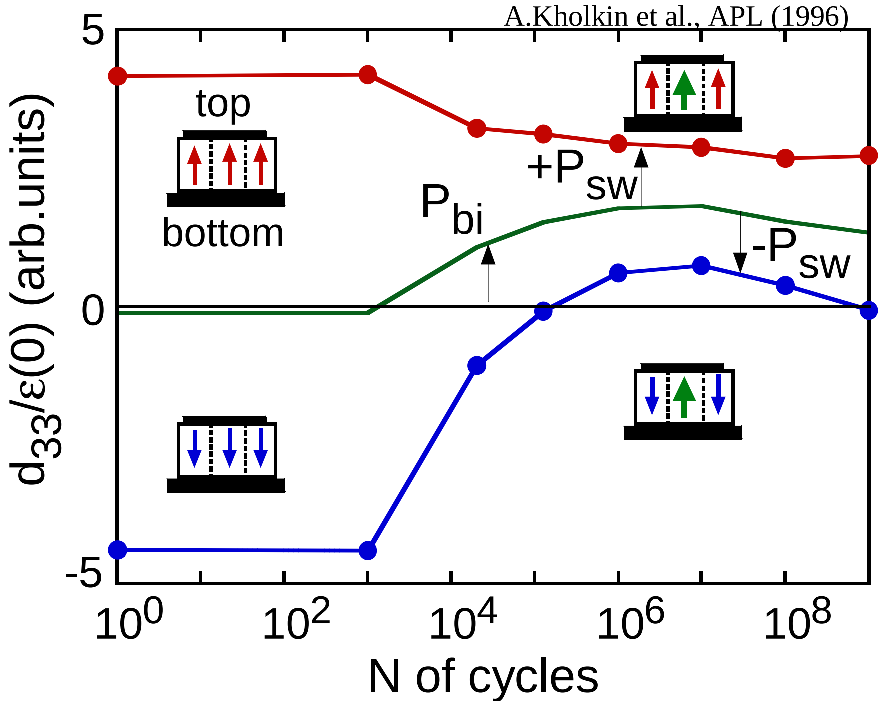

$$P_{bi}=d_{33}/(2Q_{eff}\varepsilon_o\,\varepsilon)$$

UV-induced poling

d_{33} loop of virgin film

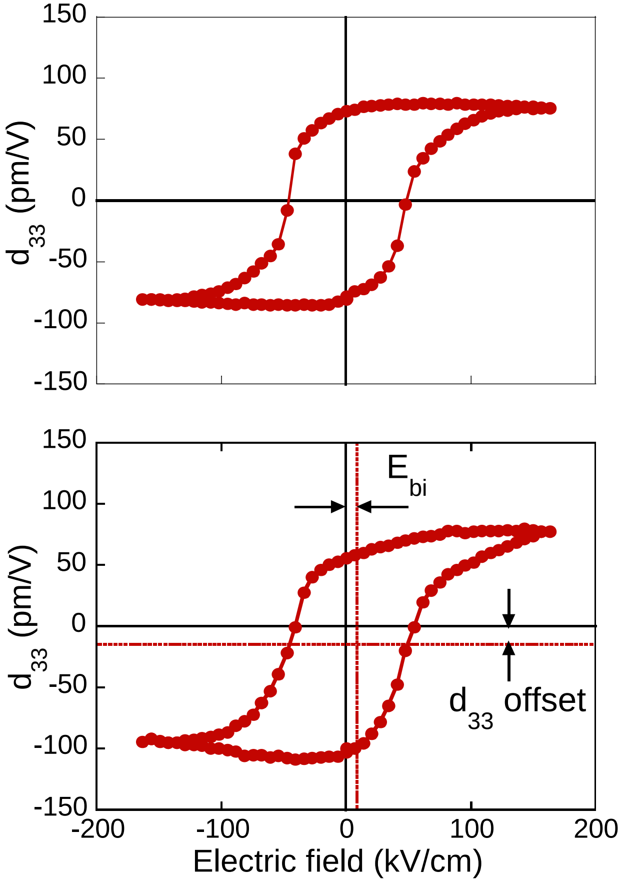

d_{33} loop of illuminated film

Photoinduced poling effect

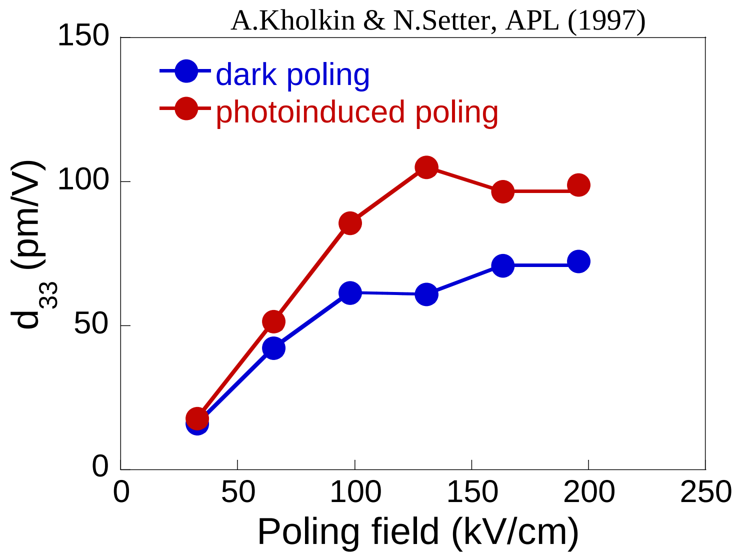

$$d_{33}=2Q_{eff}\varepsilon_o\,\varepsilon\,P_{bi}$$

Downscaling of actuators

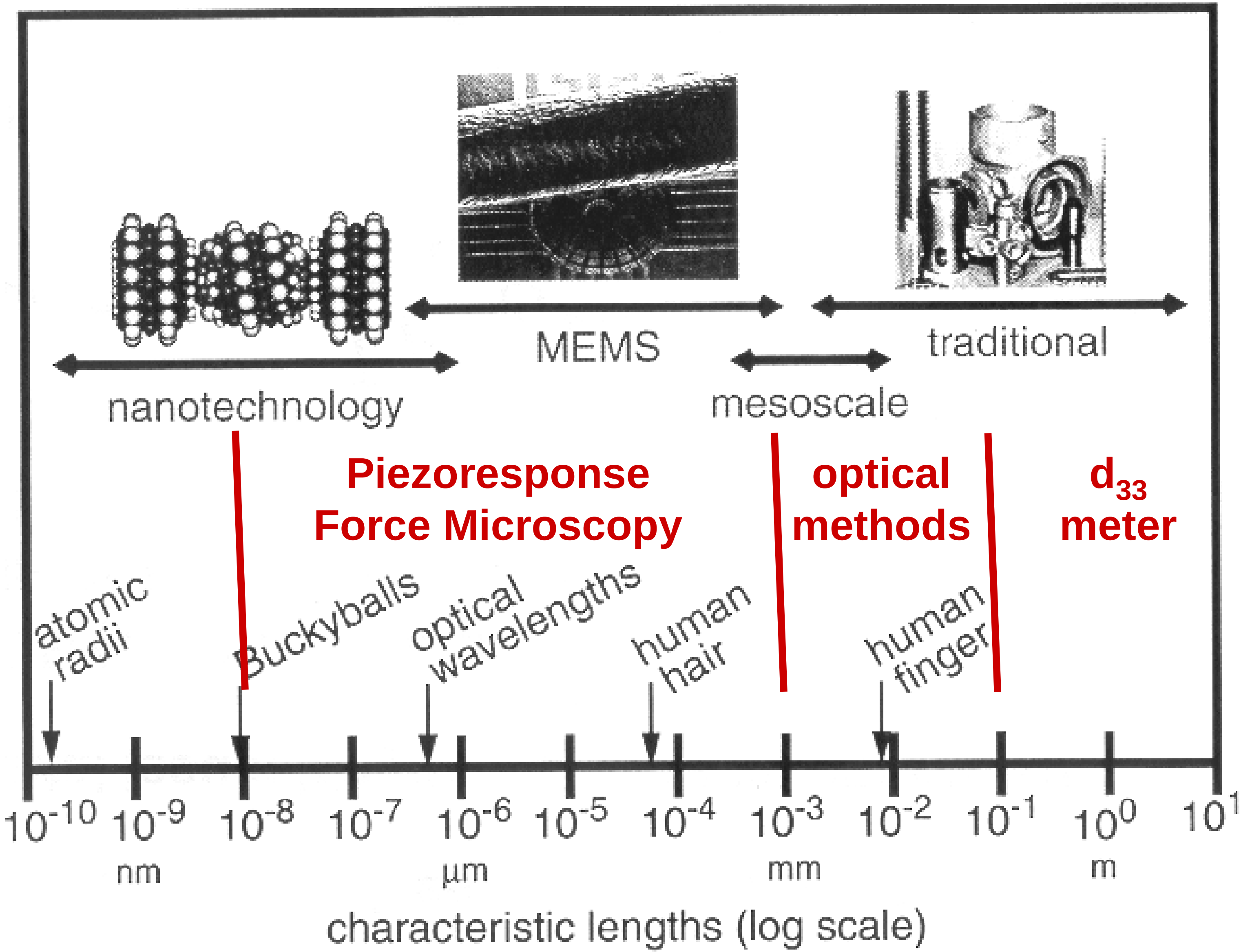

Local characterization: Piezoresponse Force Microscopy

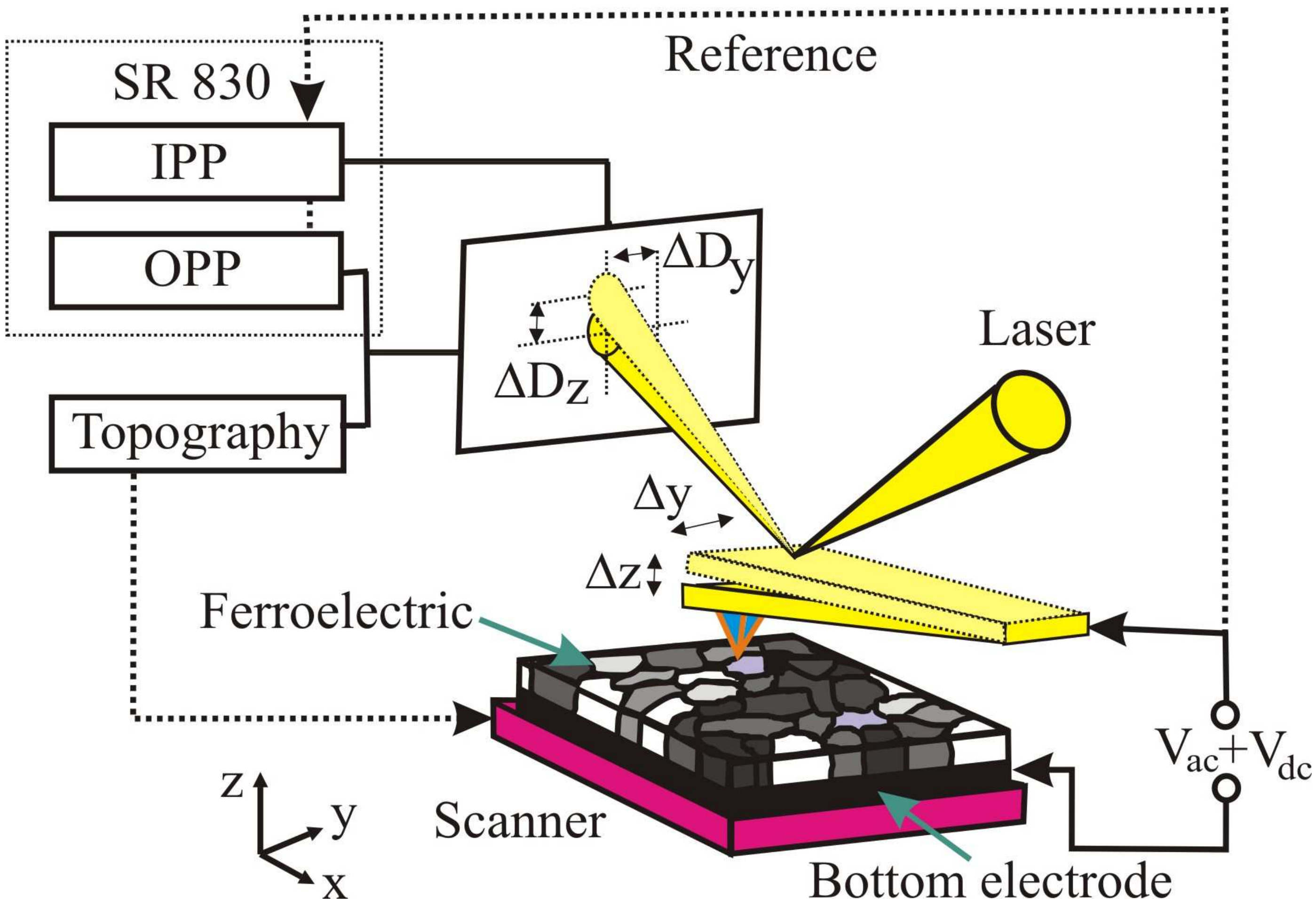

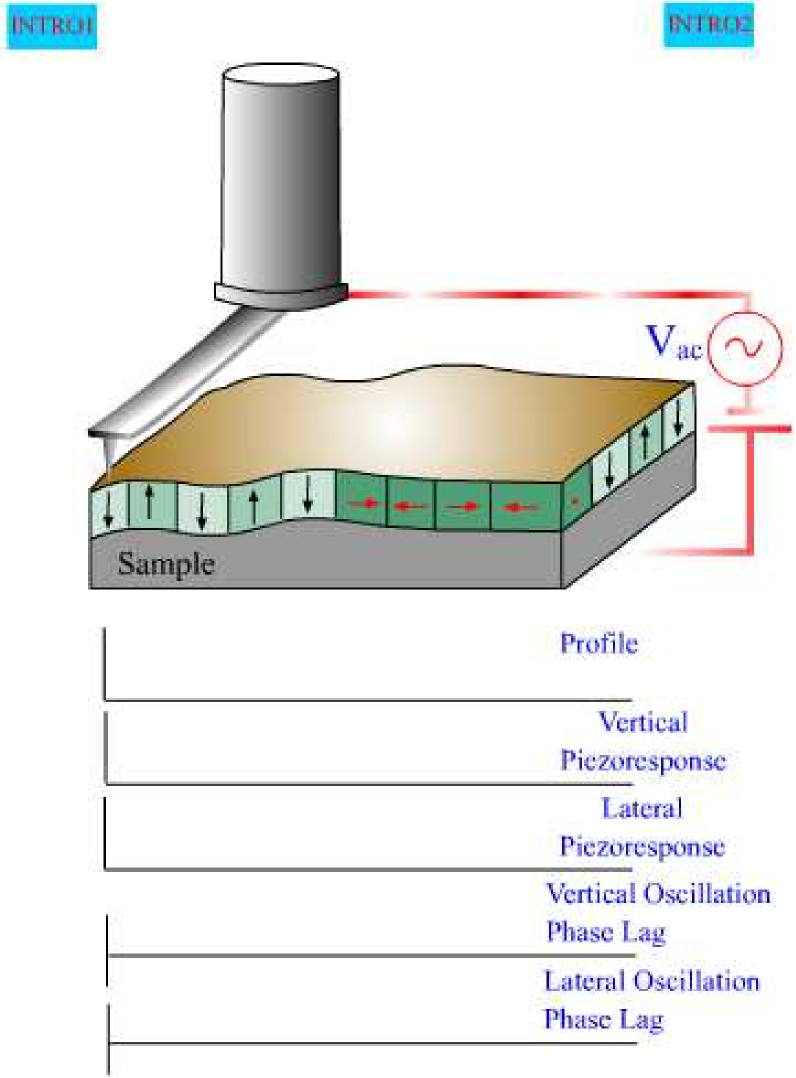
INTRO1
INTRO2
V_{ac}
Sample
Profile
Vertical Piezoresponse
Lateral Piezoresponse
Vertical Oscillation Phase Lag
Lateral Oscillation Phase Lag

1-st pass. Sample profile acquisition.

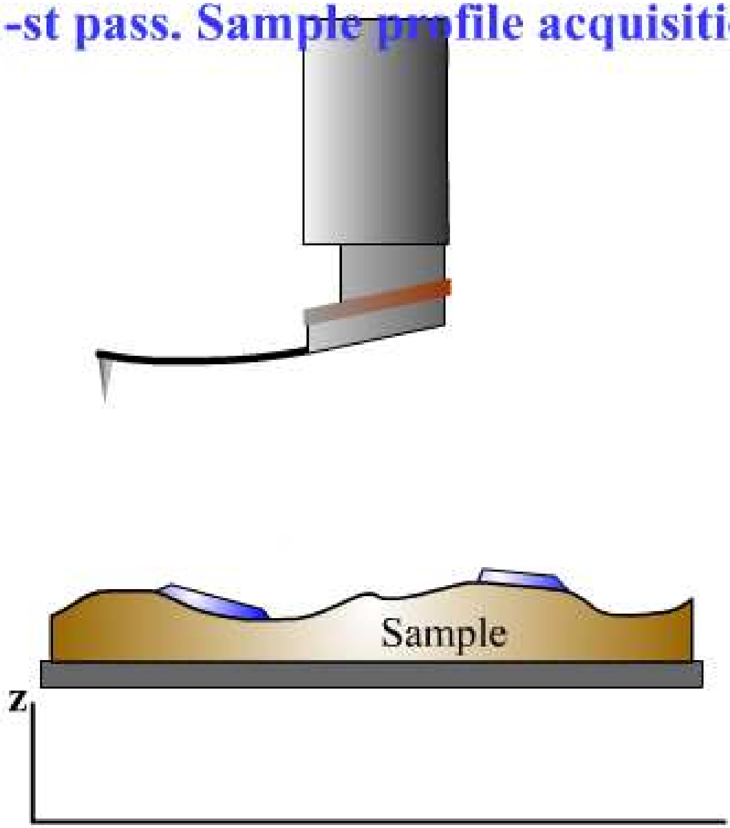

 www.ntmdt.com

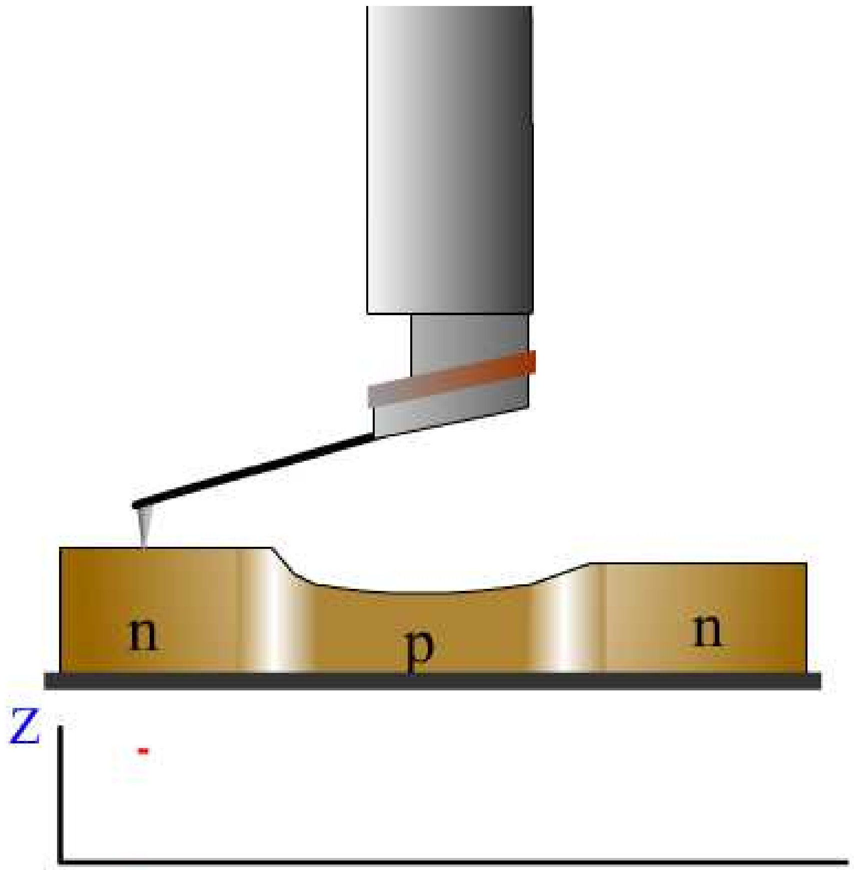
n
p
n
Z

PFM vs. EFM

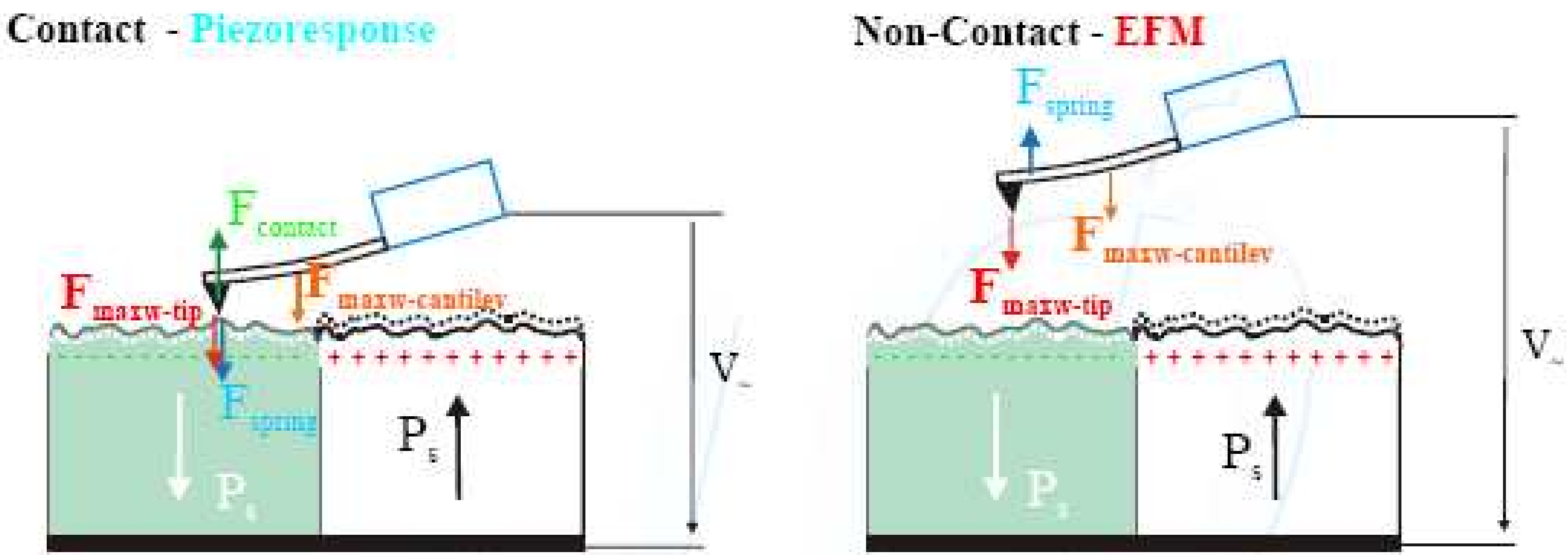

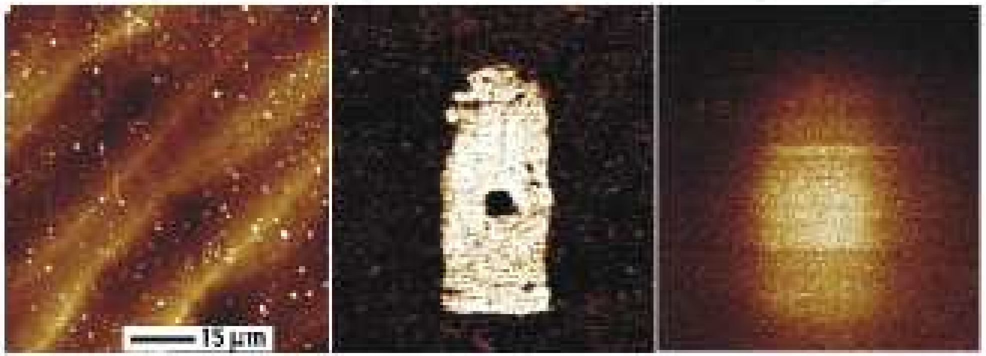

Topography z - Piezoresponse EFM-Surface charge

KFM and EFM for domain imaging

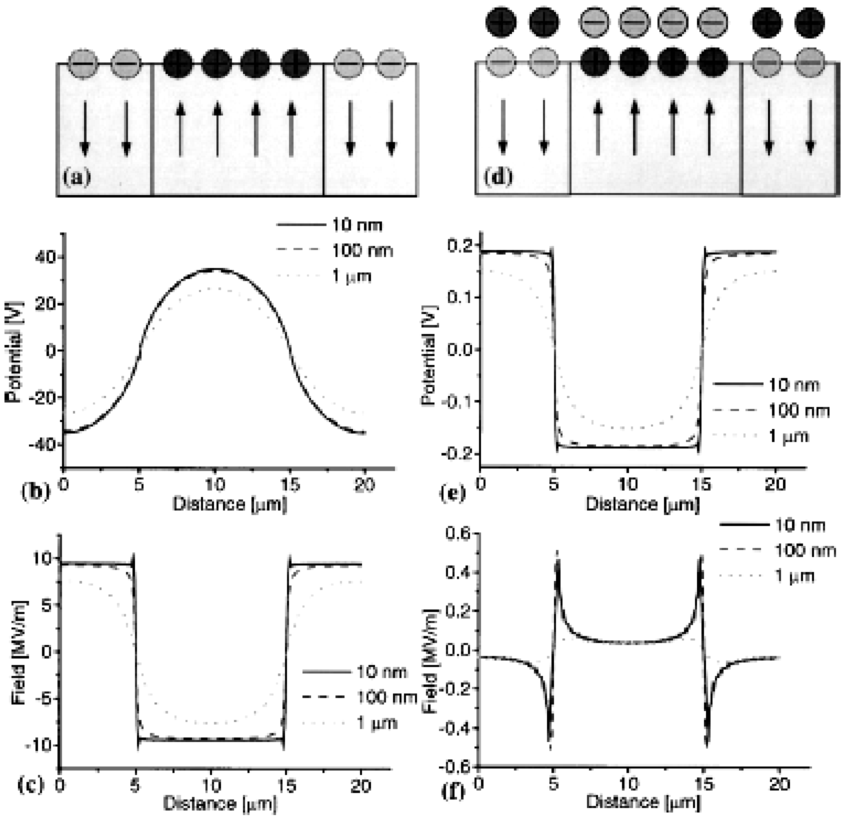

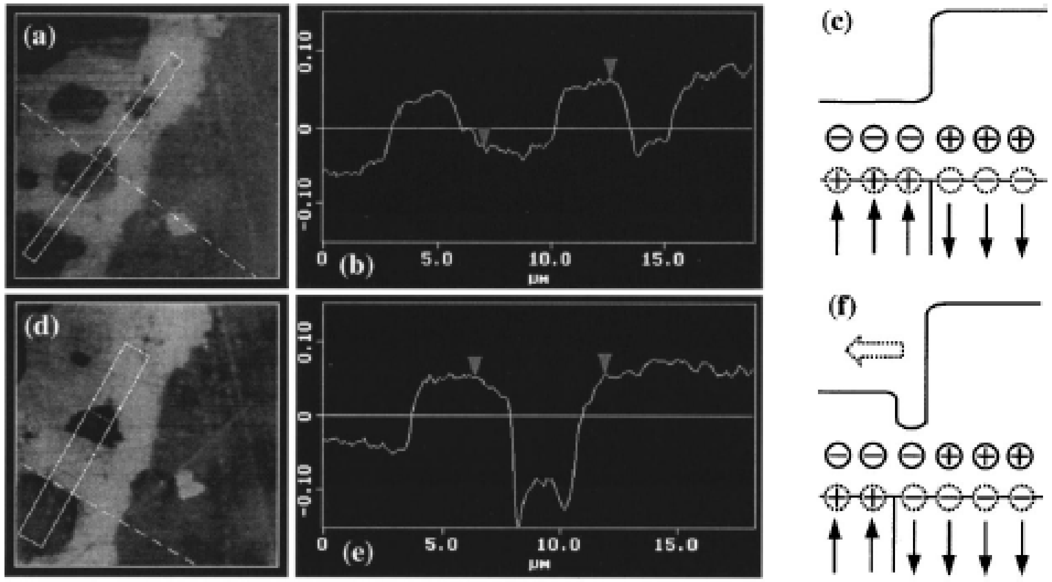

Kalinin & Bonnell PRB (2001)

Advantages/disadvantages of PFM

- Much higher resolution: limited by tip diameter
- Control of polar state: new applications of ferroelectrics: e.g., nanolithography and self-assembly routines
- Local domain engineering and interaction with defects
- Vizualization of small domains impossible in the past
- Multiferroics and magnetoelectric interaction on the nanoscale
- Slow acquisition
- Difficult to get reliable absolute values of d_{33}
- Not easy interpretation: electrostatics

Potential distribution and effective d_{33}

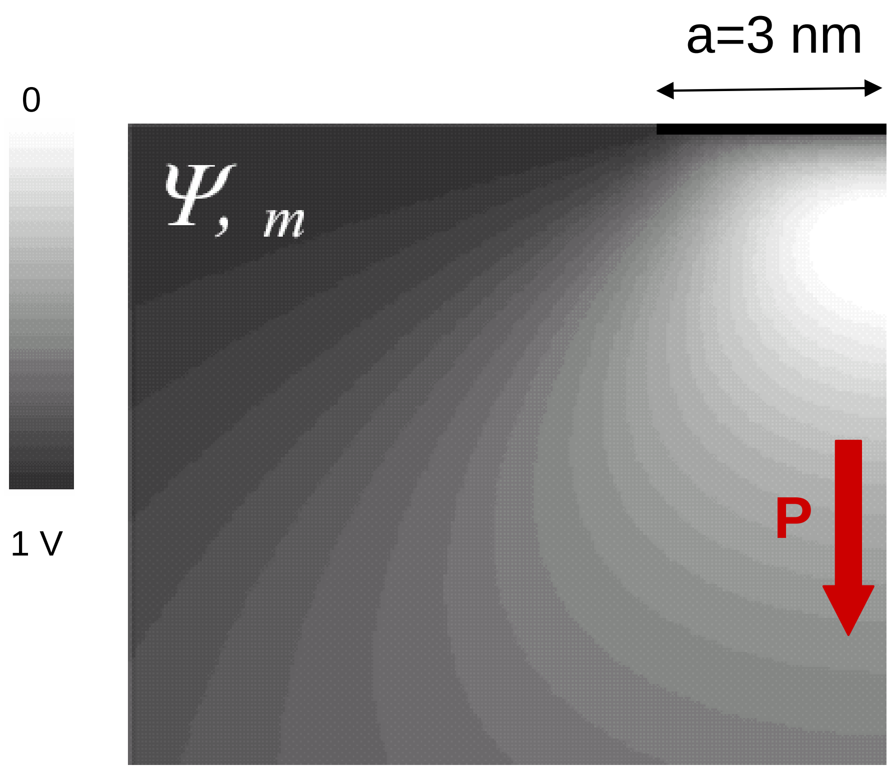

BaTiO$_3$ (V_{appl}=1 V)

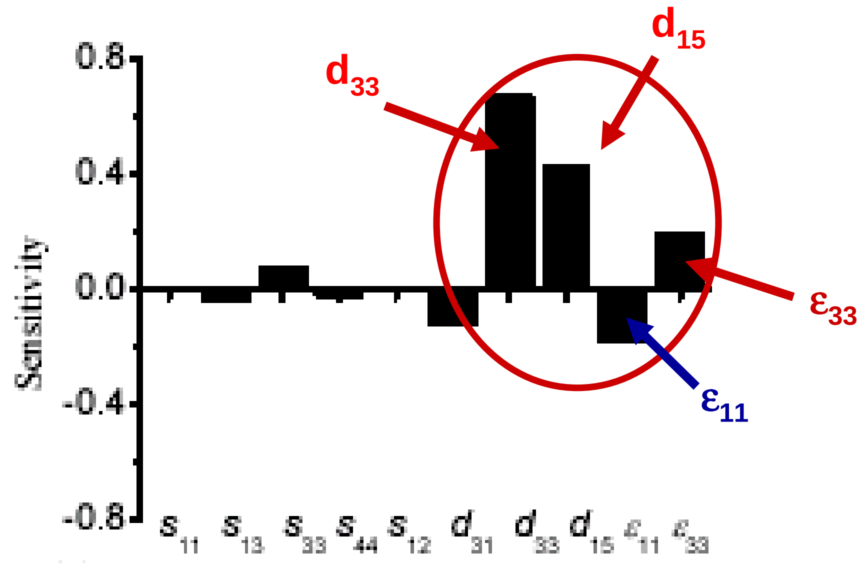

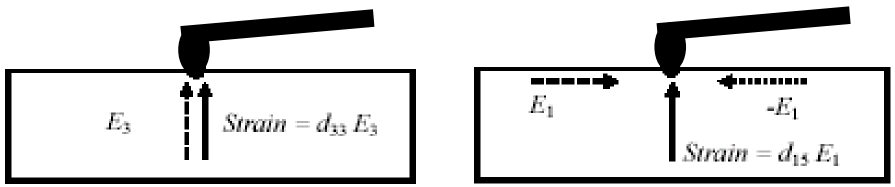

d_{33} contribution d_{15} contribution

Kalinin et al, Phys. Rev. B (2004)

Influence of interface layer

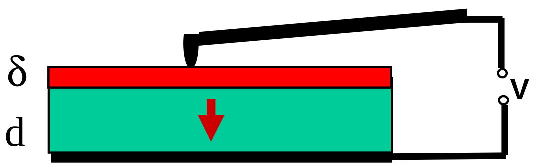

$$\left(\mathbf{d}_{33}\right)_{\mathbf{eff}} \propto \frac{\mathbf{A}_{1\omega}}{\mathbf{V}_{ac}} = \frac{\mathbf{A}_{1\omega}}{1 + \dfrac{\delta\varepsilon}{d\varepsilon_{\delta}}}$$

Effect of tip-surface interaction

Weak indentation

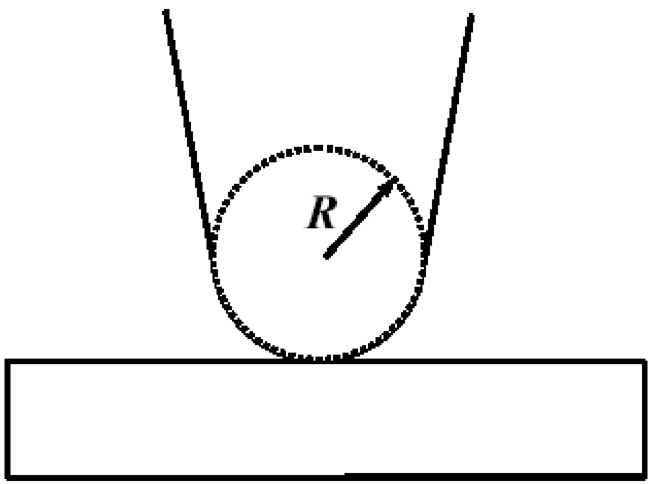

Strong indentation

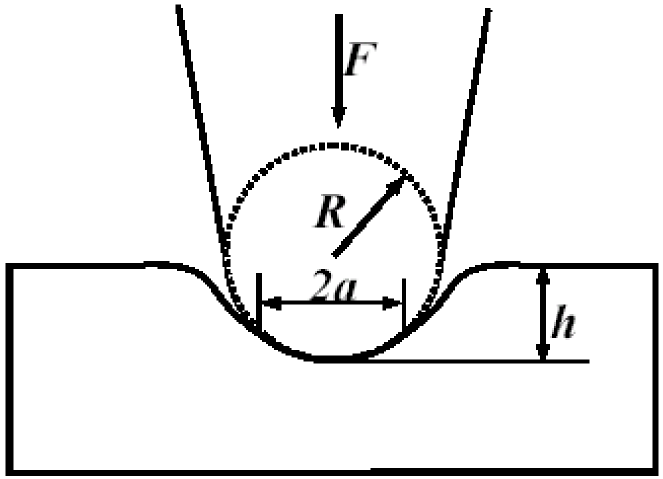

- Small contact area <<R.
- Electrostatic signal dominates electromechanical one. $F = \frac{V^2}{2}\frac{\partial C}{\partial z}$
- Distribution of E-field can be calculated using image charge models.

- Medium contact area a≤R.
- Electromechanical signal dominates electrostatic (Maxwell stress).
- Coupled electrostatic + elastic + electroelastic problems should be solved!

Local vs. macroscopic measurements

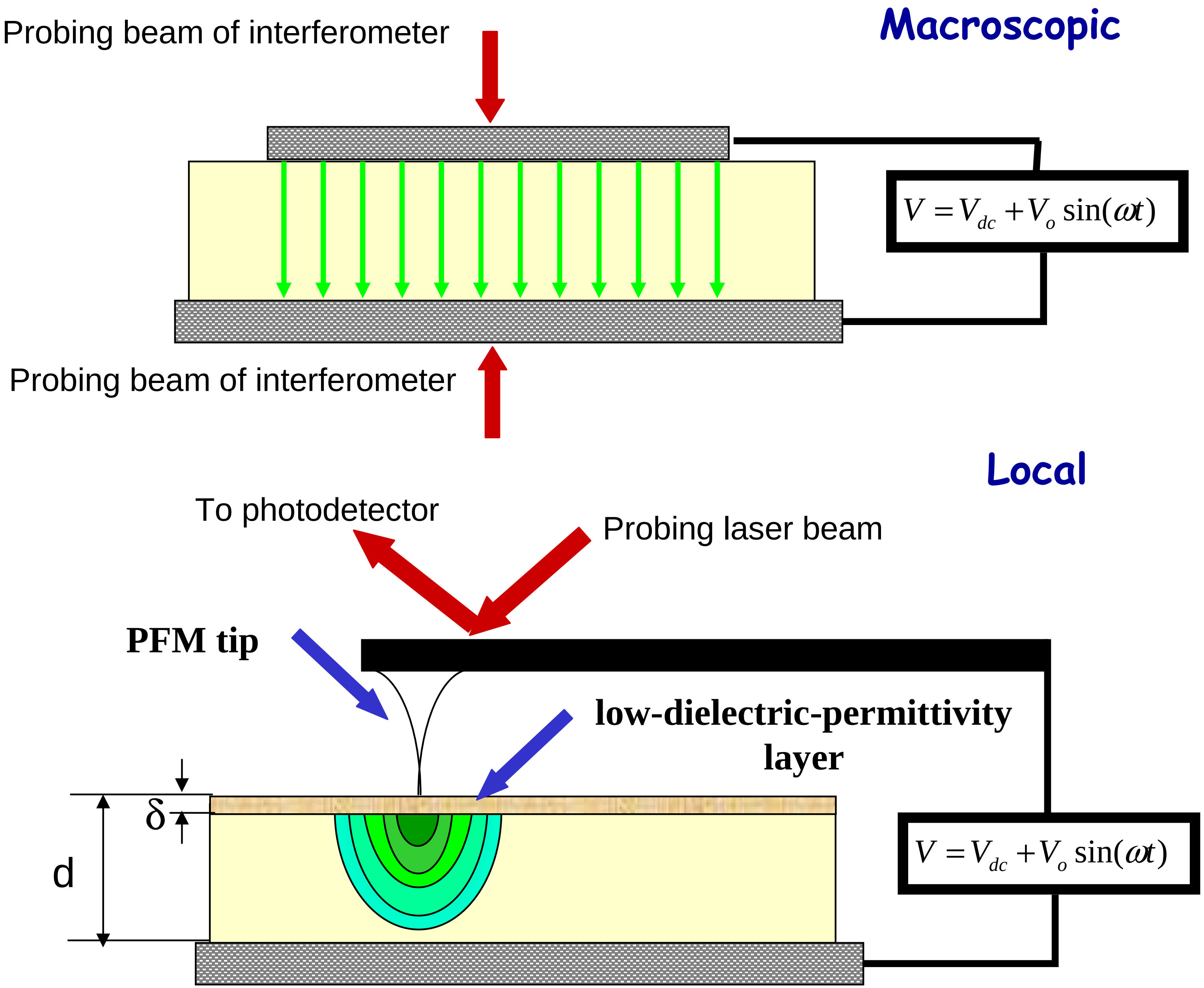

Piezoelectric hysteresis

Strain in monodomain ferroelectric with centrosymmetric paraelectric phase

$$S = QP^2(E) = Q[P_s + P_{ind}(E)]^2 = QP_s^2 + 2Q\varepsilon_o\varepsilon P_s E + QP_{ind}^2$$

For small ac-field $E = E_{dc} + E_o \sin(\omega t)$

1st harmonics of ac-strain $S_{1\omega} = \underbrace{2Q\varepsilon_o\varepsilon P_s}_{d_{33}=\text{const}} E_o \sin(\omega t)$

If polarization is changed by E_{dc}, **$d_{33}=f(E_{dc})$** and can be formally rewritten as

$$\boxed{d_{33}(E_{dc}) = 2Q\varepsilon_o\varepsilon(E_{dc})P(E_{dc})}$$

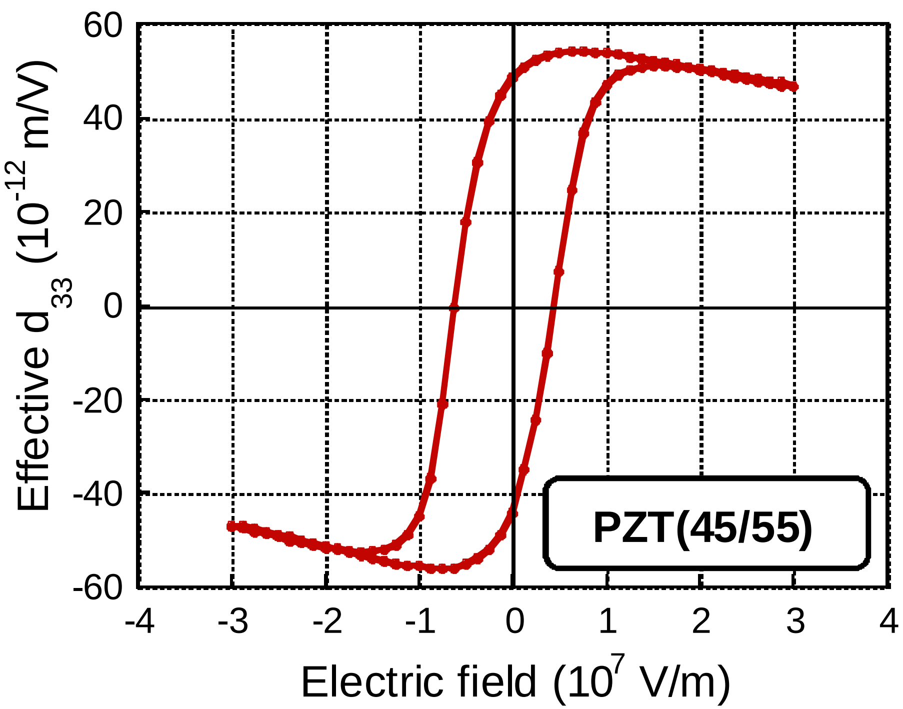

P(E) reconstruction

Simultaneous measurements of d_{33}(E) and ε(E)

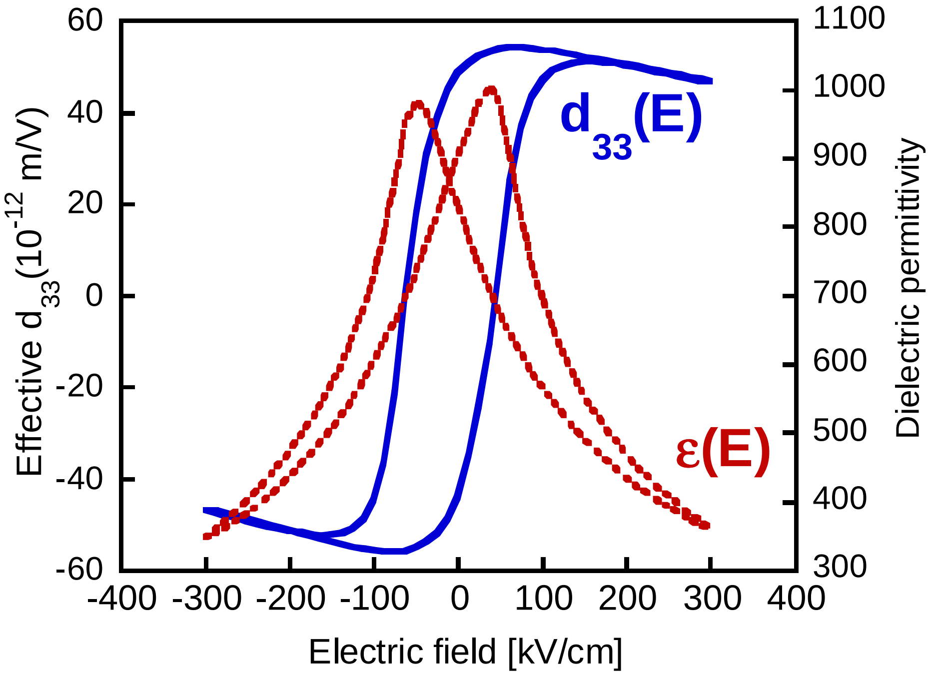

Comparison of P(E) and reconstructed from d_{33}/ε

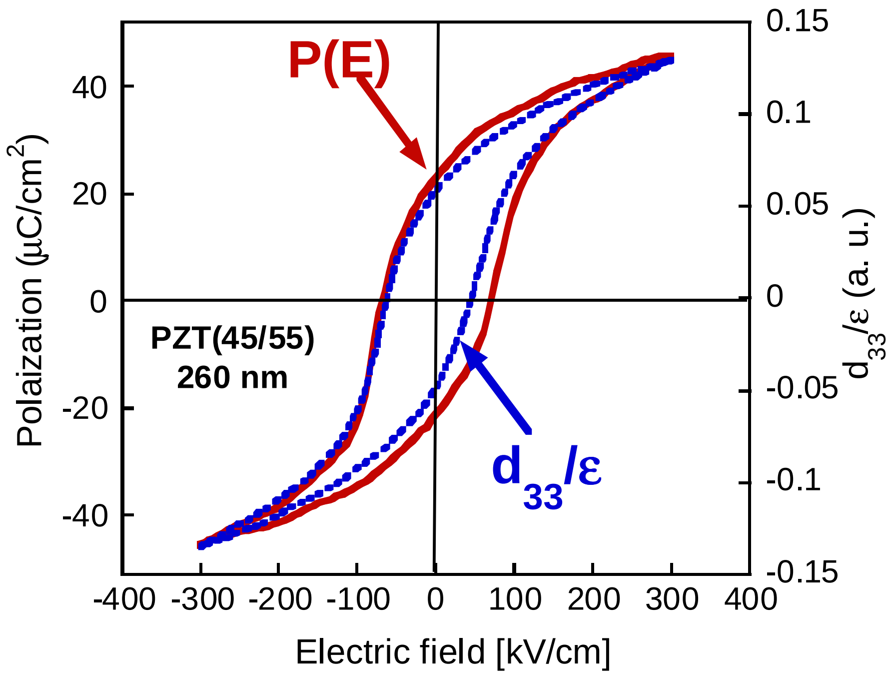

- **Polarization hysteresis is close to d_{33}/ε(E) hysteresis**
- **d_{33}(E) shape is determined by both ε(E) and P(E)**

Kholkin et al, JAP 89, 2001

Influence of electrostatics

Two modes of voltage application

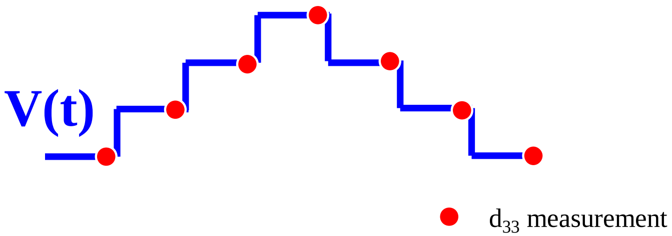

Step mode

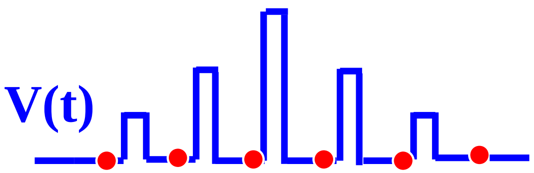

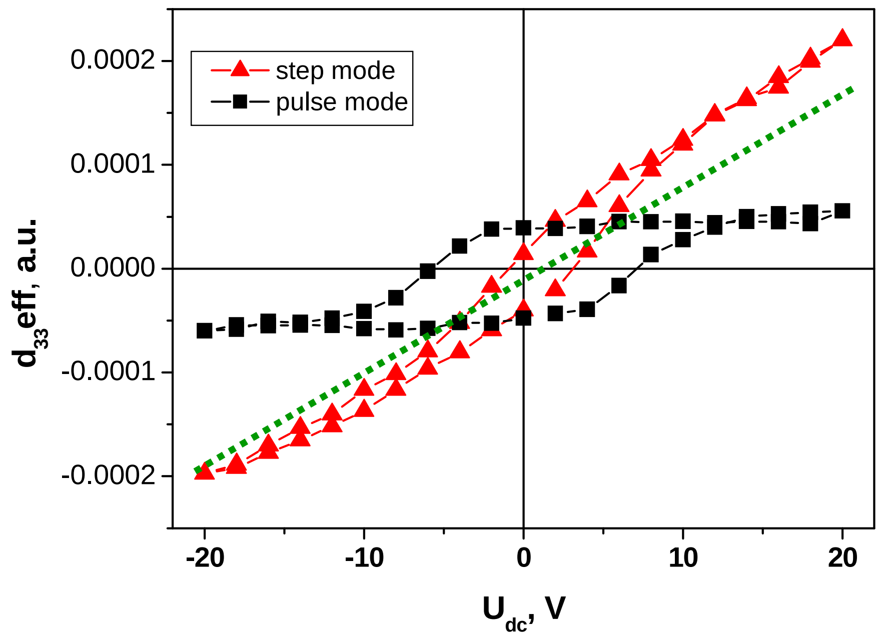

Pulse mode

$$A\cos\varphi = \underbrace{-\frac{K}{k_{lever}}\frac{\partial C}{\partial z}(V_{dc}+V_k)}_{\text{Electrostatic term}} \pm d_{33}V_o$$

Hong et al., JAP (2001)

- **Electrostatic interaction distorts the shape of the hysteresis in step mode and simulates polarization offset if $V_k \neq 0$**

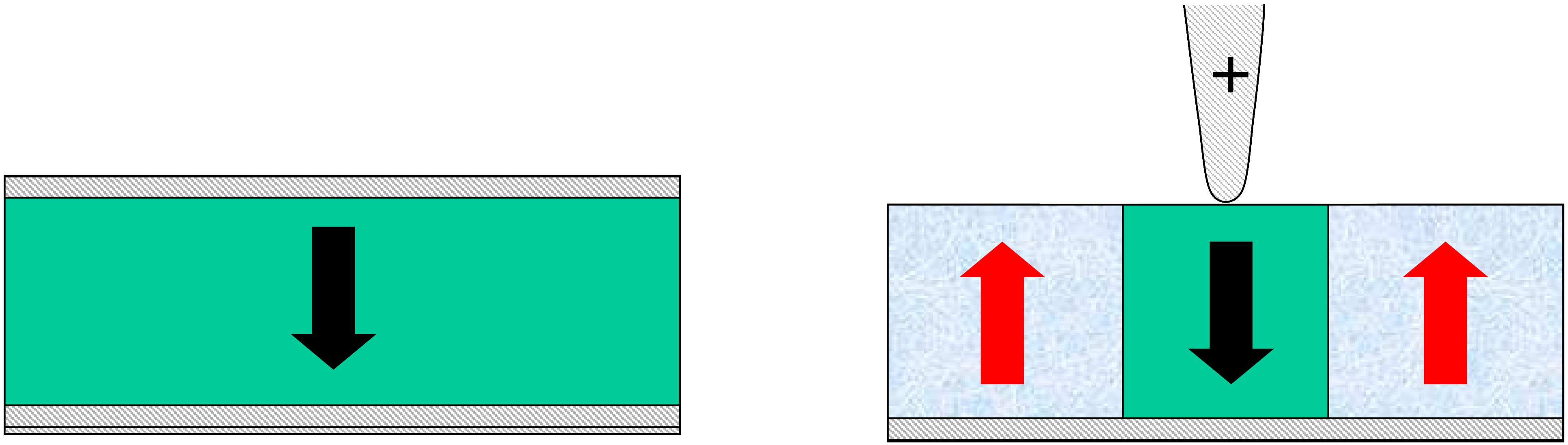

Origin of piezosignal

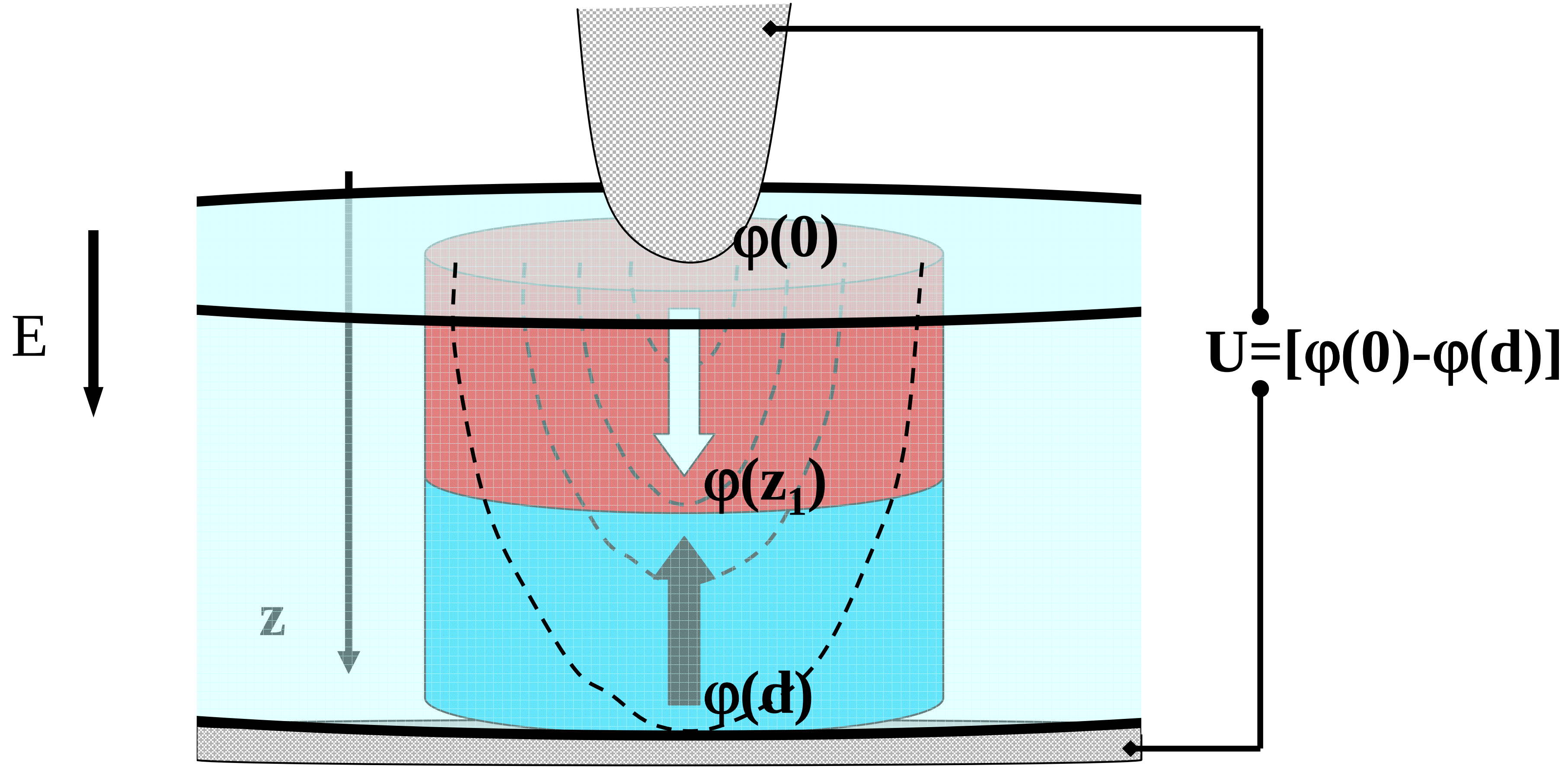

$$\Delta l=\int_0^d d_{33}(z)E(z)dz=d_{33}\int_0^{z_1}E(z)dz-d_{33}\int_{z_1}^{d}E(z)dz=$$

$$=d_{33}[\varphi(0)-2\varphi(z_1)+\varphi(d)]=d_{33}\{U-2[\varphi(z_1)-\varphi(d)]\}$$

$$\Delta l=(d_{33})_{eff}U\Rightarrow(d_{33})_{eff}=d_{33}\left\{1-\frac{2[\varphi(z_1)-\varphi(d)]}{U}\right\}$$

Wu et al., Nanotechnology 16 (2005)

E_c at $\varphi(z_1)=\dfrac{\varphi(0)+\varphi(d)}{2}$

$$\boxed{d_{eff}\propto\alpha\gamma d_{33}\left[1-\frac{2R}{R+\dfrac{P_S U_{dc}\ln(\varepsilon)}{\varepsilon\sigma_W}}\right]}$$

Hysteresis in PZT films

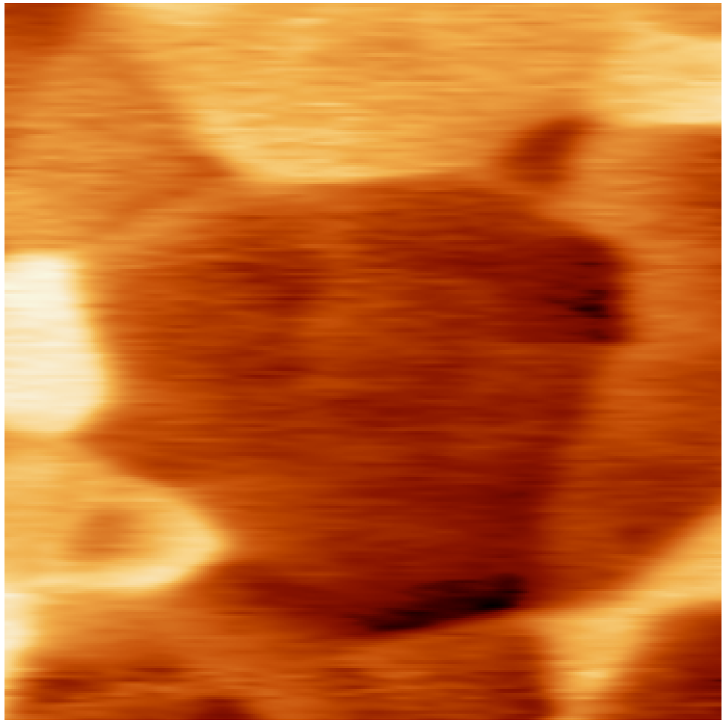

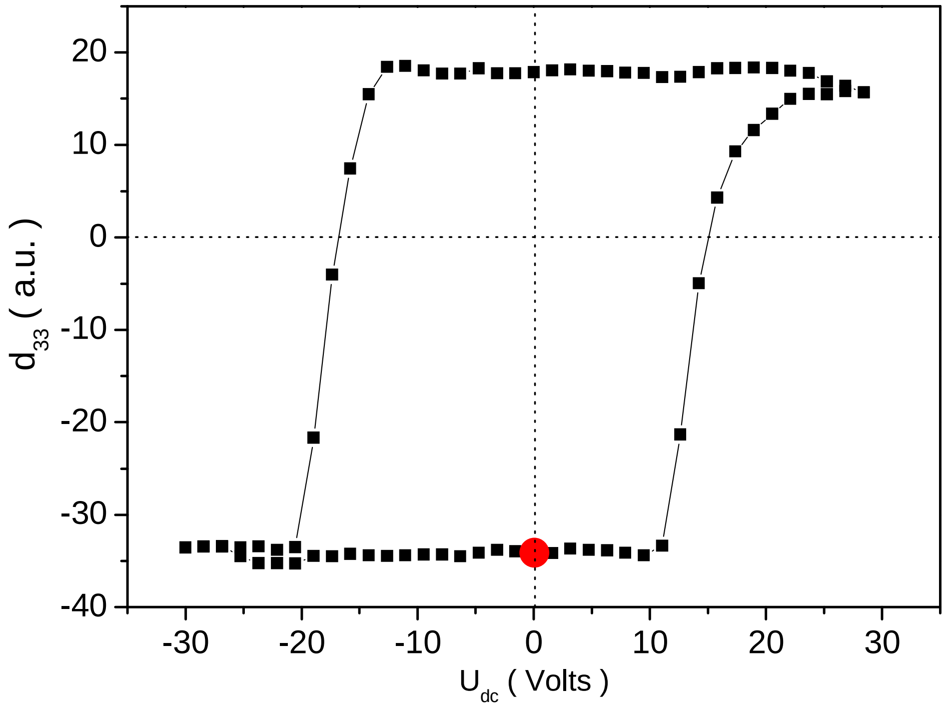

Vertical vs. horizontal hysteresis

piezoresponse vs. V_{dc}

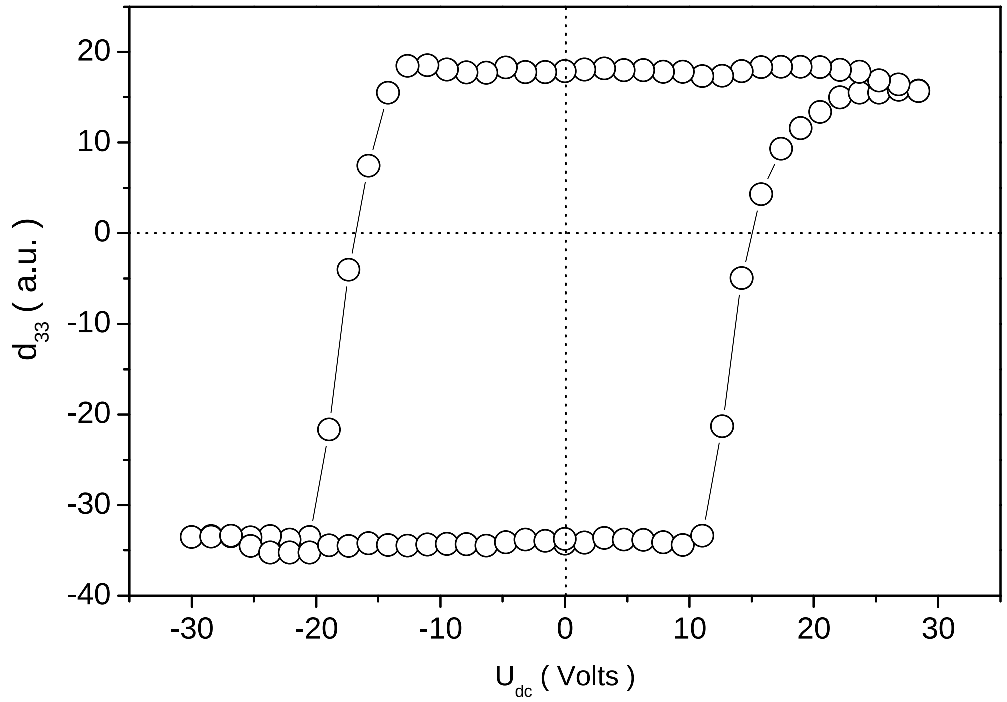

domain size vs. V_{dc}

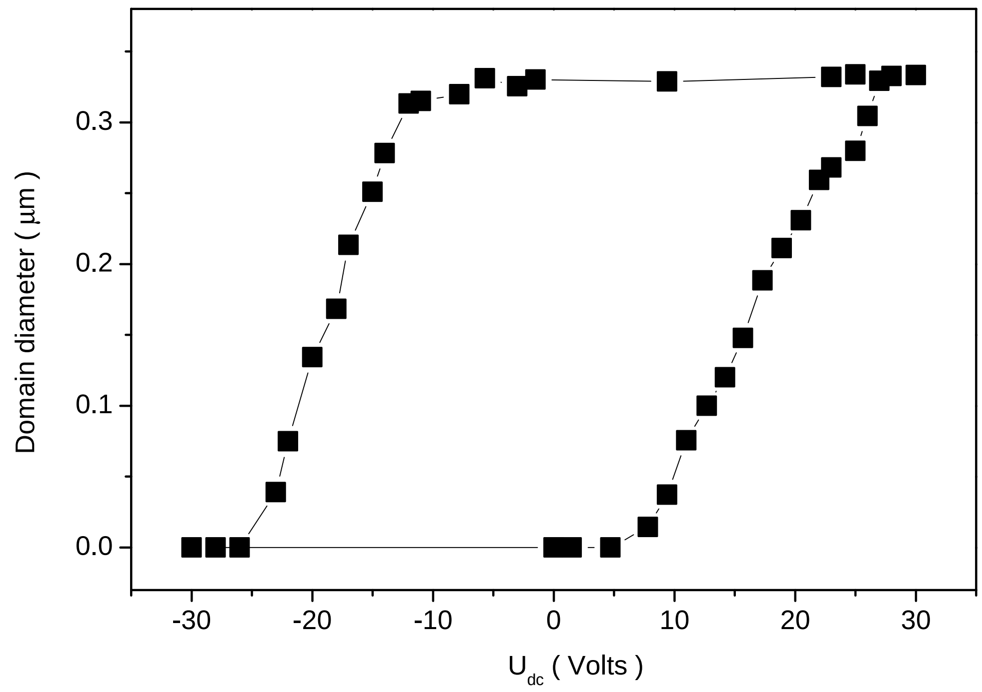

$$V_{out}=\alpha d_{33}V_{ac}f[l(V_{dc})]$$

$$r(V_{dc})=[S(V_{dc})/\pi]^{1/2}$$

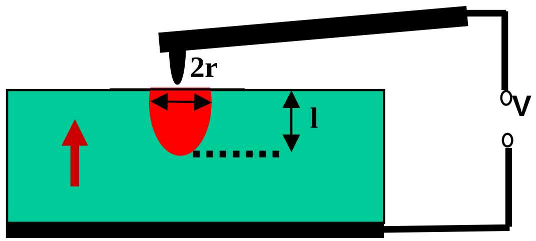

Effect of PZT composition

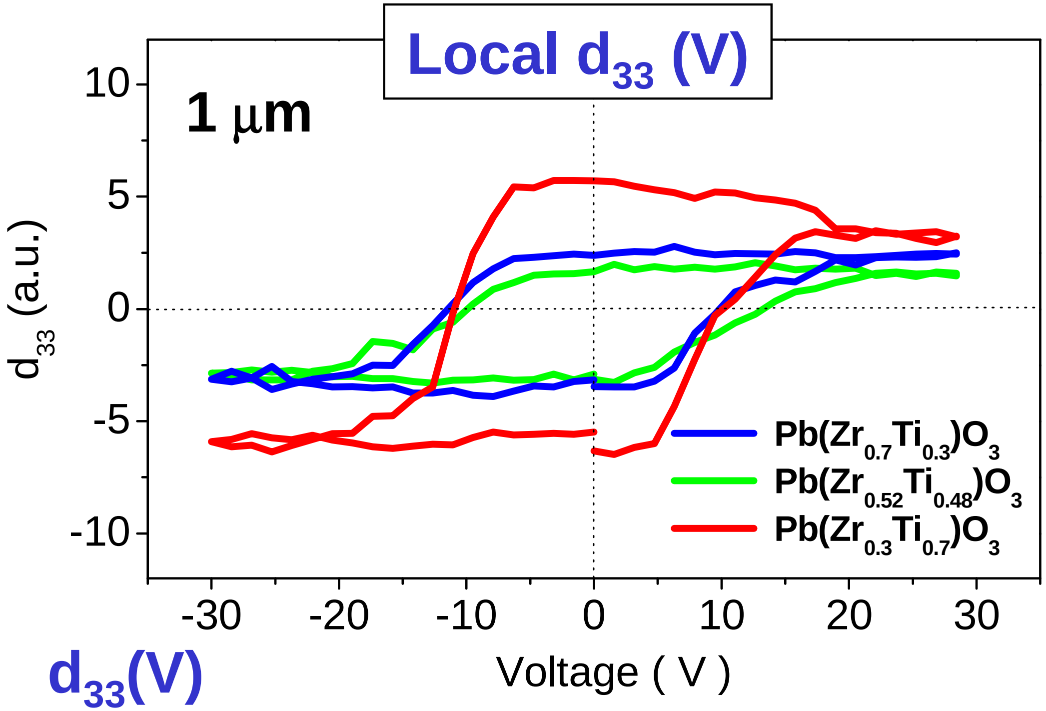

PZT films
1 μm, sol-gel
INOSTEK

d_{33}(V)

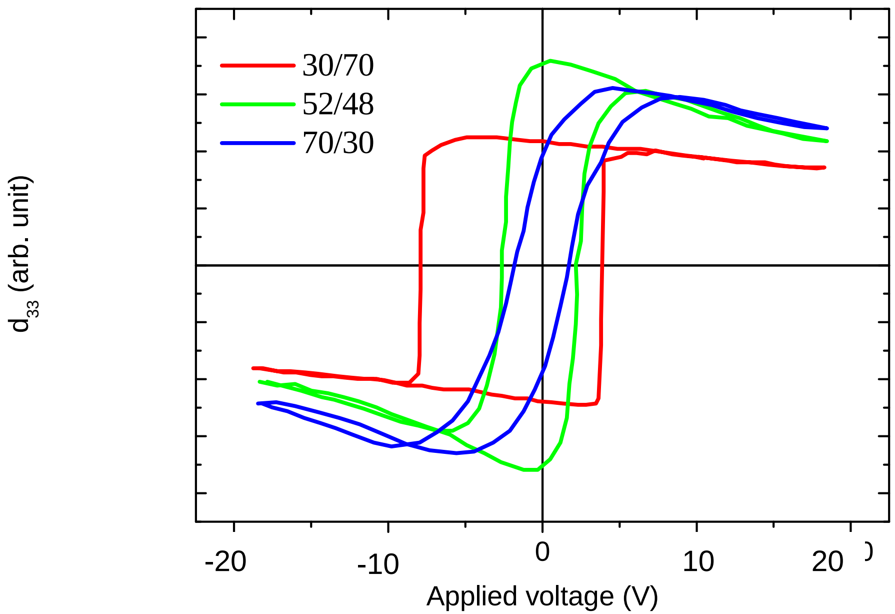

P(V)

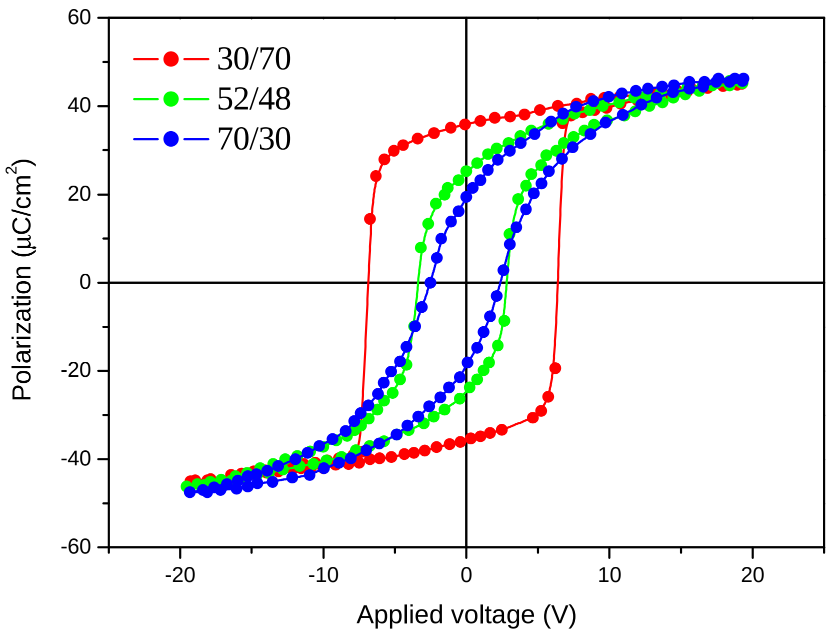

Bdikin et al, J. Electroceram. (in press)

Effect of dielectric constant

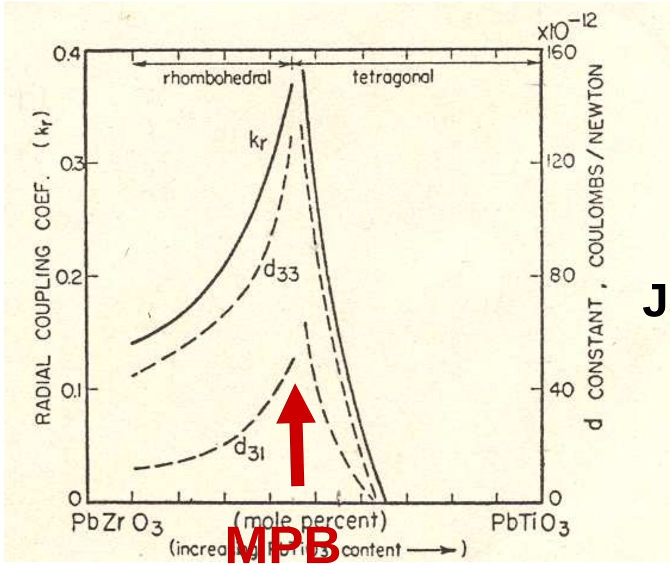

Jaffe et al., J. Appl. Phys. (1954)

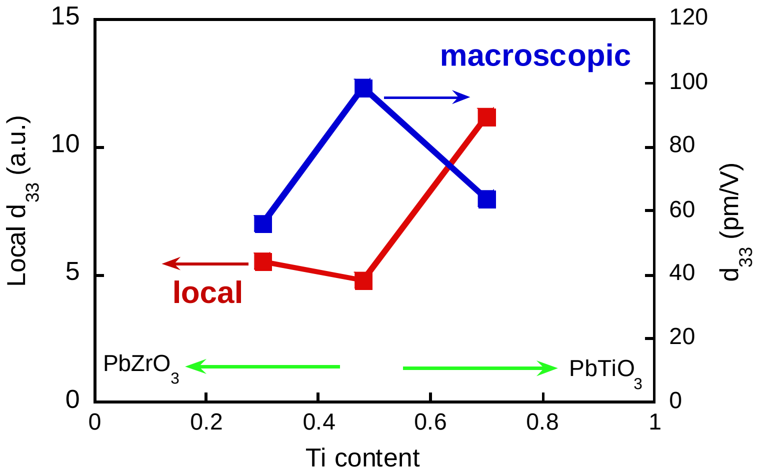

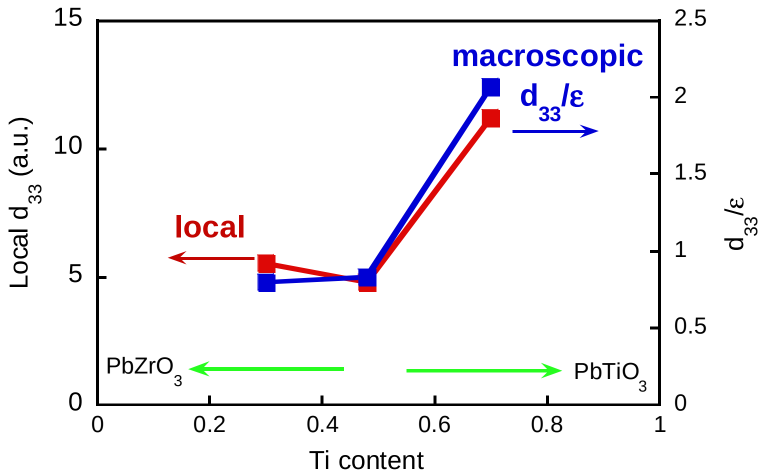

- **Local d_{33} is inversely proportional to dielectric constant**

$$(d_{33})_{eff} \propto \frac{A_{1\omega}}{V_{ac}} = \frac{A_{1\omega}}{1+\dfrac{\delta\varepsilon}{d\varepsilon_{\delta}}}$$

Effect of topography

Macroscopic loop

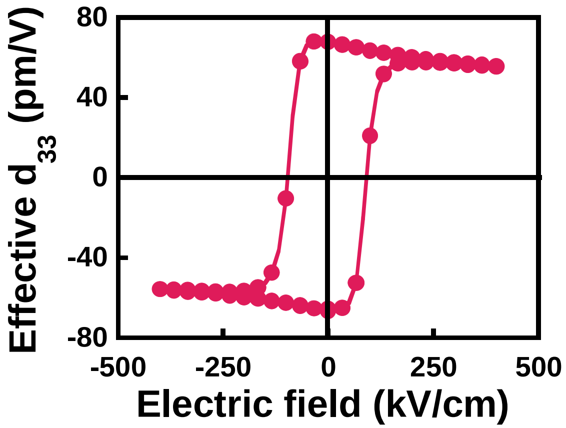

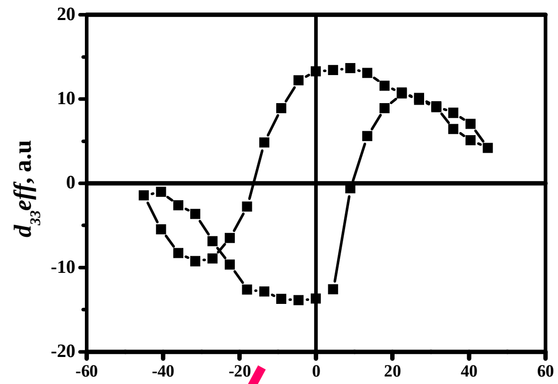

Nanoscale loops

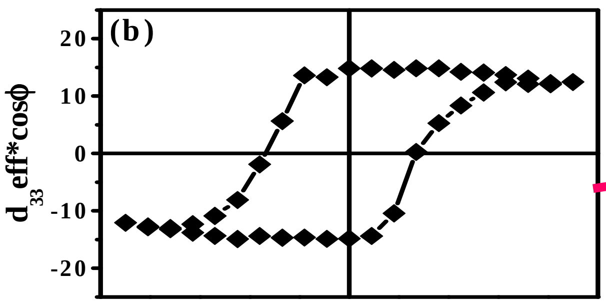

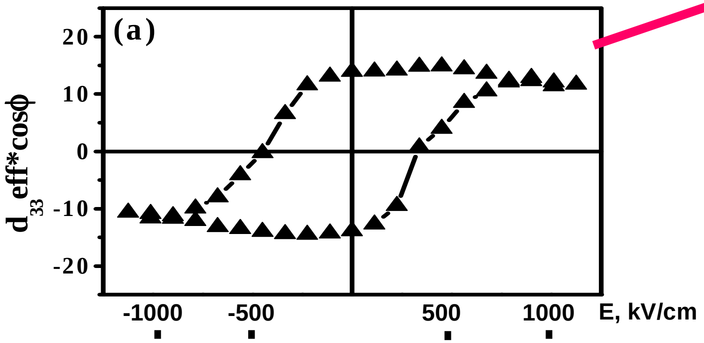

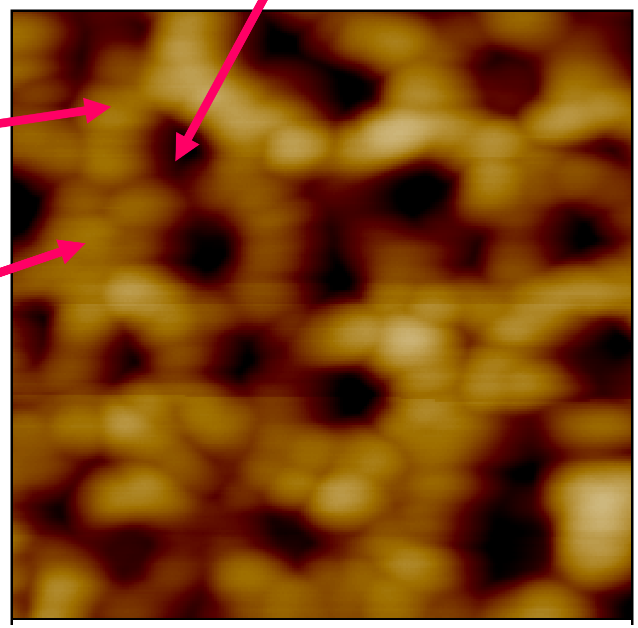

$PbTiO_3$: 24%Ca

Shvartsman et al., Ferroelectrics (2003)

Domains in Airvillius-type materials

Ferrodistortive Ferroelectric	$570 < T_{c2} < 650$ K → 2nd order	Ferrodistortive Paraelectric	$770 < T_{c1} < 800$ K → 2nd order	Paraelastic Paraelectric
$A2_1am$		$Amam$		$I4/mmm$

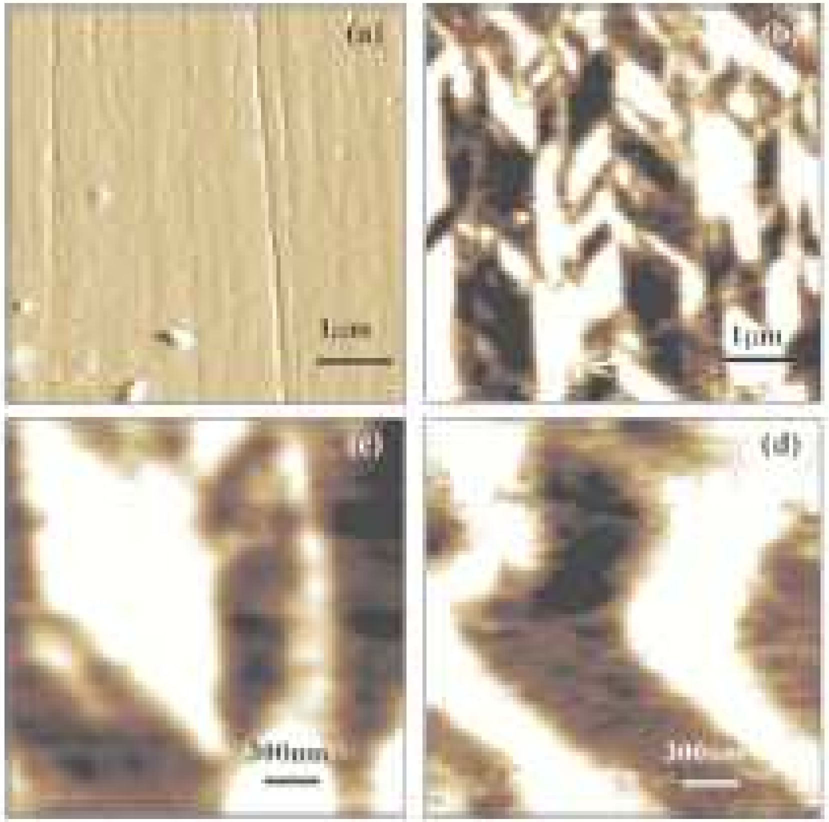

FIG. 2. (Color online) Topography (a) and lateral piezoresponse images (b)–(d) obtained for the (001) face of SBT crystal. The image (d) was acquired after rotating the sample by 90° relative to its position in image (c).

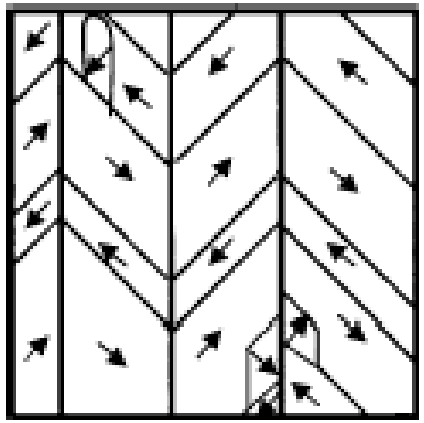

FIG. 3. Reconstructed domain structure of the SBT single crystal. The cross section of domain pattern in the *ab* plane is depicted. Arrows show the polarization directions.

Amorin et al., Appl. Phys. Lett. (2006)

Phase diagram of PZN-PT

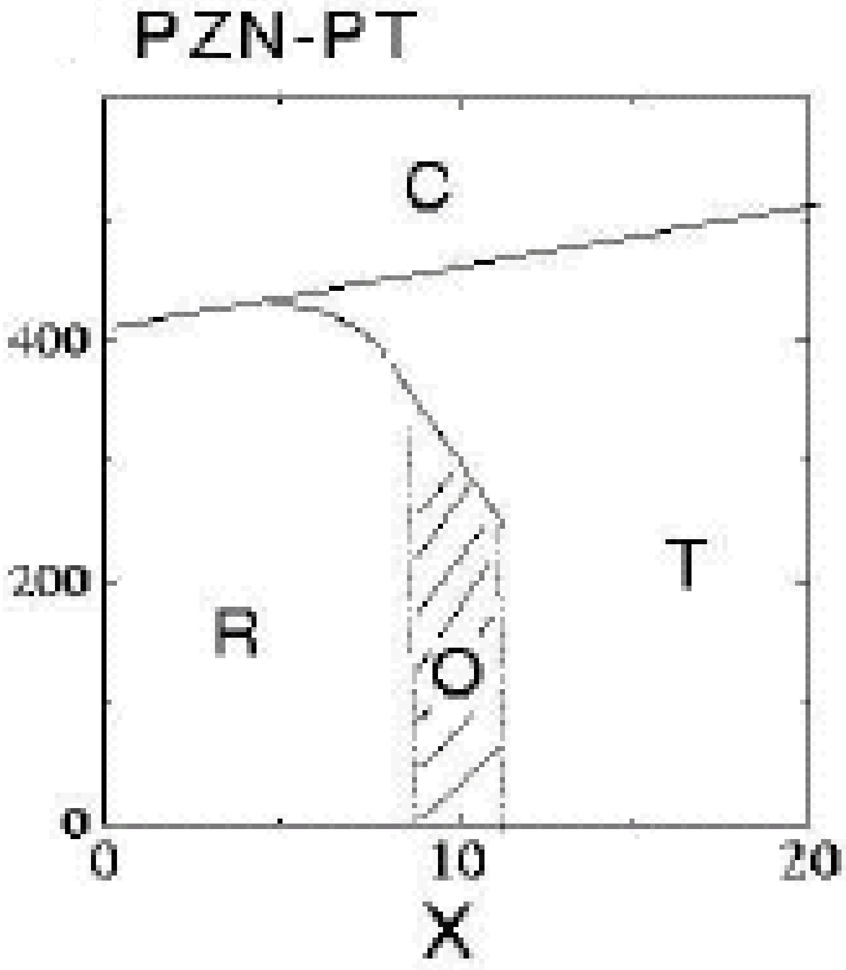

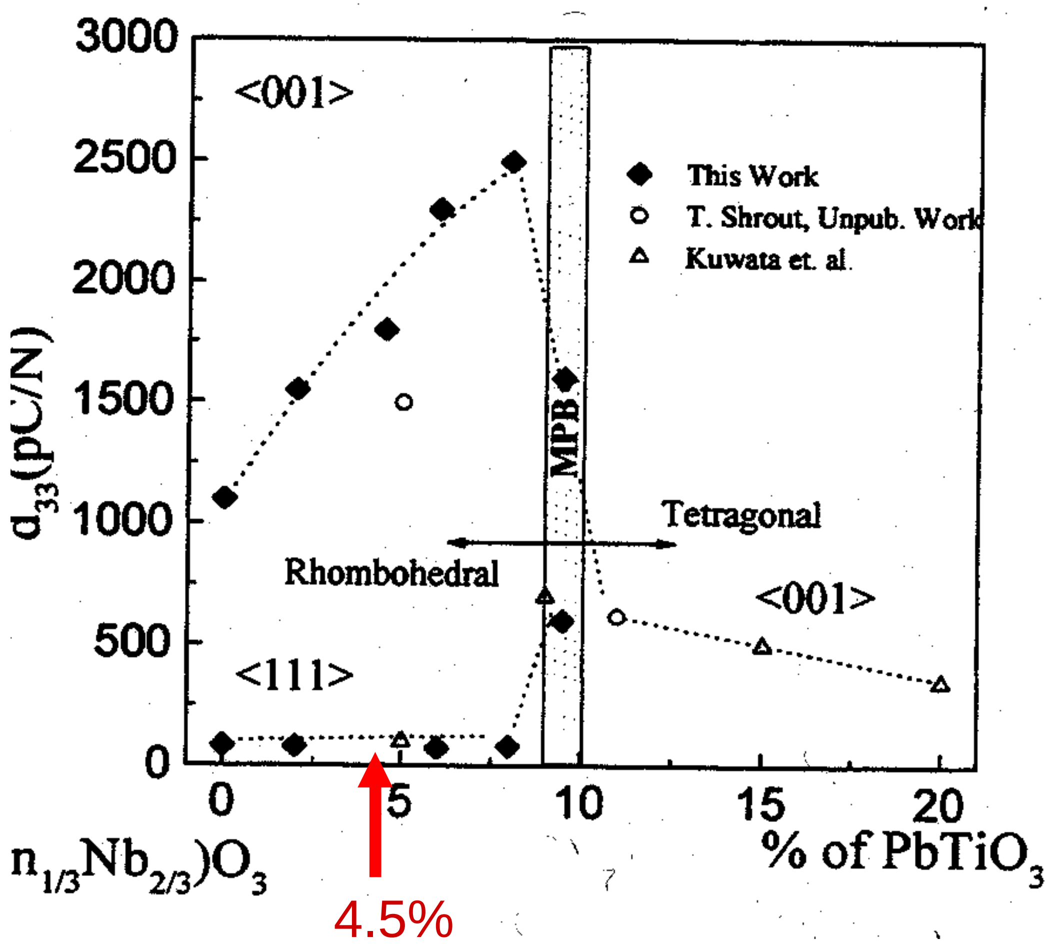

(001)

(111)

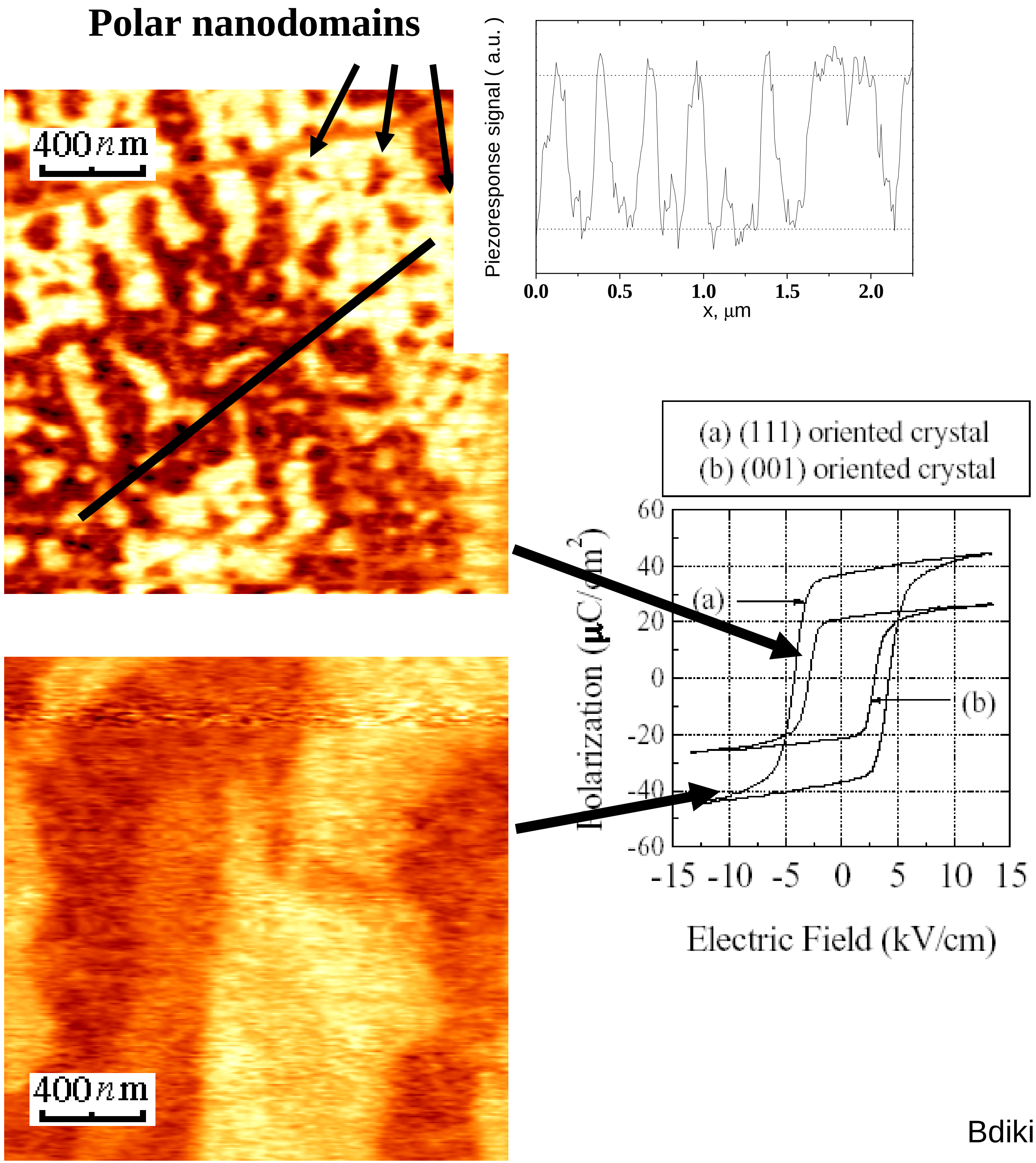

Bdikin et al, APL (2003)

Poling by the tip

virgin +30 V, 10 s +90 V, 20 s

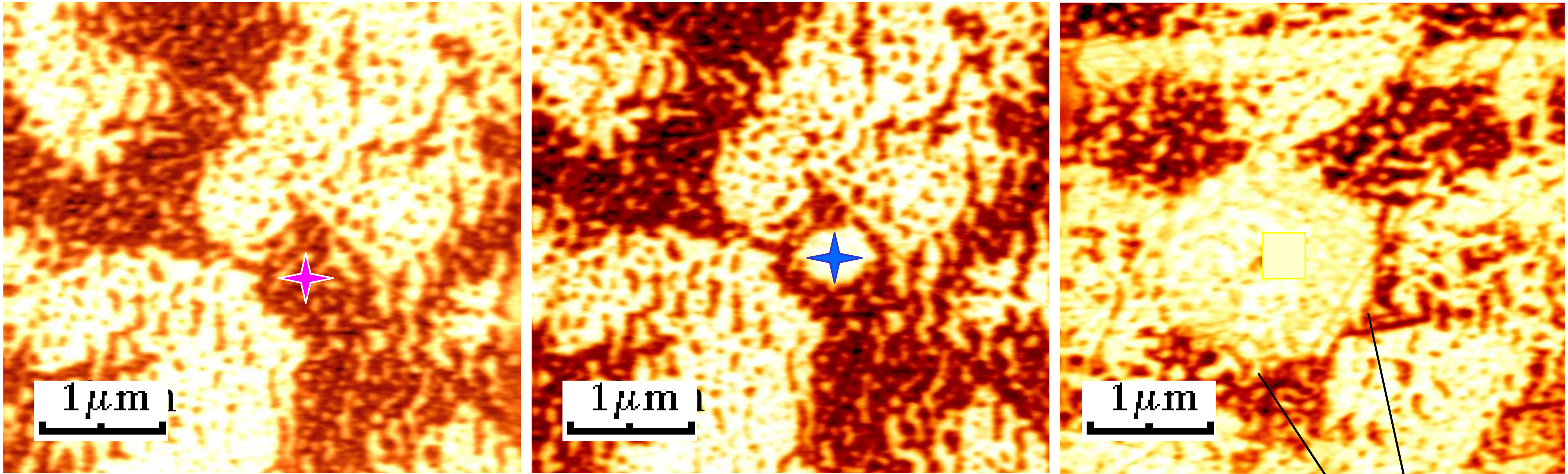

Faceted domain walls

- **Poling does not remove nanodomains**
- **“Normal” micron-sized domains can be written**

Bdikin et al, APL (2003)

Hysteresis comparison

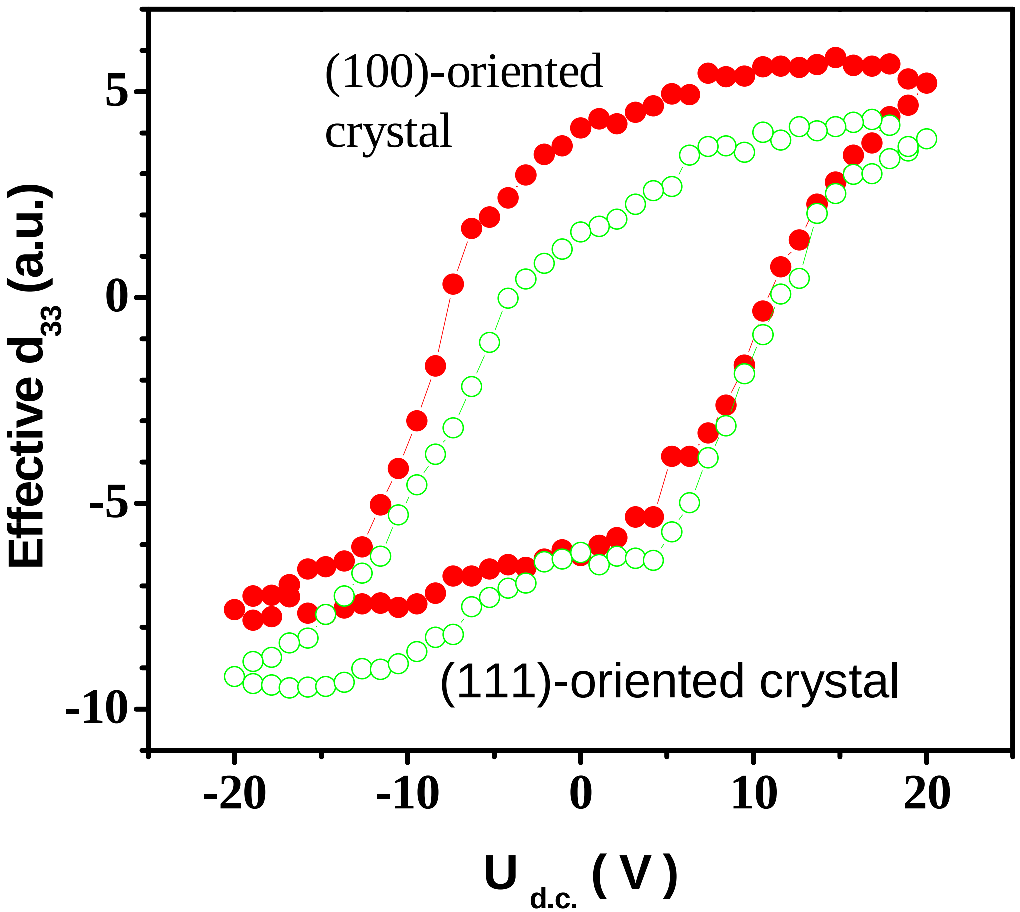

- **Local properties are comparable** ➡ **giant piezoresponse is related to nanodomains**

Mechanical stress effect on hysteresis

Soft PZT

depoling

Depinning of domain walls

Hard PZT

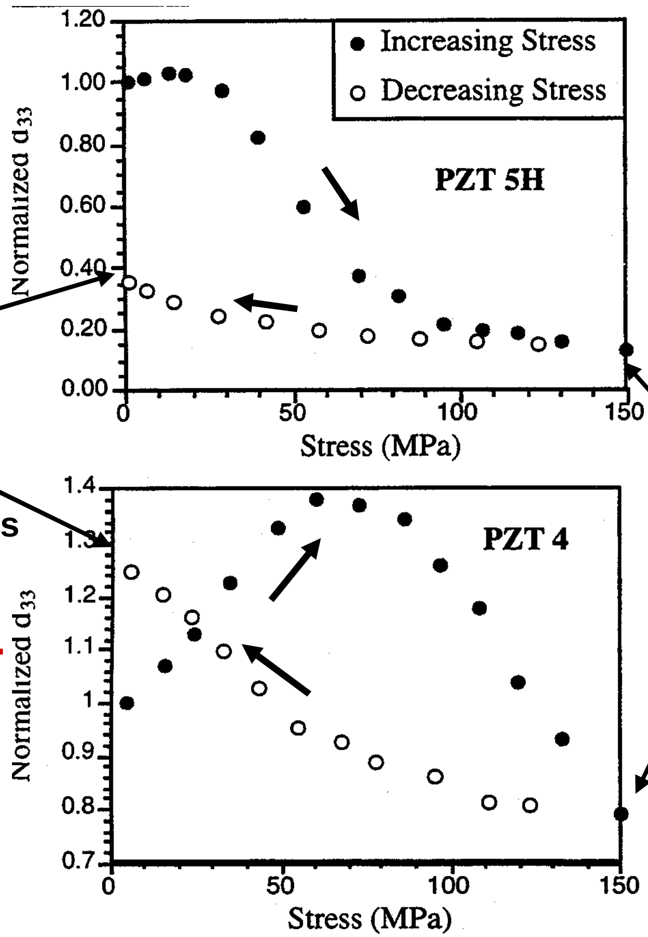

ferroelastic switching

Zang et al, J. Mater. Res. 12, 236 (1997)

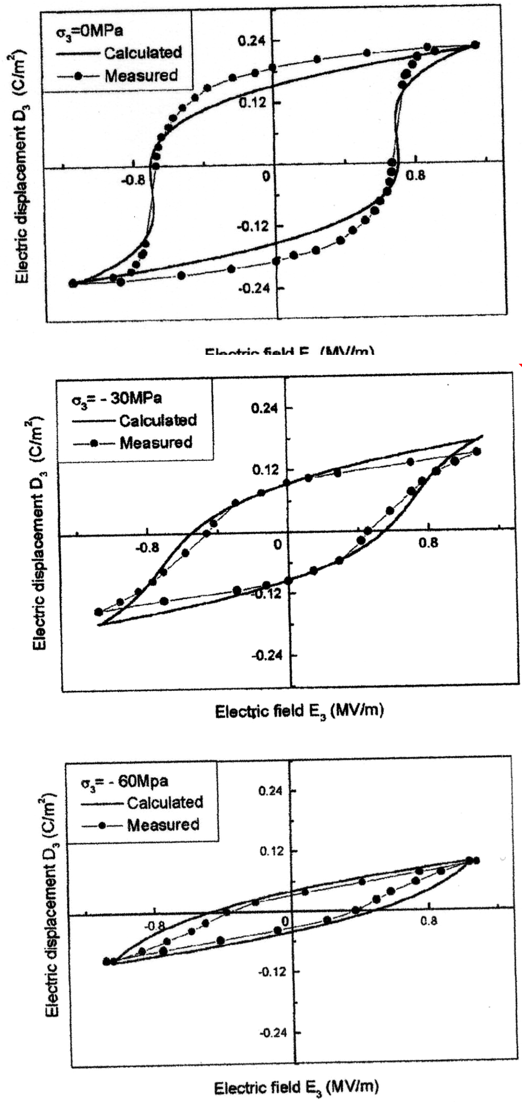

-30 MPa

-60 MPa

Fang & Li, J. Mater. Sci. 34, 4001 (1999)

- Compressive strain (| | P) results in depoling (soft PZT) through ferroeleastic domain wall motion

Stress by PFM: $PbTiO_3$-La films

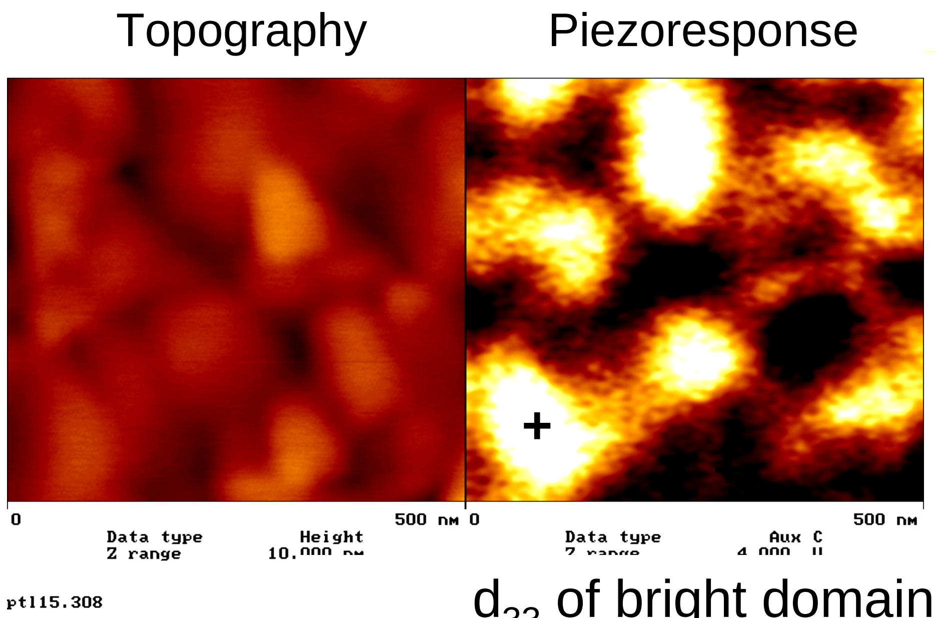

- Sol-gel spin-on technique
- Thickness ≈340 nm
- (001)/(100) preferred orientation
- Grain size 50-150 nm
- High piezoelectric anisotropy

d_{33} of bright domain vs. force

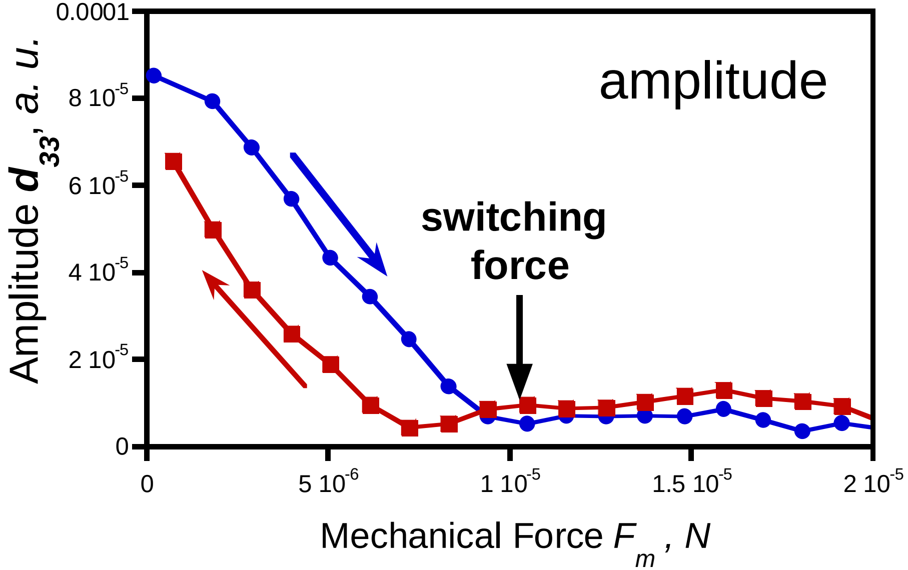

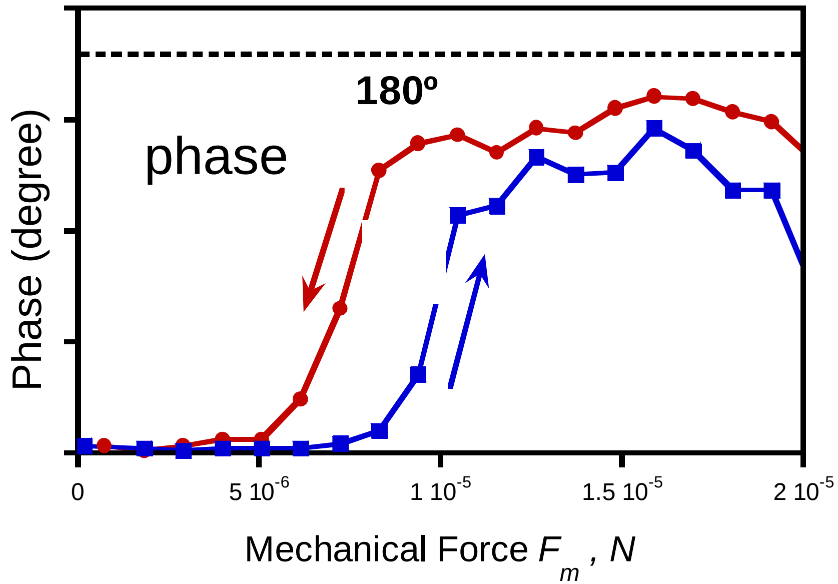

Kholkin et al, Appl. Phys. Lett. (2003).

Hysteresis suppression

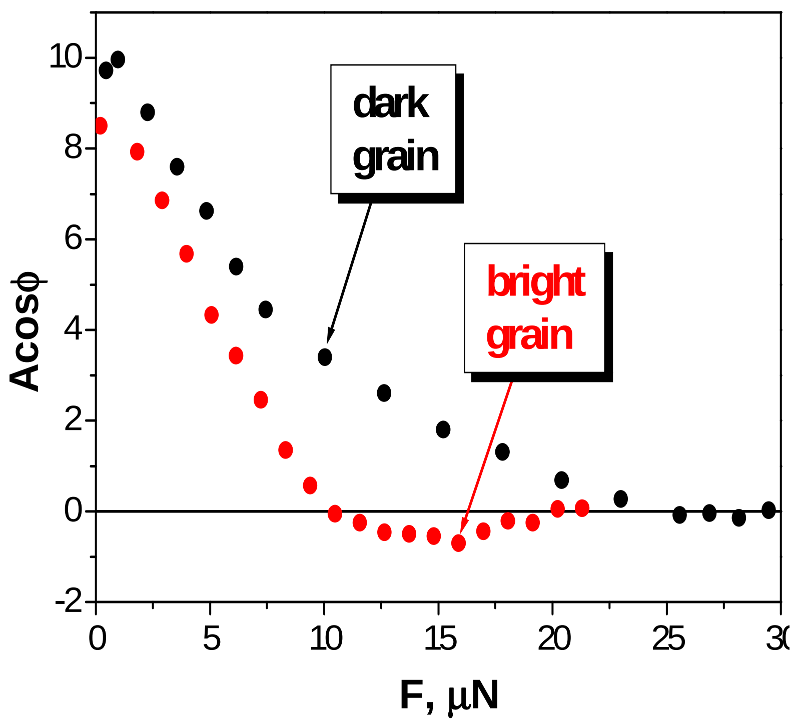

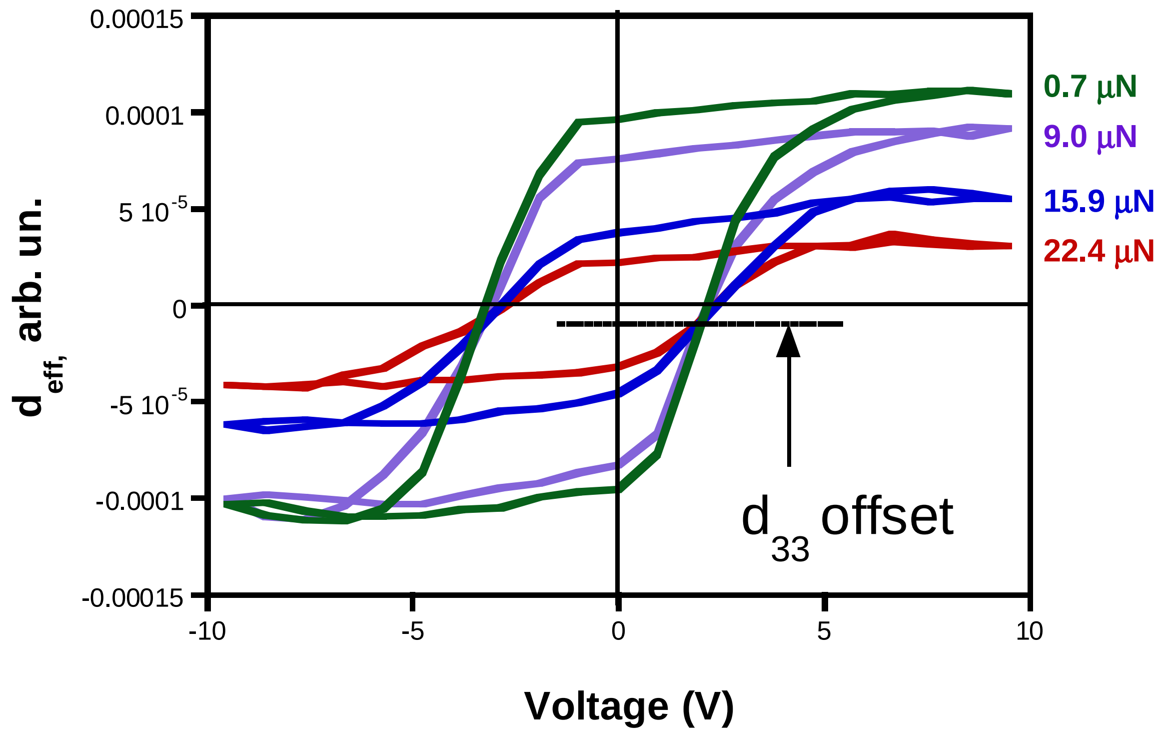

- d_{33} suppression depends on the initial contrast
- Hysteresis is suppressed with strong polarization offset

Kholkin et al, Appl. Phys. Lett. (2003).

Non-linear thermodynamic approach

σ_3

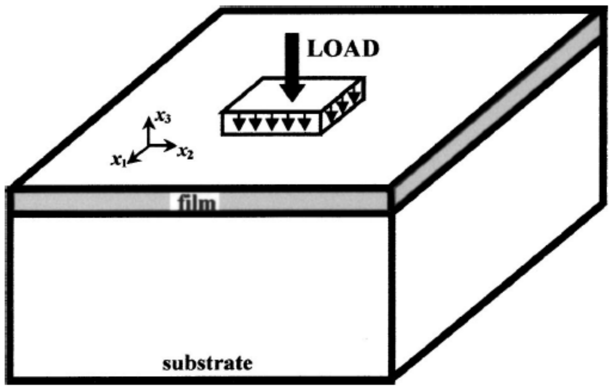

$$S_1 = S_2 = S_m = \frac{b^* - a_0}{a_0} = const$$

- misfit strain

$$S_6 = 0$$

Modified thermodynamic potential

$$\tilde{G} = G + S_1\sigma_1 + S_2\sigma_2 + S_6\sigma_6$$

$$\tilde{G} = \frac{(S_m - s_{12}\sigma_3)^2}{s_{11}+s_{12}} - \frac{1}{2}s_{11}\sigma_3^2 + a_1^*(P_1^2+P_2^2) + a_3^*P_3^2$$
$$+ a_{11}^*(P_1^4+P_2^4) + a_{12}^*P_1^2P_2^2 + a_{13}^*(P_1^2+P_2^2)P_3^2 + a_{33}^*P_3^4$$
$$+ a_{111}(P_1^6+P_2^6+P_3^6) + a_{112}[P_1^4(P_2^2+P_3^2) + P_2^4(P_1^2+$$
$$+ P_3^4(P_1^2+P_2^2)] + a_{123}P_1^2P_2^2P_3^2,$$

where $a_1^*, a_{ij}^*, a_{ijk}^*$ are dielectric stiffnesses at constant stress

e. g. $\quad a_1^* = a_1 - \frac{Q_{11}+Q_{12}}{s_{11}+s_{12}}S_m + \frac{Q_{11}s_{12}-Q_{12}s_{11}}{s_{11}+s_{12}}\sigma_3$

Renormalization leads to

$$\begin{cases} S_m^\sigma = S_m - (s_{11}+2s_{12})\sigma_3, \\ T_\sigma = T - 2\varepsilon_0 C(Q_{11}+2Q_{12})\sigma_3. \end{cases}$$

Emelyanov et al. , Phys. Rev. B (2003)

Phase diagrams under stress

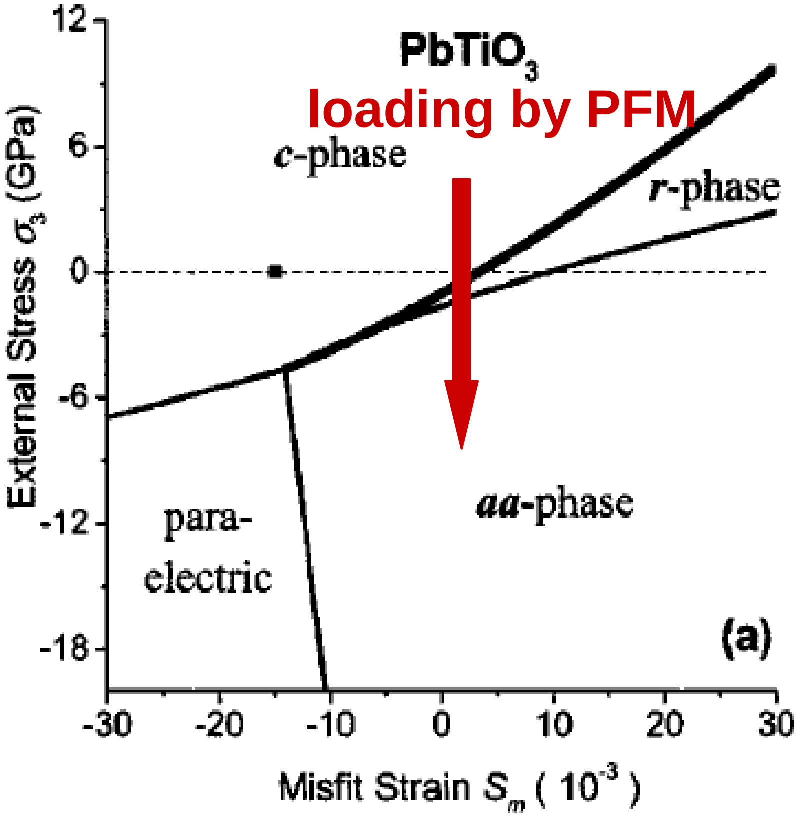

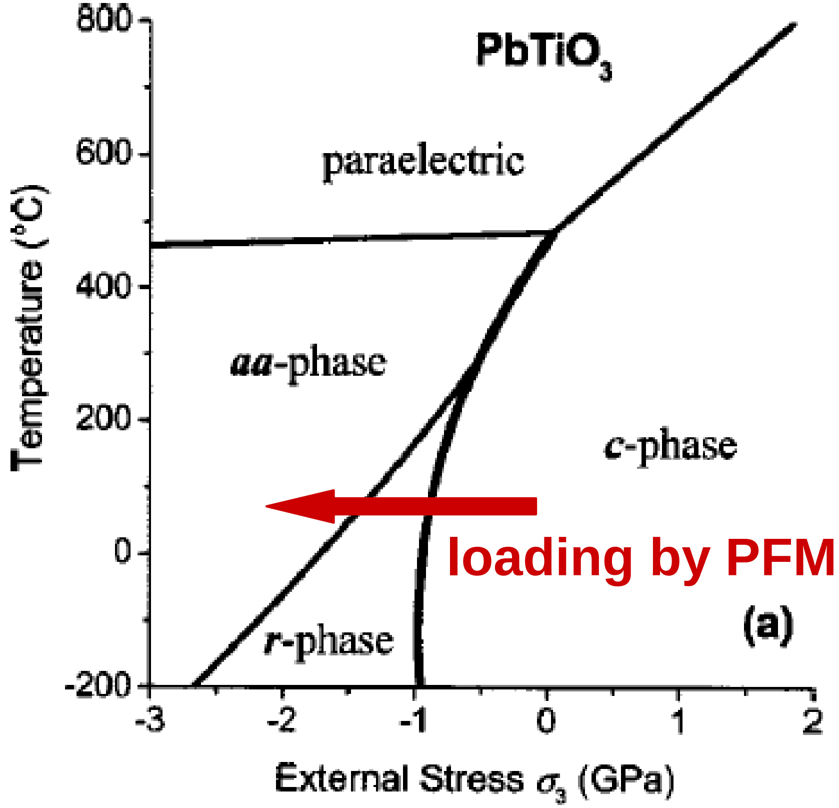

- **Phase transition into *r*- and *aa*-phases is possible under high compressive stress**

Emelyanov et al., Phys. Rev. B (2003)

Local parameters under stress

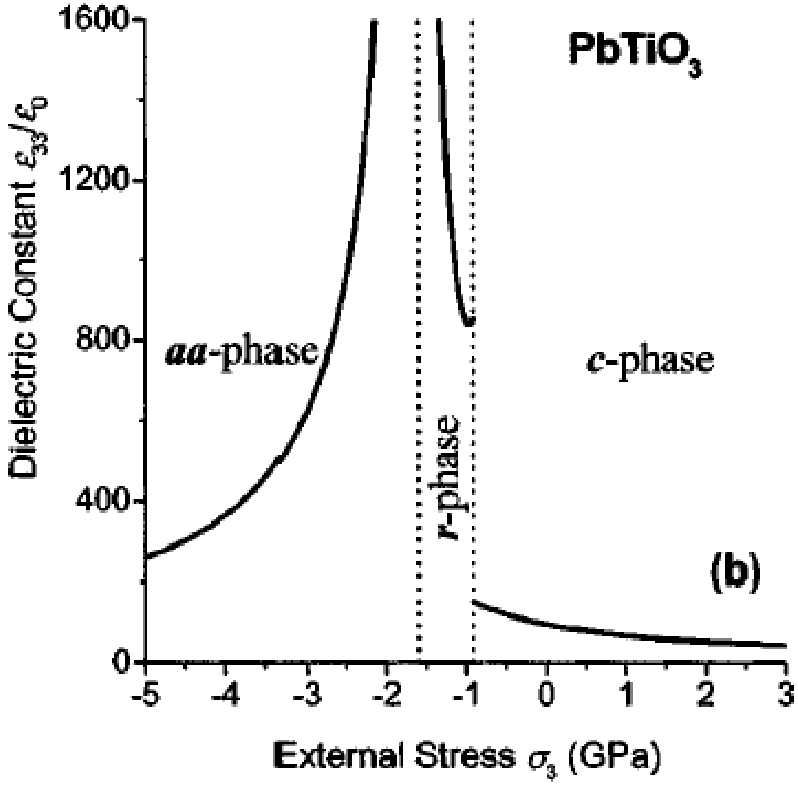

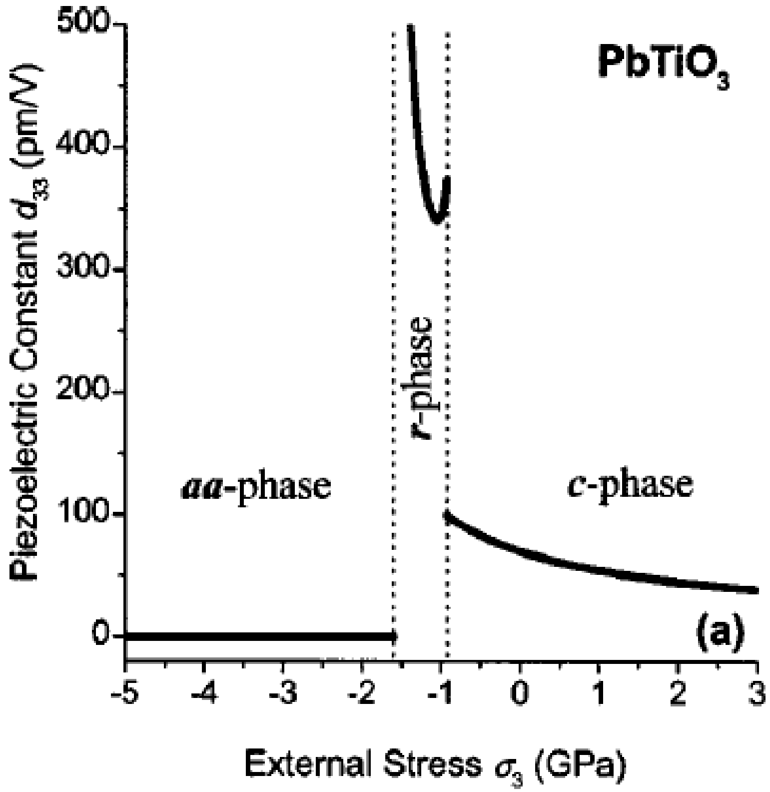

- **Proper stress design of microdevices may enhance materials properties near stress-induced phase transitions**

Emelyanov et al, Phys. Rev. B (2003)

Tentative explanation of asymmetry

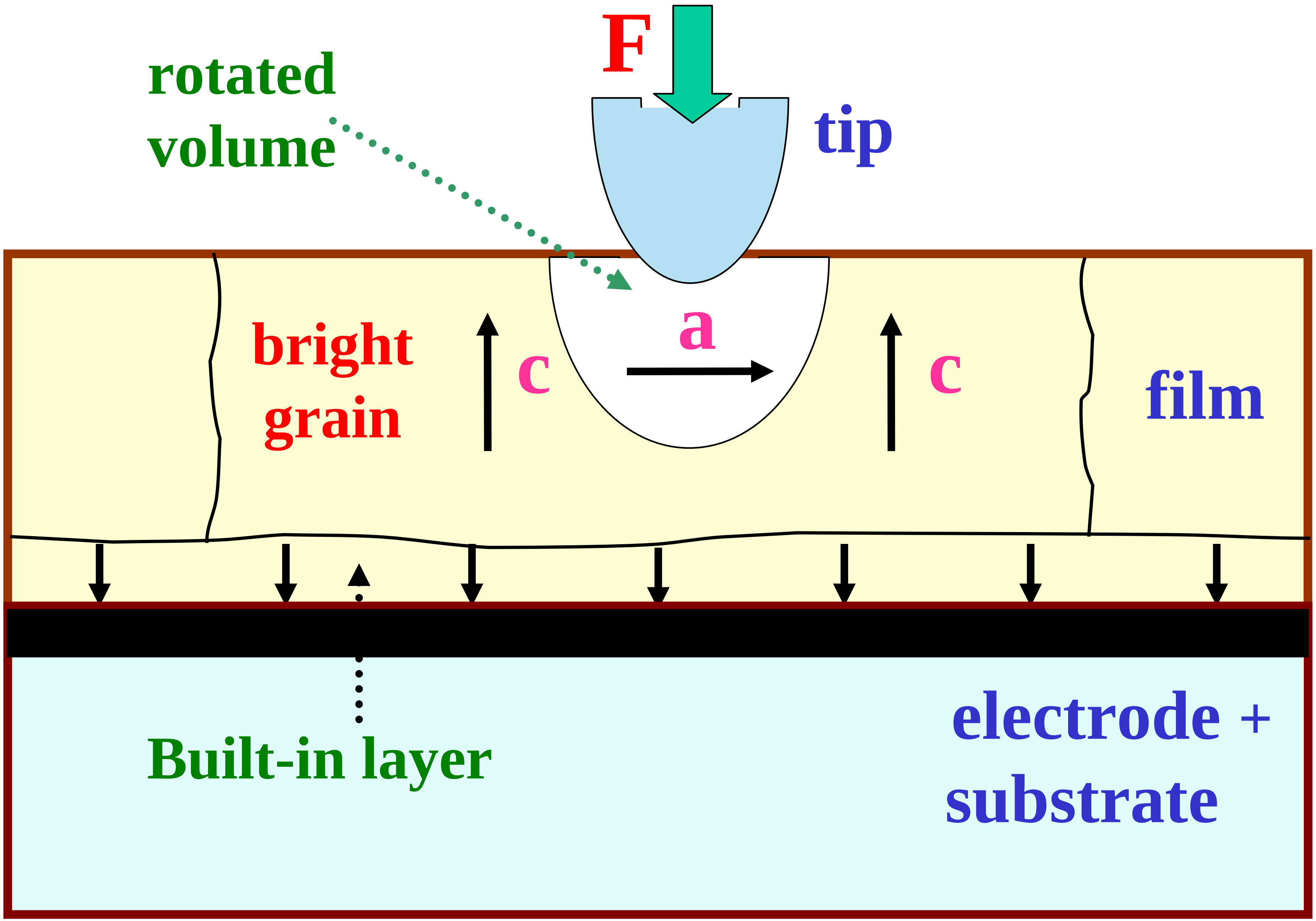

Mesoscopic disorder in relaxors

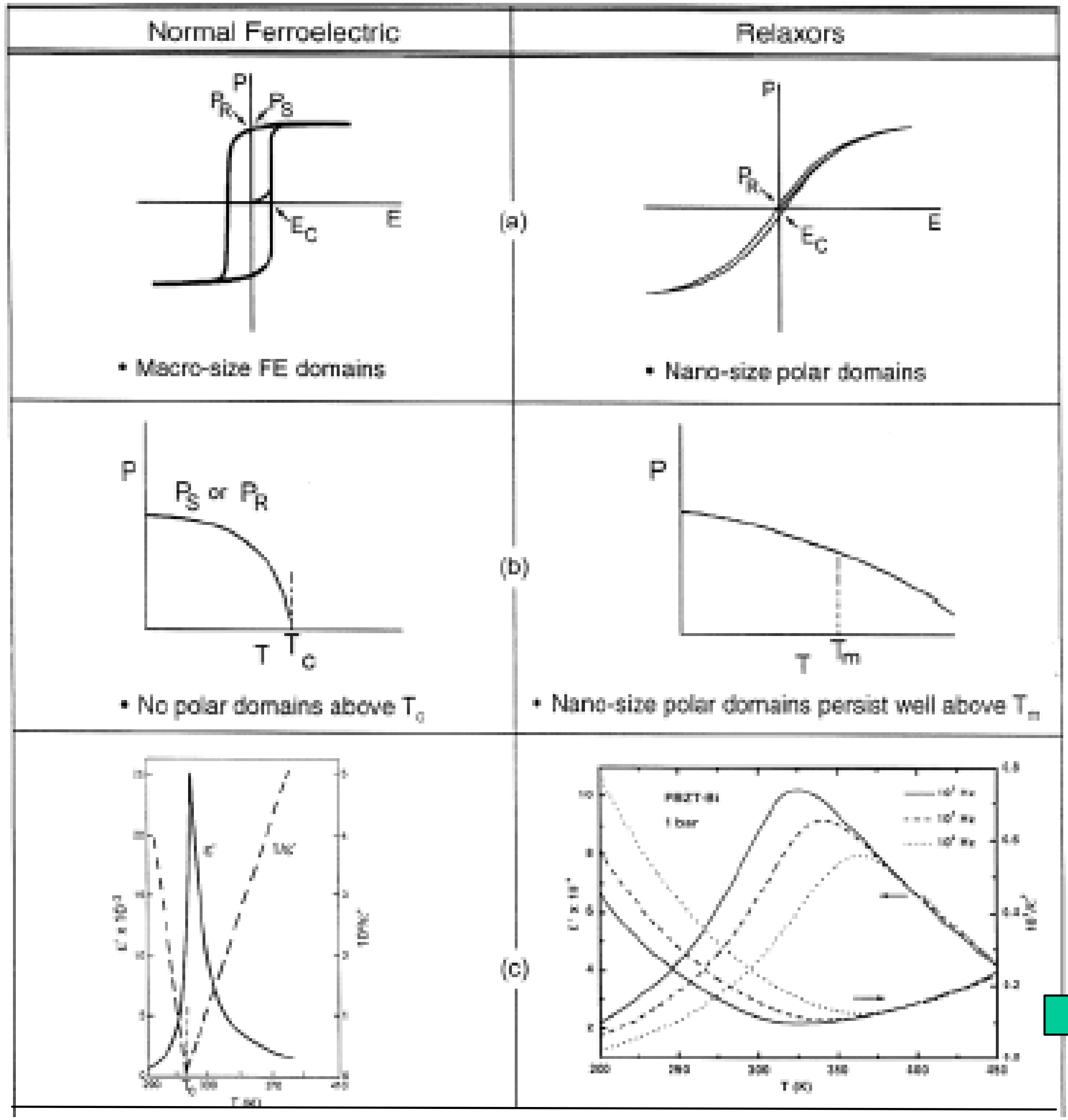

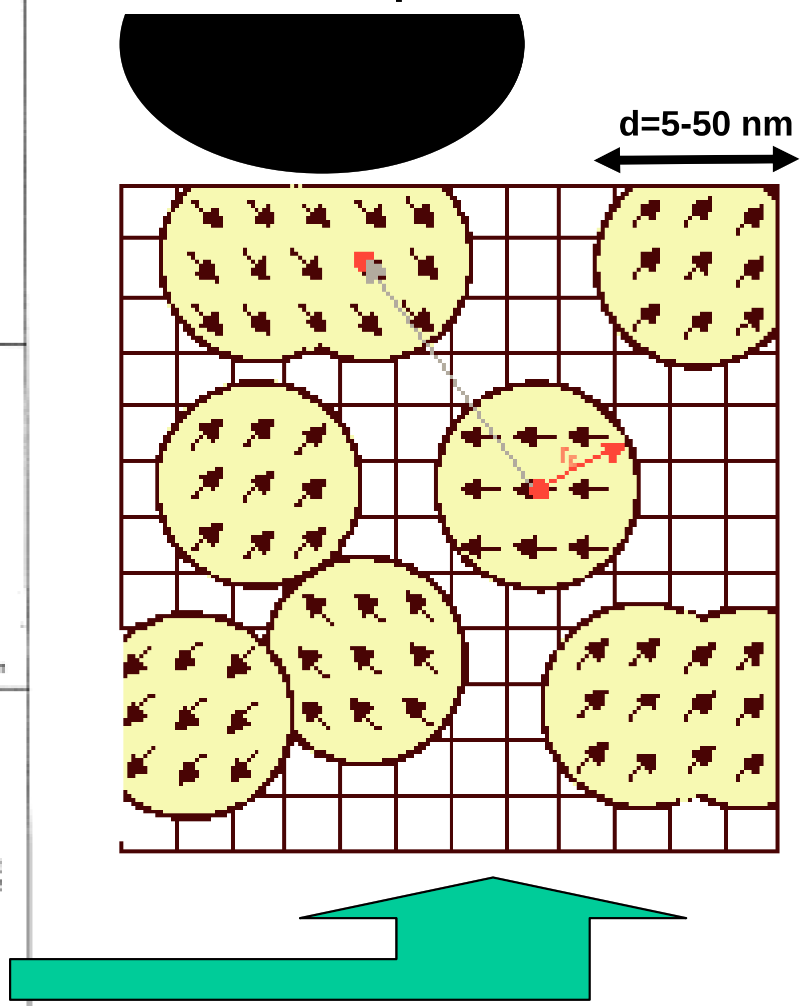

Polar clusters
(nanodomains)

Phase diagram of (Pb,La)(Zr,Ti)O_3

studied composition

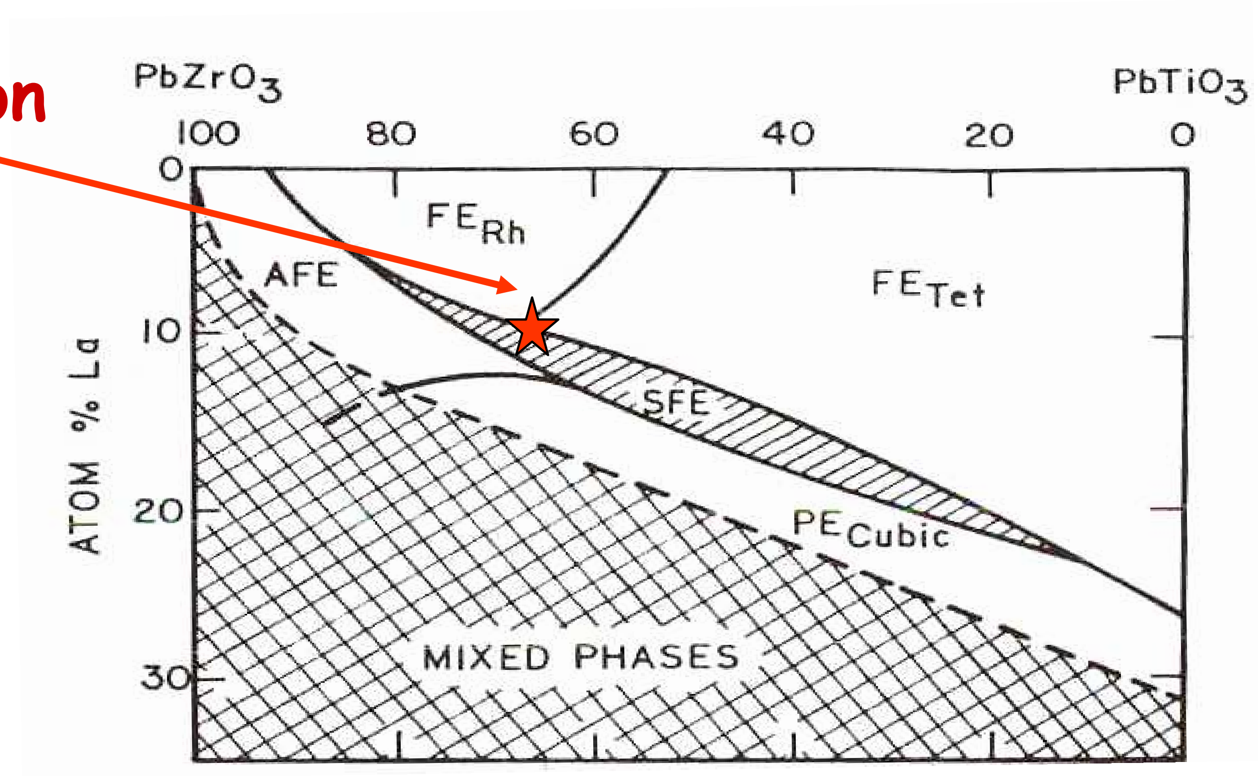

- **Relaxor "ergodic" cubic phase at room temperature**
- **No piezoelectric activity at large scale**

Domains in virgin ceramics

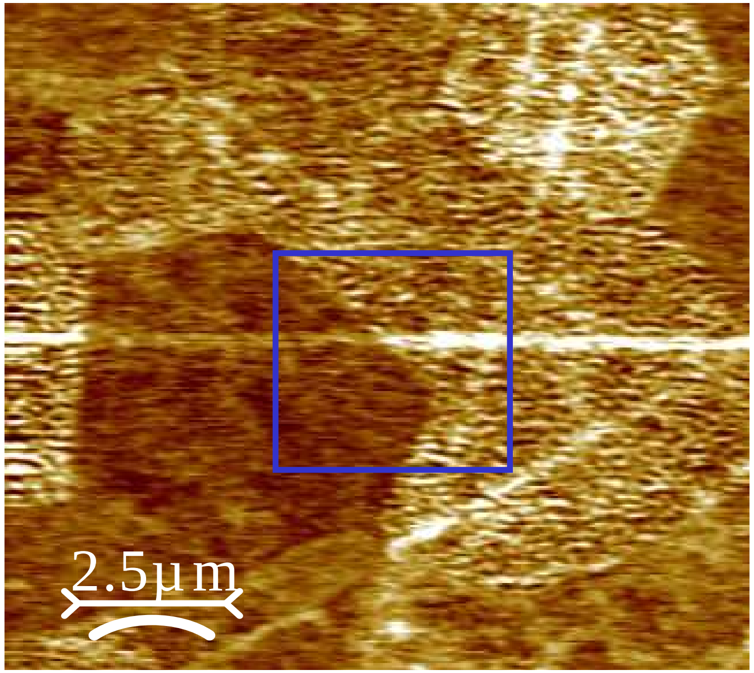

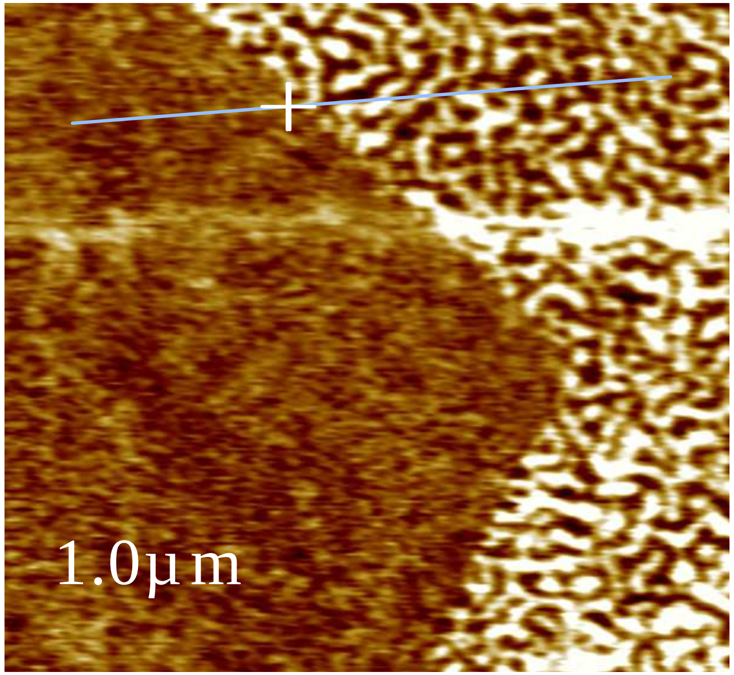

vertical piezoresponse

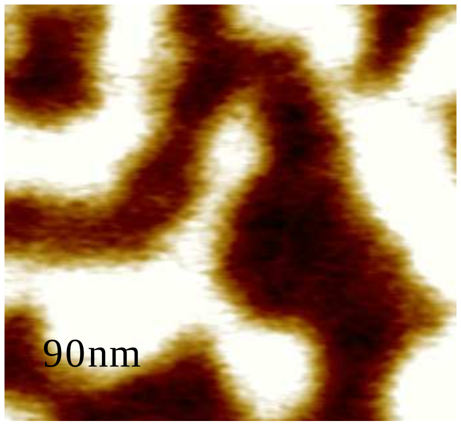

lateral piezoresponse

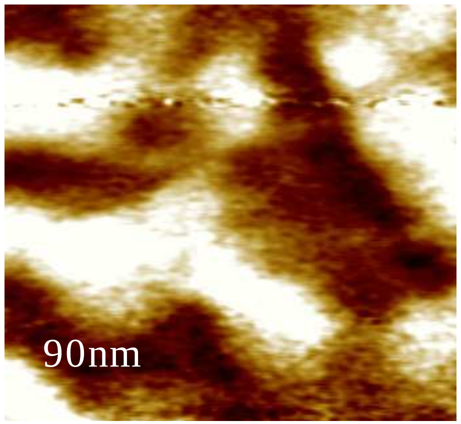

reconstructed domains

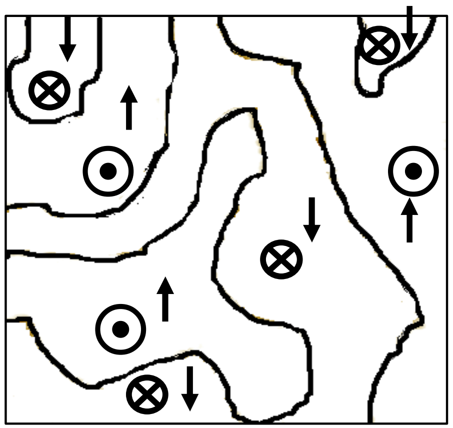

Poling and tip-induced phase transition

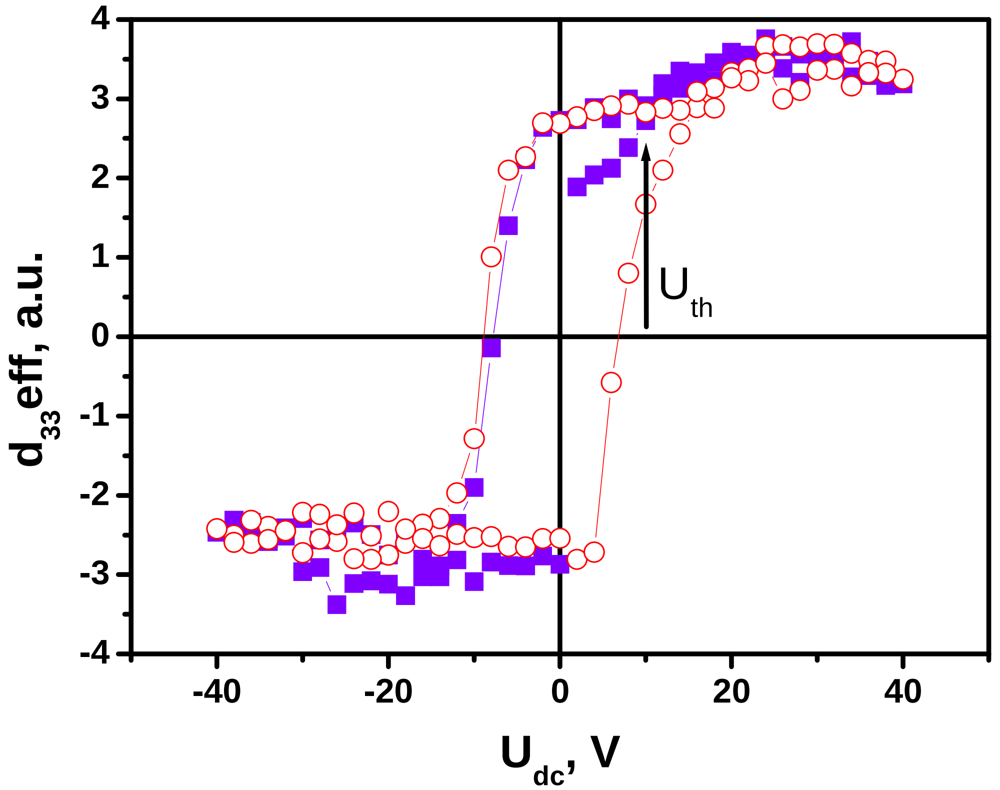

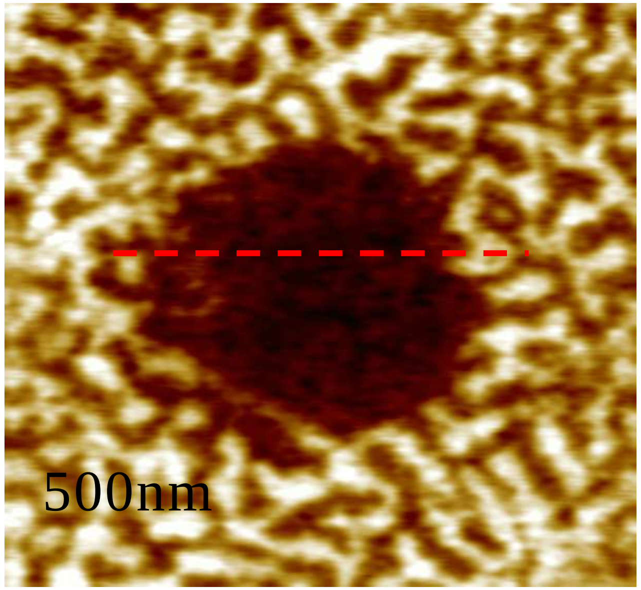

- **Threshold-like increase of piezoresponse signifies bias-induced phase transition**
- **Further hysteresis is due to evolution of ferroelectric phase**

Kholkin et al, APL (2005)

Polar nanoclusters in PMN-10%PT

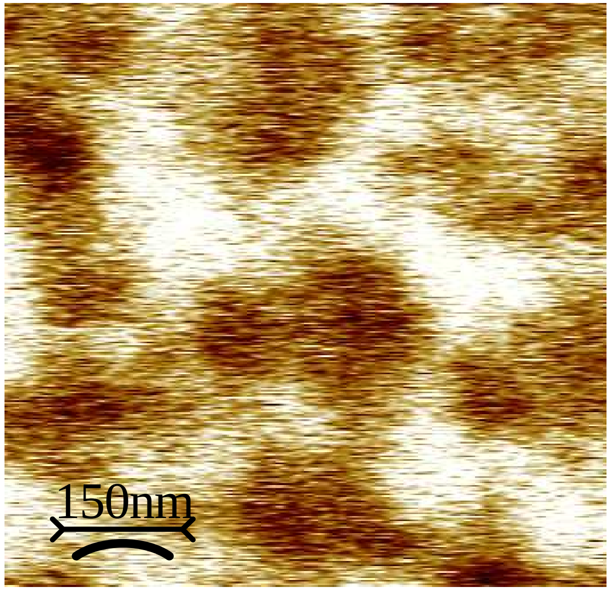

piezoresponse

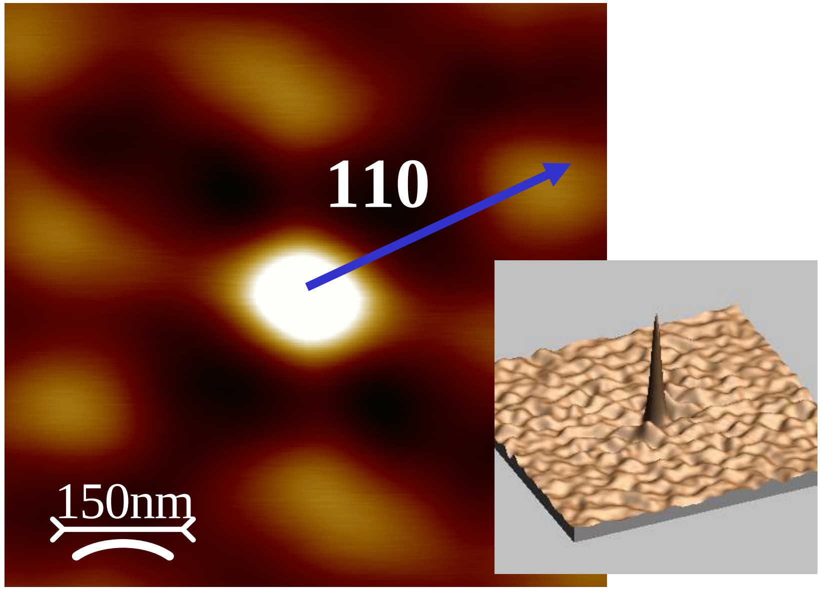

autocorrelation image of d_{33}

$$C(r_1, r_2) = \sum_{x,y} D(x, y) D(x + r_1, y + r_2)$$

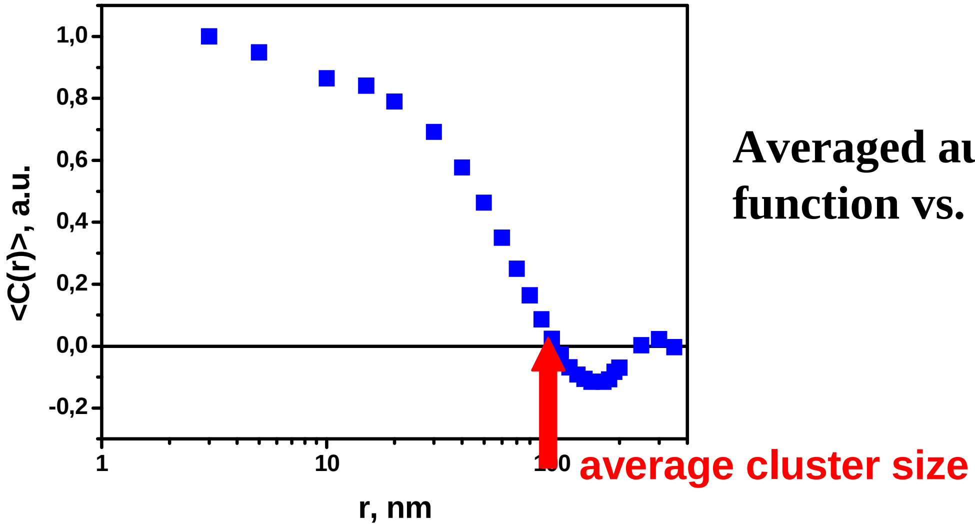

Averaged autocorrelation function vs. distance

Aging in ferroelectrics

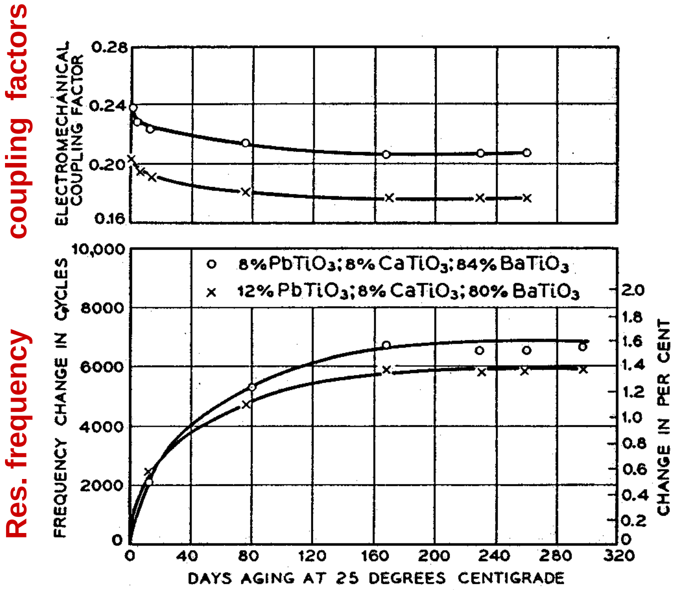

Mason (1954)

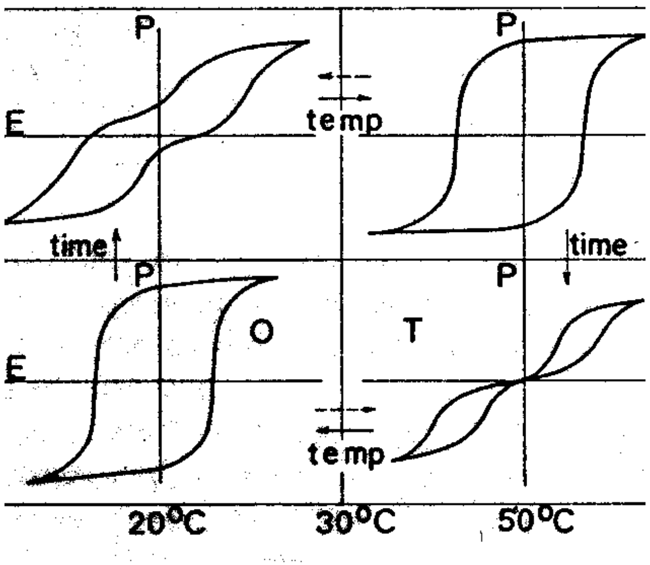

Jonker (1972)

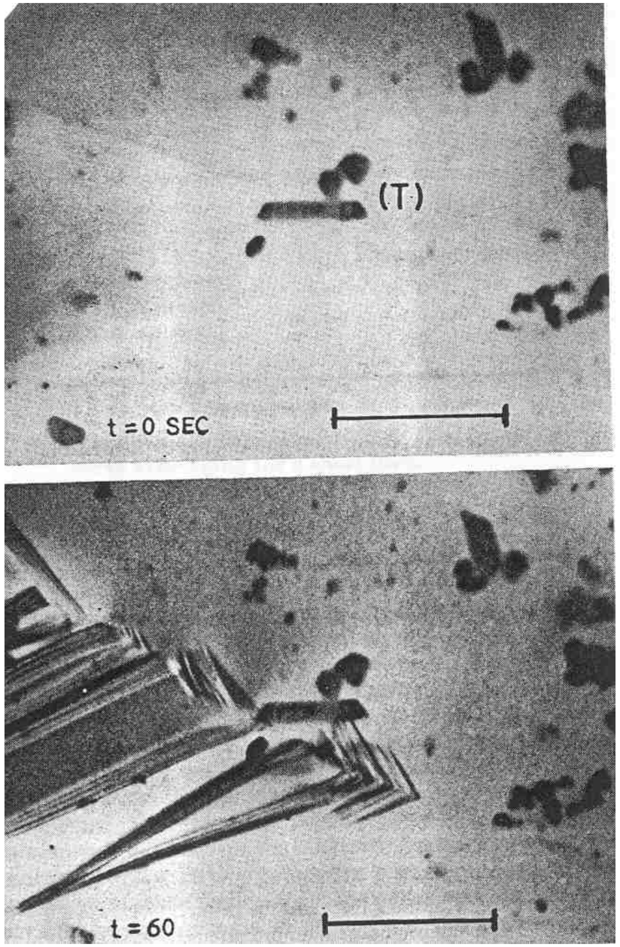

Bradt & Ansell (1968)

Formation of new 90º domain walls

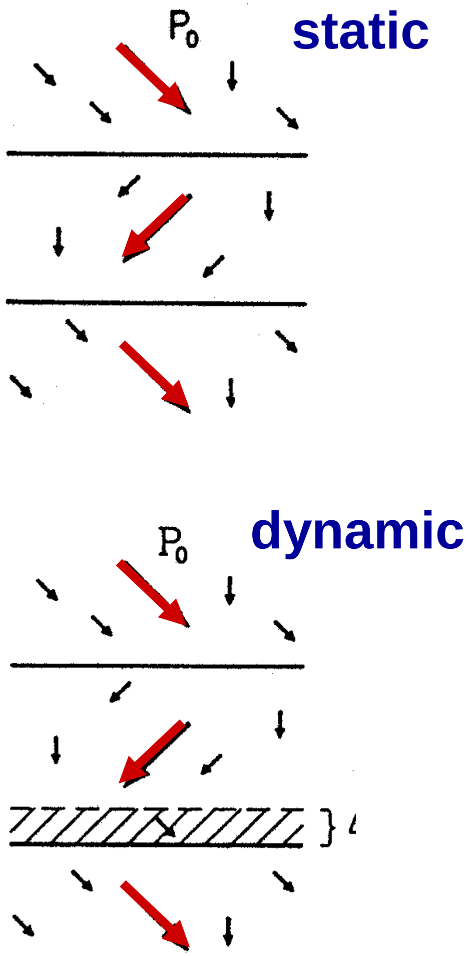

Robels & Arlt (1992)

Stabilization of existing walls by polar defects

Piezorelaxation at the nanoscale

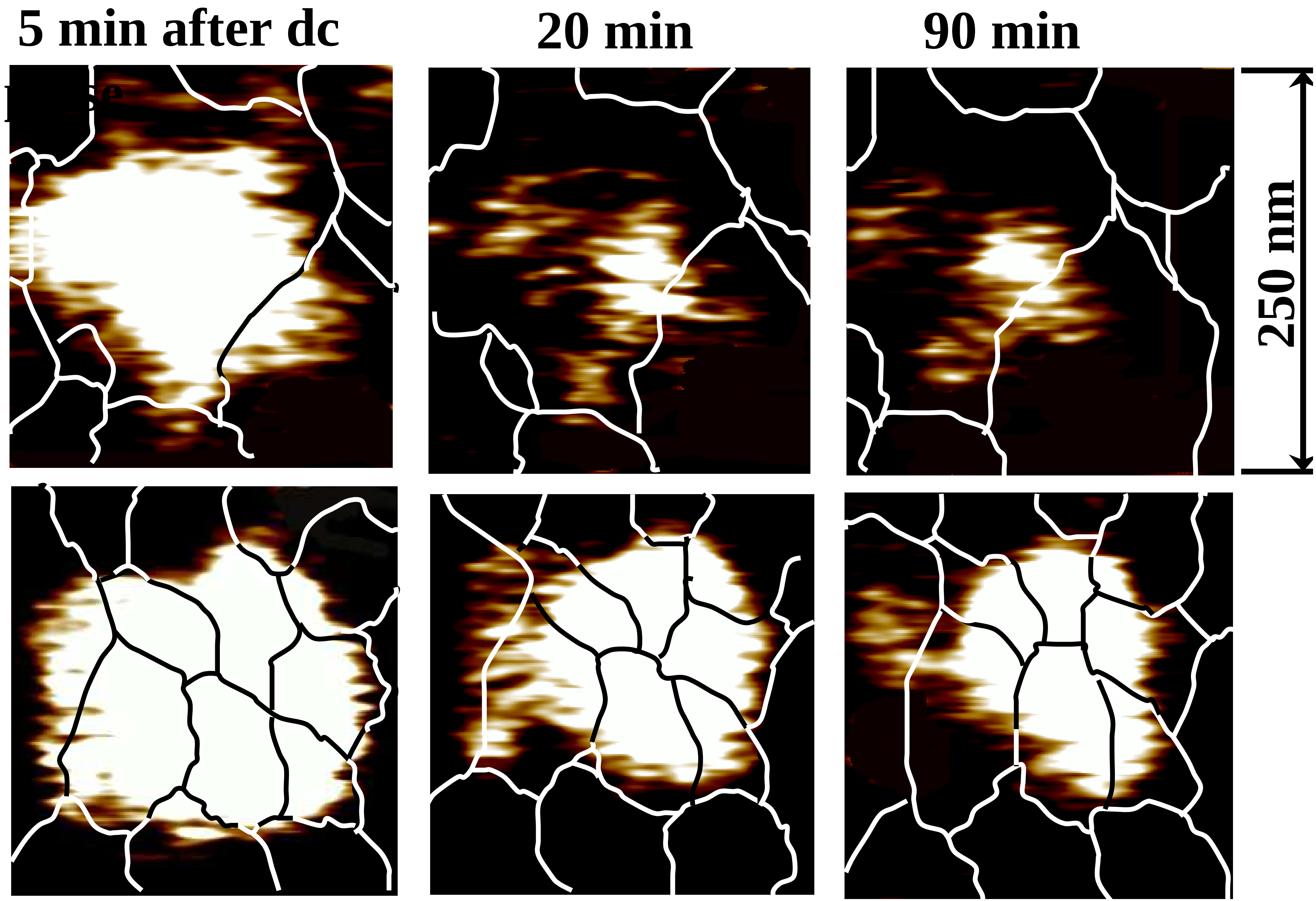

Piezorelaxation vs. grain size

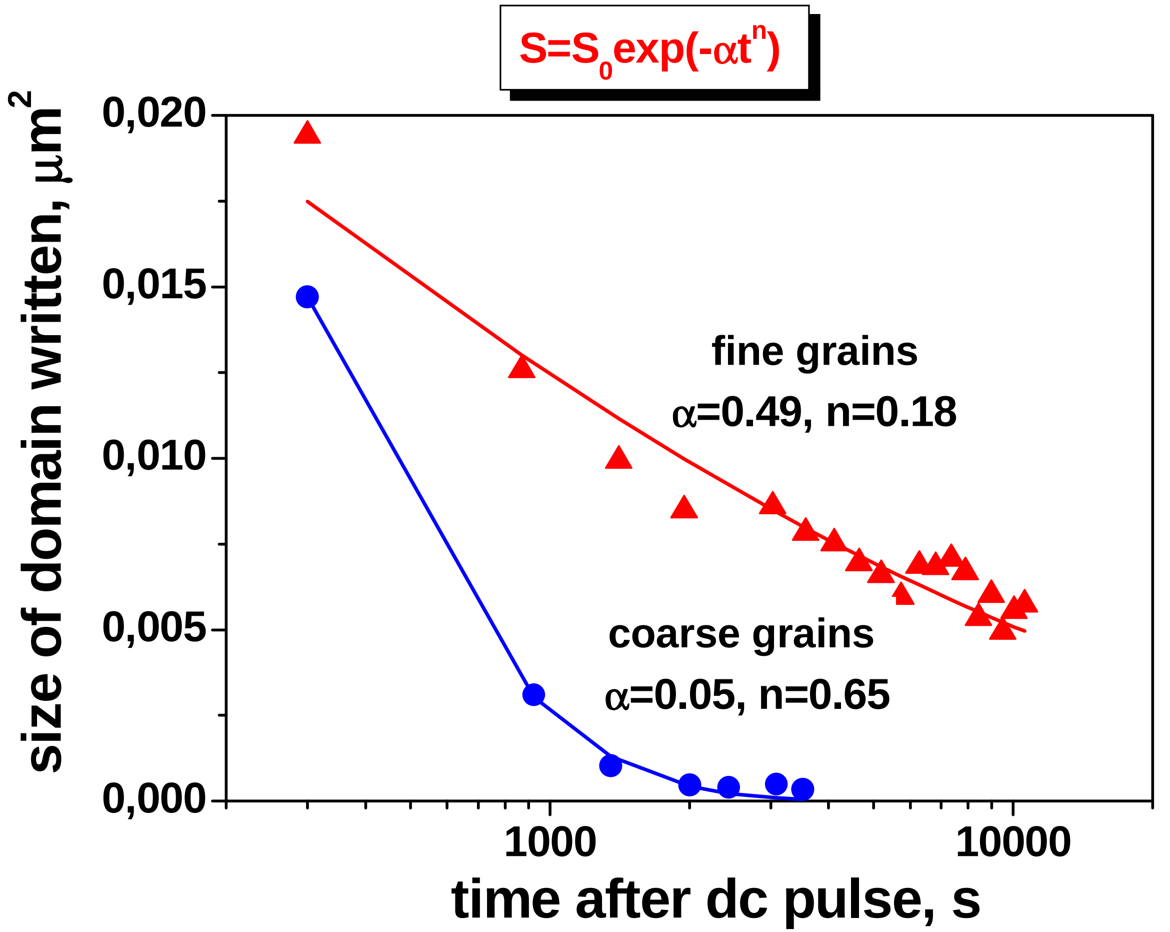

- Stretched exponential dependence is typical for systems with the broad spectrum of relaxation times

Bipolar fatigue in piezoceramics

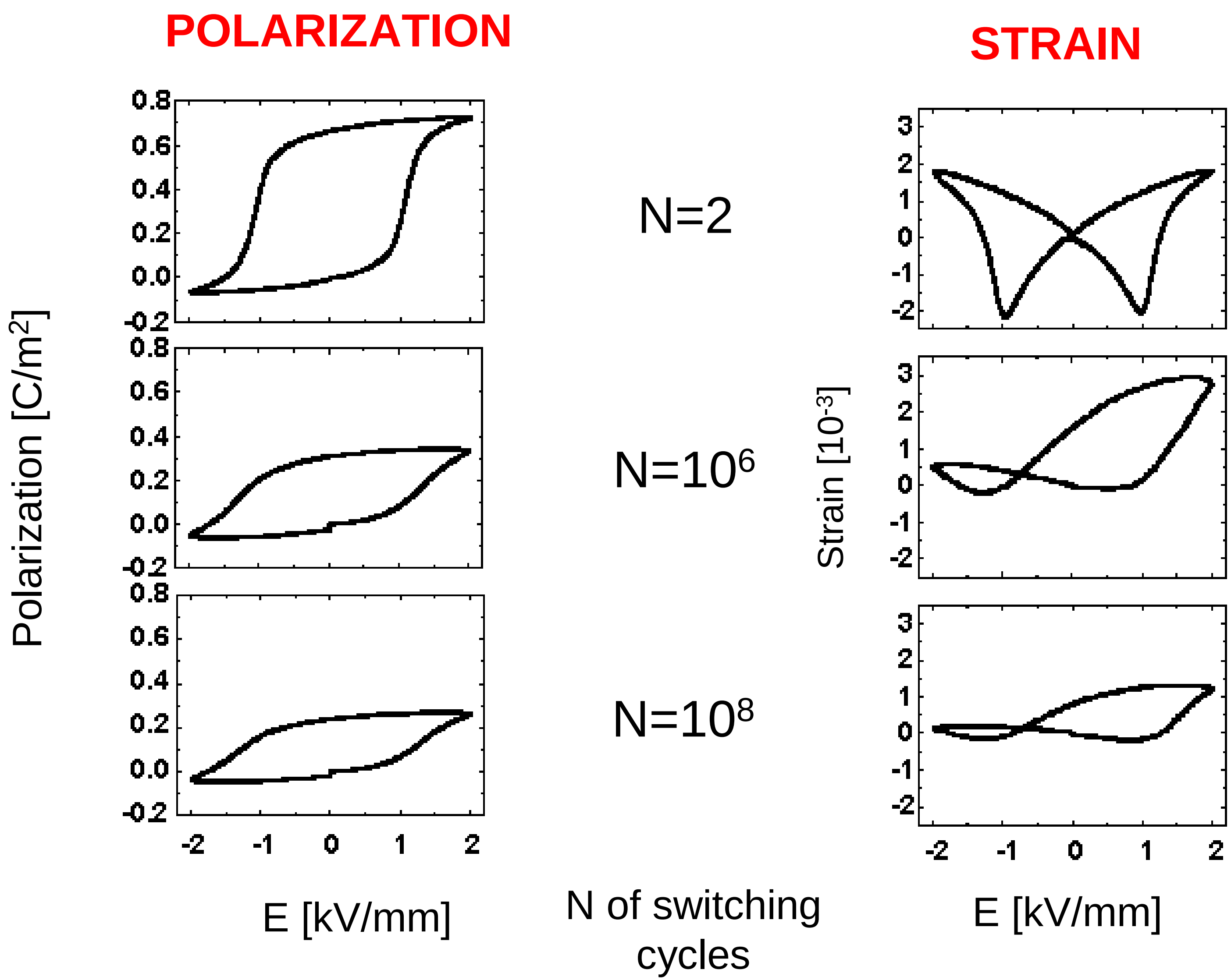

- **Strain asymmetry as a result of fatigue-induced polarization offset**

Fatigued vs. virgin piezoceramics (PIC151)

N=0

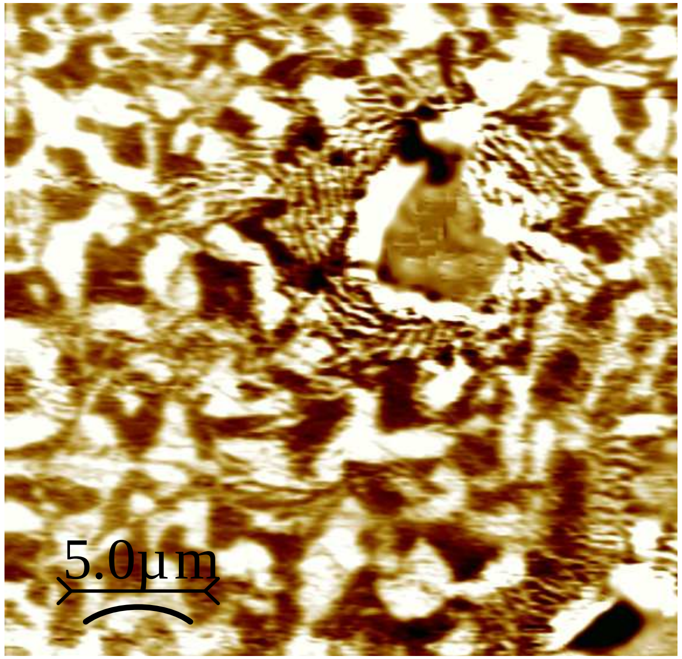

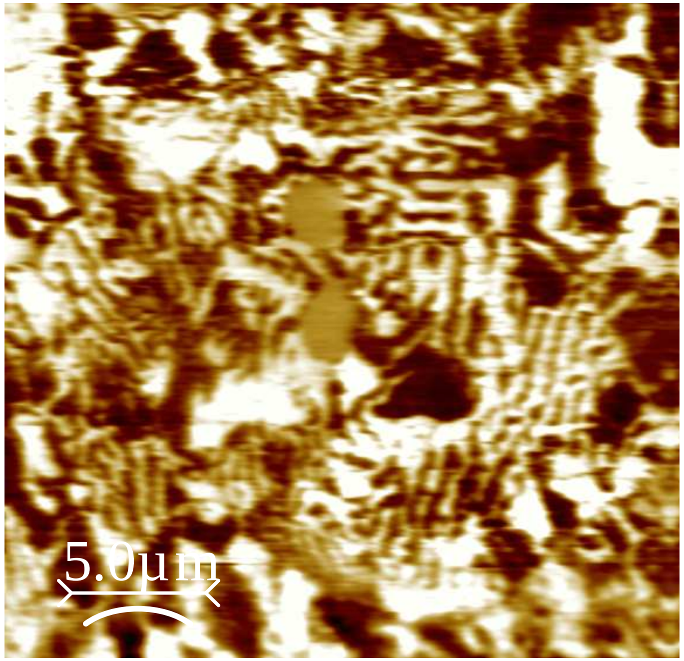

N=10^6

N=$5x10^7$

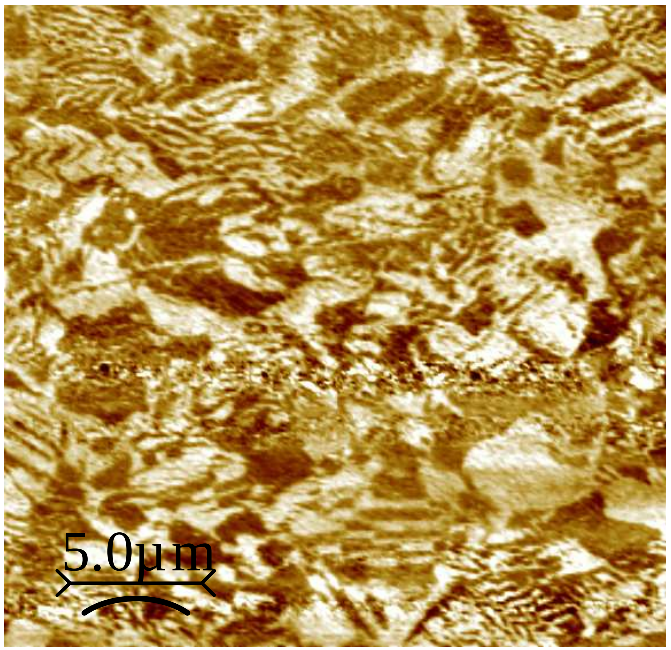

Effect of annealing

virgin sample

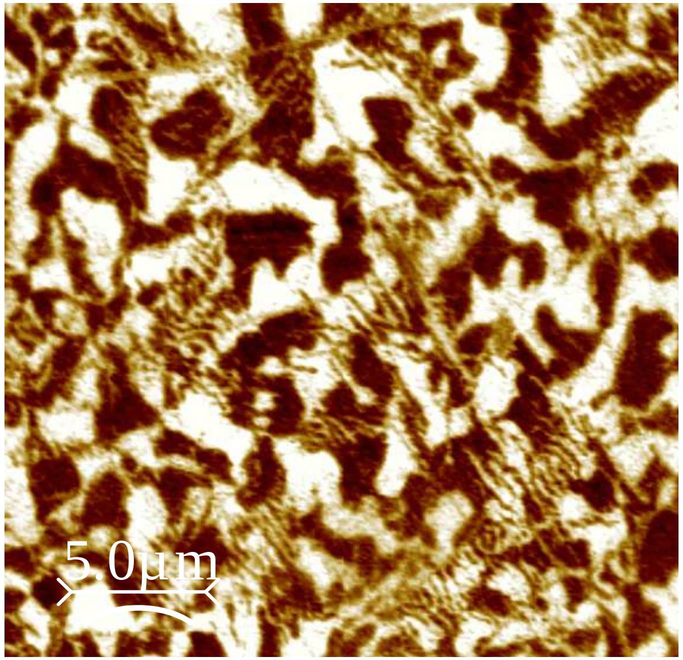

fatigued

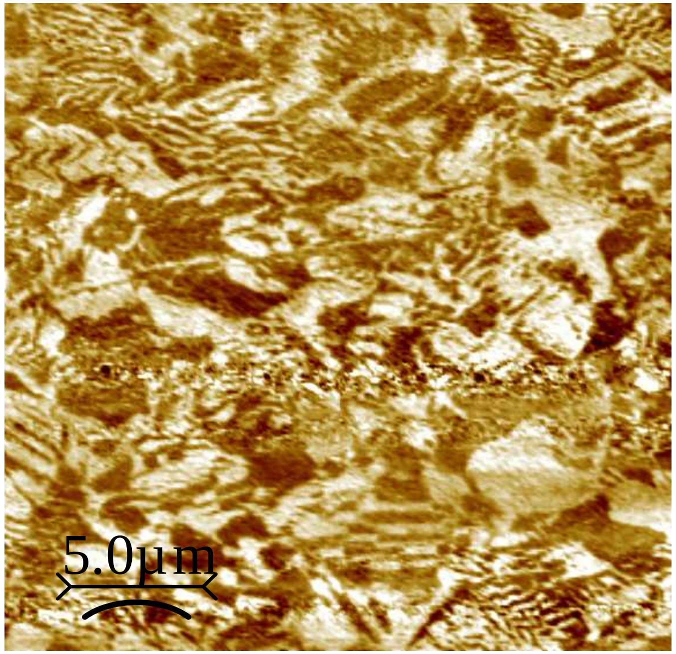

annealed

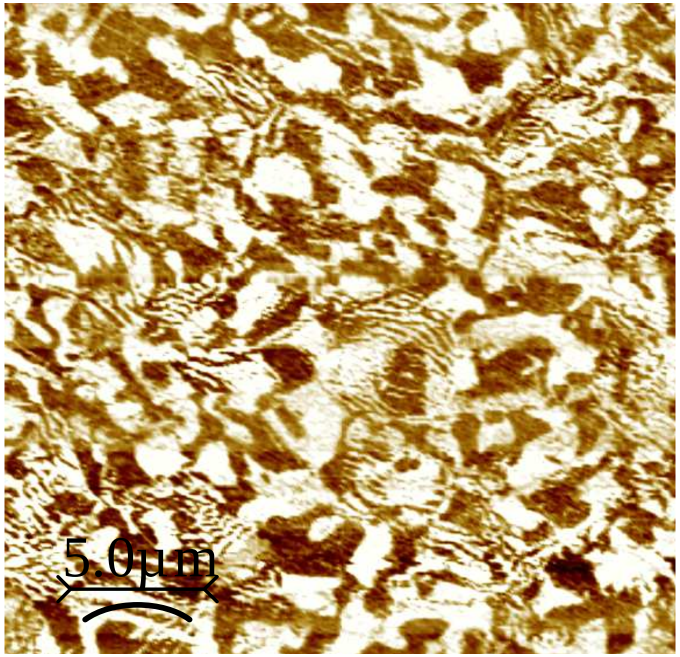

After annealing (T=700 ºC, 10 h) the initial ratio between 180º and ferroelastic domains is restored along with the rejuvenation of switchable polarization.

Concentration of stripe domains vs. depth

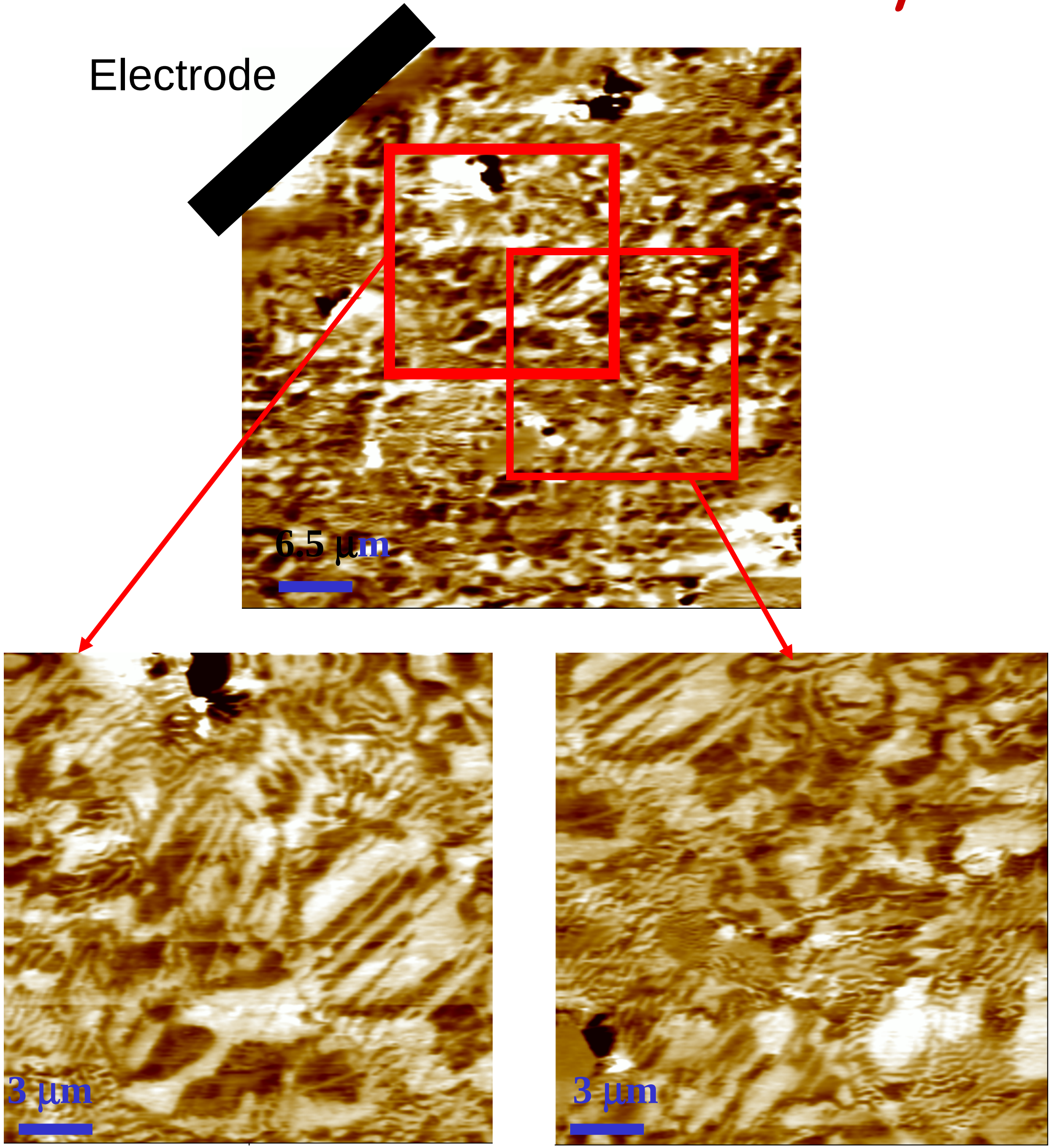

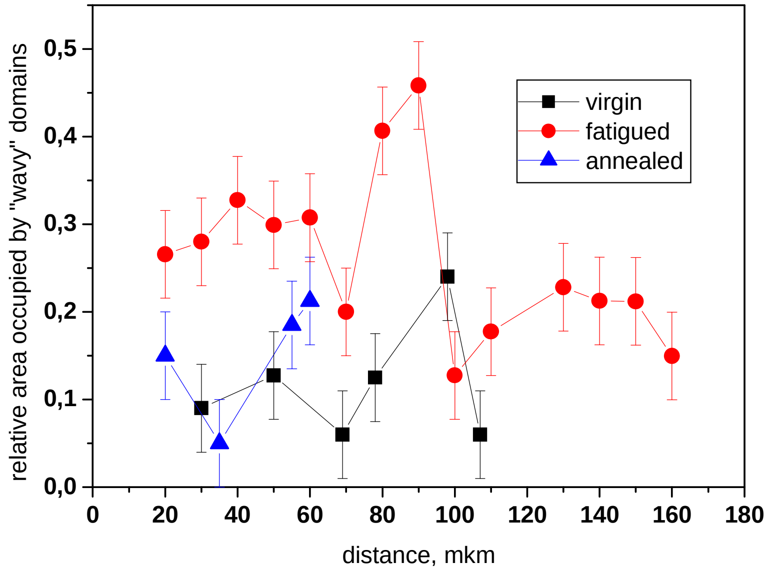

- Concentration of stripe domains decreases with the distance from the electrode
- A maximum at about 80-100 µm below the electrode

Domain distribution vs. depth

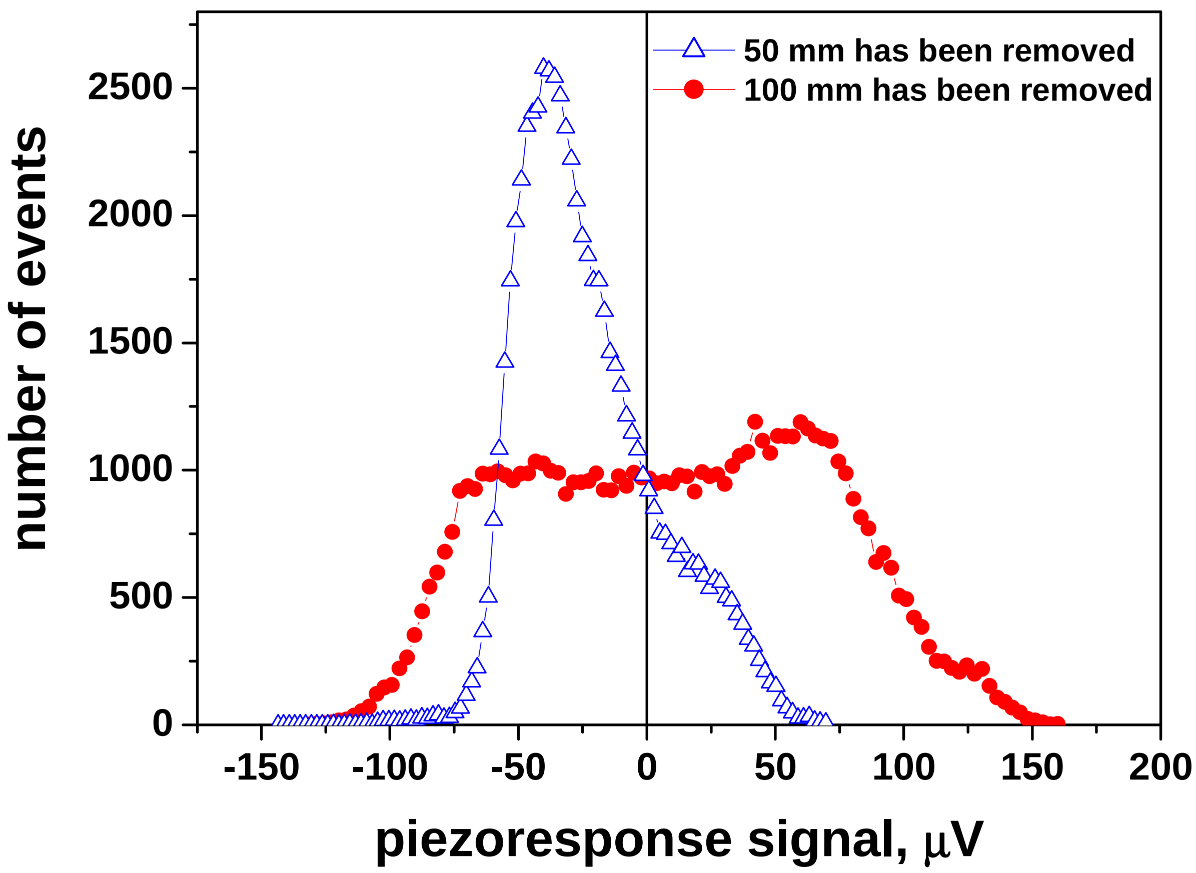

- **In fatigued areas the domain histogram is highly asymmetrical demonstrating a preference of polarization state (domain head at electrode)**
- **The symmetrical domain distribution is restored with depth**

Local polarization switching vs. fatigue

initial | **poled +30 V** | **poled -30 V**

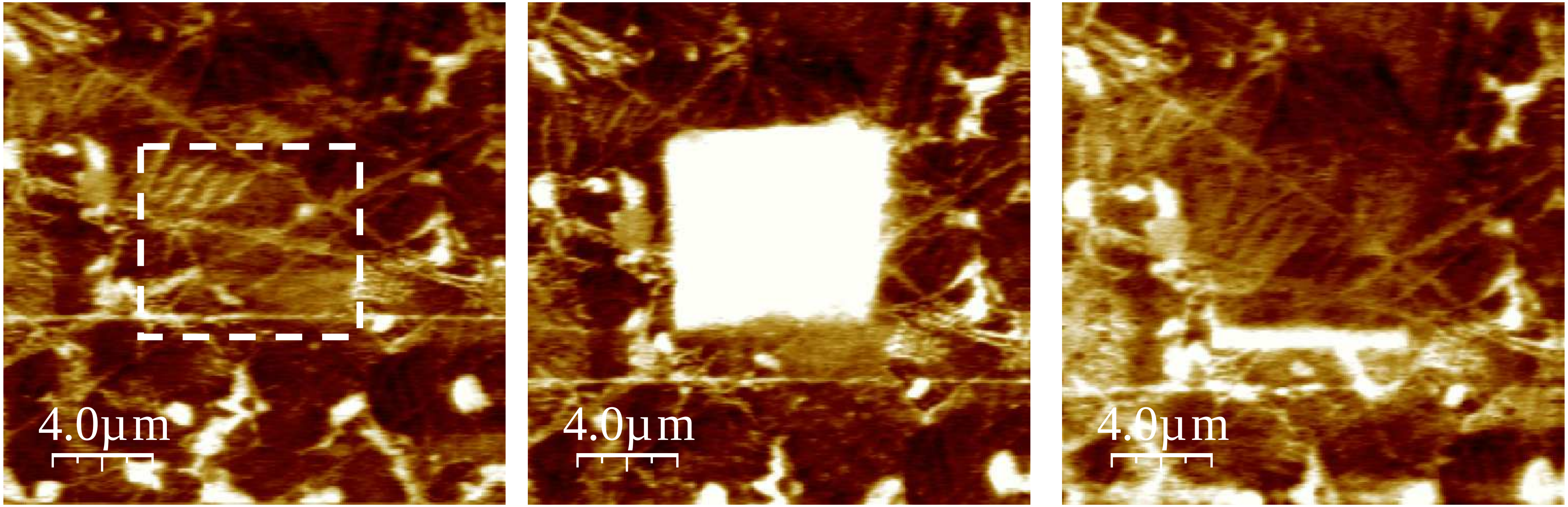

- **Local poling is different for both directions of poling field**
- **Pinning mechanism might be applicable for fatigue in ceramics**

Conclusions:

- ***Miniaturization requires integration of piezoelectric/ ferroelectric materials using Si-based technology***

- ***Laser interferometry is an indispensable technique for the piezoelectric measurements in thin films down to nm thickness***

- ***Piezoresponse Force Microscopy (PFM) can be used for integrated piezoelectrics provided the mechanism of the tip-surface interaction is understood***

- ***PFM is suitable for the local study of polarization reversal, aging and fatigue in ferroelectrics including relaxors***